Finite Element-Based Non-Linear Dynamic Soil-Structure Interaction

Terry Bennett MEng

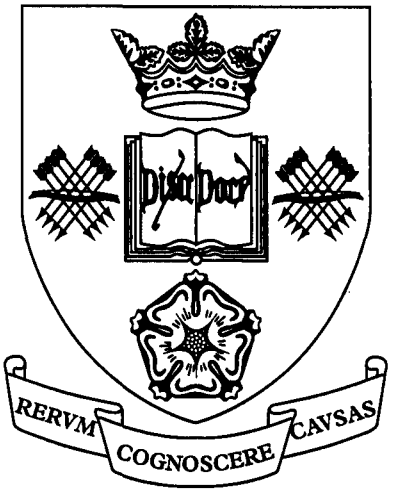

This thesis is submitted for partial consideration towards the degree of Doctor of Philosophy in

The Department of Civil and Structural Engineering

at the University of Sheffield

January 2001

ACKNOWLEDGEMENTS

First and foremost I would like to thank my Mom, Dad and brother Sonny for all those words I don't quite know how to write.

Roger, I would like to thank you for, if not understanding, then tolerance of my good self. Your seemingly infinite enthusiasm has been both inspirational and bewildering. I have learnt much more from you than computational mechanics.

To my colleagues in Dept. of Civil and Structural Engineering thanks for the help, advice, jam sessions, footy matches, and theological discussion(!). In particular I would like to thank the other members of the Computational Mechanics Team - Mihail, Jens, Sultan, Benebdellah, Forrest and Yi.

I would like to express my gratitude for the financial support for this project, from an EPSRC Departmental Scholarship and with partial support from MAST MAS3-CT95-0041 (1996-1999) Probabilistic Design Tools for Vertical Breakwaters.

My Colleagues at TNO Bouw (The Netherlands) have shown great understanding in my acclimatisation to the land that they call home and the world of work.

Finally I can not thank enough my good friends during my 7 years in Sheffield, in particular 94, 102, Dan and Diane, Pob, Hairy, Tina, Paul and Charlotte, Mat and Ben, Jonead and many others too numerous to mention. Special thanks to Little Mat for 7 years of friendship and help with the final push.

ABSTRACT

The modelling of unbounded domains is an important consideration in many engineering problems, for example in fluid flow, electro-magnetics, acoustics and solid mechanics. This thesis focuses on the problem of modelling elastic solids to infinity, with the specific purpose of modelling dynamic soil-structure interaction (DSSI). However, the reader should be aware that the techniques presented may also be adapted to address those other physical phenomena.

The need for techniques to model the soil domain to infinity and a qualitative introduction into the problems associated with dynamic soil-structure interaction are outlined in chapter 1. This is done to illustrate why such an abstract mathematical concept of modelling infinite domains has an important role to play within the design process of large, safety critical, civil engineering structures.

A brief review of a number of alternative ways of addressing this problem is given in chapter 2. Their relative strengths and weaknesses along with the typical applicability of the techniques is discussed. A consequence of this review is the identification of a very promising rigorous approach [59] which is singled-out for further study. A detailed explanation of this (Consistent Infinitesimal Finite Element Cell Method, CIFECM) method is then given in chapter 3. Attention is restricted to the use of the technique for solving the 3-D vector wave equation in the time domain.

The features of the non-linear dynamic finite element code, into which the CIFECM has been incorporated, is highlighted in chapter 4. The non-linear (microplane) material model for quasi-brittle materials is described along with the solution strategy employed. It should be mentioned that the soil is treated within this thesis as drained linear elastic medium. The method of coupling the CIFECM into the dynamic equation of force equilibrium for both directly applied and transmitted loading regimes is detailed.

Application of the code follows in chapter 5; firstly by introducing the simplest test problem of one finite element coupled with one CIFECM element to model a surface foundation. Comparisons are made between the dynamic displacements resulting from the method and standard FE solutions obtained from the use of extended meshes and fixed boundary conditions, along with a study of the influence input variables. Following these examples a larger (more realistic) engineering problem is tacked involving the simulation of an aircraft impact on a reinforced concrete nuclear containment vessel. This represents the first use of the method in a 3-D non-linear structural analysis problem. The results illustrate the practical implications of including DSSI in the analysis.

In chapter 6, a series of general observations on the method are made with an assessment of its value together with a discussion on its wider application to other engineering fields. Possible future developments to make the method more computationally efficient are finally suggested.

Contents

List of Figures

Chapter 1

Introduction to Dynamic Soil-Structure Interaction

In the standard structural analysis of a building, typically the superstructure would be considered to be supported on an infinitely stiff base. However, in certain important cases the influence of the foundations on the response of the structure may be considerable, for example, when a stiff structure is sited on a relatively soft foundation.

Dynamic soil-structure interaction analyses may be important in examining the structural response to many types of loading, but it is in earthquake engineering (where the effects of founding safety critical structures on deep soft soil layers) where the effects are most noticeable.

Stress waves entering the soil layer(s) from the structure will spread over a greater area with increasing depth. This will result in increased energy absorption of the full dynamic system. If a structure is founded upon a relatively large depth of soil, the foundation soil can be considered to extend horizontally to infinity and vertically downwards to infinity (half-space), thus no reflections of the outgoing stress waves will occur. In such cases this *radiation* damping can lead to a strongly reduced response.

There are a number of ways in which the interaction of the structure with its founding material will affect its dynamic response. Each of the separate interaction effects needs to be considered in an analysis to ascertain whether the founding material will have an effect upon the response of the structure. More flexible soil foundations will result in the full dynamic (soil and structure) system becoming softer, serving to reduce the fundamental frequency of excitation of the complete system significantly. The overall effect upon the structural response will be dependant upon

the frequency of the loading, but may lead to a reduction of the stresses induced within the structure, despite larger total displacements. If a structure is founded upon rock, no rotations at the base of the structure are possible. However, rocking motion will occur in most foundations, there being considerable importance for tall structures. Similarly, shearing and torsion effects between the structure and its founding material are ignored in the analysis of a structure treated as being founded on bedrock.

Distinction may be made between the types of loading, depending upon whether the loads are applied directly on the structure, as is the case with blast and impact problems or problems where reciprocating machines apply a regular excitation, or the load is transmitted through the soil to the structure from an external source, as is the case with earthquake loading or from remote vibrations (induced from a nearby railway for example).

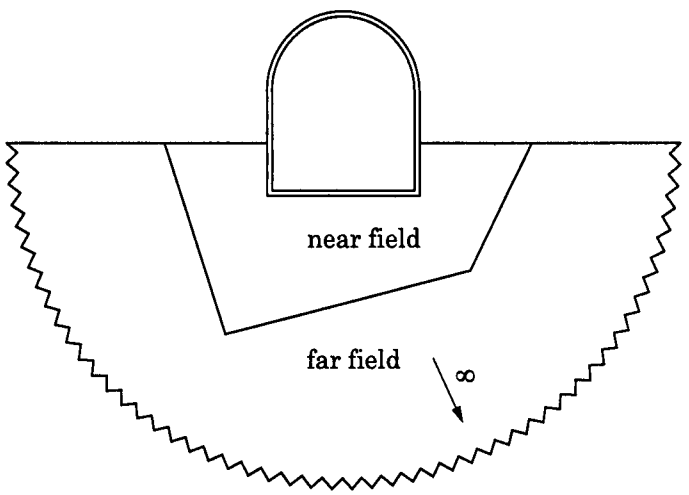

Figure 1.1: The Near and Far Fields

The soil directly below the structure is referred to as the near field and may contain material non-linearities. The remaining extent of soil is assumed to behave linearly, and is named the far field (fig.1.1). The assumption of linearity in the far field can be justified for most load cases, and is an inherent assumption in earthquake analysis where a two stage procedure needs to be carried out.

In an earthquake analysis the effect of the input ground motion upon the site without the presence of the structure is first carried out, the forces and/or displacements upon the soil-structure interface are then used as the input for the analysis of the full soil and structure system (fig.1.2). In order that such a two stage procedure is valid, the principle of superposition is automatically implied. The material properties of the soil extending to infinity can be selected such that the strains calculated

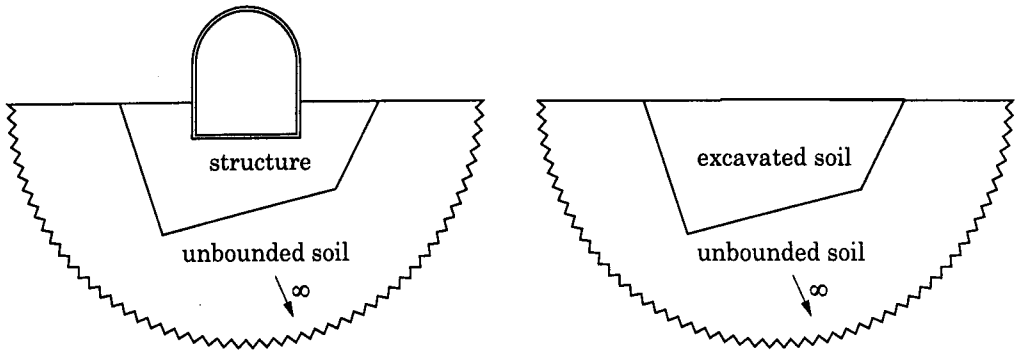

Figure 1.2: (a) Soil and Structure System; (b) Free Field

conform with those that might be expected, requiring a degree of experience on the part of the analyst.

At present the field is still limited in that a full non-linear analysis is not possible (e.g. permanent settlements of a structure due to the far field) many of the most significant features in a soil-structure interaction problem can be modelled with today's Finite Element technology. For example, both the structure and near field soil can be analysed with non-linear response with reasonable confidence using sophisticated constitutive models (although this itself remains a highly active research area), and uplift of the structure from its foundations may be modelled by the use of frictional contact elements.

In the frequency domain analysis it is possible to evaluate the dynamic response of structures by performing a series of uncoupled single degree of freedom (SDoF) analyses at discrete frequencies for multi-degree of freedom problems. The associated *eigenvalues* are calculated based on the mass matrix $[M]$ and the stiffness matrix $[K]$. For a N degrees of freedom problem, there are N associated frequencies each possessing a corresponding mode shape.

In order that non-linear effects may be included within an analysis, it is necessary to perform a step-by-step, iterative (causal) approach. When performing a time domain analysis, it is necessary to invoke a numerical time integration procedure. This procedure forms a relationship between the three unknown updated vectors $\{\ddot{d}\}$, $\{\dot{d}\}$ and $\{d\}$. If the solution is based on the previous time t, the method is classed as an *explicit method.* If it is based on the new time $t + \Delta t$, the method is known as an *implicit method.*

Both linear and non-linear dynamic problems can be treated in the same manner using a time domain approach. The only difference being that an iterative non-linear solution strategy is required to be nested within an implicit time stepping

scheme when solving non-linear problems. Within this thesis, only the time domain analysis is considered.

A realistic simulation of the dynamic response of an important structure must include consideration of the degree of soil-structure interaction likely and detailed coupled analyses be performed if necessary. Currently, most existing general purpose Finite Element codes do not include this capability and although specialist algorithms exist, there remains much work to be done in linking advanced far field modelling techniques to existing Finite Element codes.

Chapter 2

Alternative Methods of Modelling the Dynamic Far Field

This chapter presents a review of the concepts underlying a number of existing numerical methods for modelling the dynamic far field. The study examines those methods which may be coupled with a conventional Finite Element analysis of the structure (and possibly the *local* soil in the immediate vicinity of the structure). This is presented in a conceptual manner, in order to demonstrate the many techniques available to model problems where the effects of considering unbounded founding material are of differing importance.

Note that for linear problems, the dynamic far field may be analysed either in the frequency domain or the time domain. In the frequency domain approach, the solution applicable to the whole duration of the analysis is determined at discrete frequencies. The complete solution (for all examined frequencies) is given by superposition of each of the frequency dependent results. Transfer functions relating the response to the excitation can be calculated and, by use of the Fourier transform, the displacement in the time domain determined.

If the structure, or the near field soil, behaves non-linearly then the analysis *must* be performed in the time domain using a step-by-step integration procedure. The method adopted in this thesis (see chapter 3) operates either the frequency or the time domain. Not all the techniques reviewed in this chapter exhibit this flexibility. This review is limited to time domain procedures, for a thorough review of dynamic soil-structure interaction in the frequency domain the reader is directed to the classic text book by Wolf [56].

Methods used in the analysis of dynamic soil-structure interaction problems are categorised into two subsets

- Direct Methods
- Substructure Methods

Standard direct methods offer a simplified way of incorporating the influence of the foundation and far field into the model. These approaches are generally spatially uncoupled and temporally uncoupled (local in space and time). Approximate boundary conditions are formulated to represent the unbounded soil. In addition to modelling the unbounded soil's stiffness, reflections of the outwardly propagating waves are suppressed. In the direct methods the *radiation condition* is formulated not at infinity but at the interface where the direct method is applied (a large but finite distance from the structure). Substructure methods are constructed from a more satisfactory, mathematically rigorous, approach by respecting the radiation condition at infinity. The substructure methods are spatially and temporally coupled (non-local in space and time). Solution techniques belonging to the direct and substructure Methods will now be considered in more detail.

2.1 Direct Methods

In the direct method of analysis, the unbounded linear soil is modelled using a finite domain procedure, for example, simple analogues of physical models which do not require the calculation of the dynamic stiffness or unit-impulse response matrices for the site (unlike the substructure methods). The unbounded domain is processed in a straight forward manner along with the equations of motion for the bounded domain. The direct approximations are formulated at each node (in each appropriate direction), requiring information at the start of the time step, or at most at a few recent time steps. The boundary conditions must be frequency independent to be able to be used in a transient analysis in the time domain. The following direct methods have been considered.

2.1.1 Discrete Lumped Parameter Models

When modelling the far field, the structure can have each of its global modes of interaction modelled by simple time independent springs and dashpots. The simplest of such models simulates the vertical translation, horizontal shearing and torsion and rocking rotations as independent single degrees of freedom. These discrete elements present no great difficulties to be incorporated in most existing finite element analysis codes. Figure (fig.2.1) illustrates a two dimensional arrangement

with three degrees of freedom (3 DoF). Inherent in the *standard* discrete model is the assumption that the structure lies on the surface of the soil (that is, not embedded). The spring and dashpot coefficients are selected such that the model offers the best representation of the total soil system. If the cone models are used to determine the coefficients then the equivalent dynamic stiffness may be exact in the static case and the case corresponding to very high frequencies. However for intermediate frequencies the solution is only approximate. In order to improve the accuracy of simple model and extend it to cases where the structure lies below the ground surface, extra masses and dampers can be added to each of the degrees of freedom to provide a *lumped parameter* representation [37].

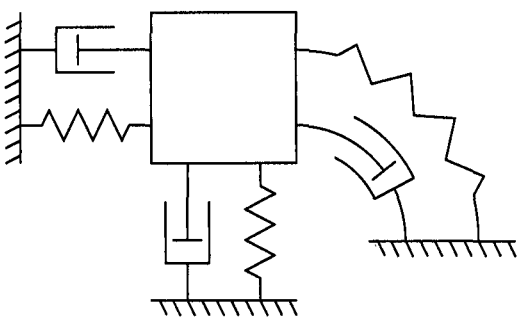

Figure 2.1: 3-DoF Lumped Parameter Model

These simple models are useful for insight into the dynamic characteristics of a given problem, or in the conservative design of structures where safety is not overly critical. The main errors associated with these methods arise from using frequency (and hence time) independent springs and dampers, and the decoupling of the global degrees of freedoms.

2.1.2 Cone Models

Cone models provide analytic expressions of wave propagation to infinity, where a solution is provided in terms of the displacements at the truncated free end of a semi-infinite cone. The approach is based on simple bar theory where plane sections remain plane. Note that only four independent degrees of freedom need be considered (rather than six; 3 translational and 3 rotational) because of the rotational symmetry about the axis of the cone. Each of the four dynamic degrees of freedom are decoupled and modelled individually by separate models.

The translational cone model is the simplest conceptually to understand. The starting point for the formulation is one dimensional wave propagation in a semi-

infinite rod. These ideas are extended to include the case where the cross sectional area of the rod increases with distance, thus approximately modelling the spreading of the area influenced by the load.

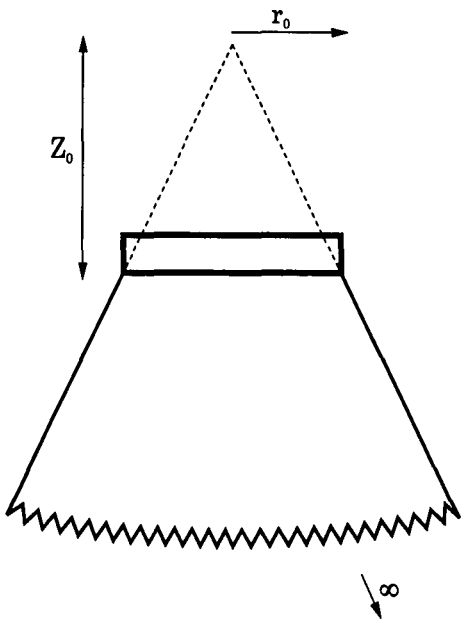

Figure 2.2: Illustration of a Semi-Infinite Truncated Cone

Identifying appropriate lengths z_0 and r_0 (fig.2.2) (which define the properties of the cone) is the major difficulty, as the system must accurately represent the unbounded soil [58]. The key assumption associated with these models is that the soil outside of the physical extent of the cone has a negligible effect on the solution. The properties derived from the cone models may be used directly as a stand alone analysis tool (which could be used, for example, for rigid base mat problems) or as a method of constructing the discrete models described above.

2.1.3 Extended Finite Element Mesh

The extended mesh approach simply involves the use of additional finite elements extending from the zone immediately adjacent to the structure, to a distance sufficiently removed (in all directions) from the structure. In the time domain this method is only accurate up until the point where the first stress waves propagating outwards are reflected back into the region of interest to the analyst (that is, the near field).

Once stress waves are reflected back from the fixed boundary into the finite element mesh, they will interact with other outwardly propagating waves causing errors in the solution. Therefore, an analysis requiring a significant time duration

will require an extremely large mesh (possibly up to several kilometres) which will be computationally prohibitive (in terms of CPU time and memory) in three dimensional analyses using current computing resources. For example, a soil with a shear modulus of $500MPa$ and density $2000kg.m^{-3}$ would require a mesh extending over 7 kilometres from the structure if an earthquake of $30s$ were to be considered. If element sizes were restricted to $10m$ (not unreasonable) and bedrock occurred $150m$ below the surface, then nearly 30×10^6 elements would be required.

Note that in the frequency domain the extended mesh solution will always be in error. This is because in the frequency domain the whole problem is assumed to oscillate at a given frequency simultaneously, so the low frequency response will be limited by the length of the extended mesh.

2.1.4 Transmitting Boundaries

The problem of wave reflection in a truncated mesh has been examined by a number of researchers [18][29][30][48]. Each has attempted to develop a form of *transmitting* (or silent) boundary which allows stress waves to be only transmitted. Weber provides a useful discussion on the distinction between local non-consistent, consistent and rational transmitting boundaries [54]. The original formulations for these boundaries started from quite different physical bases, but the final formulations can be shown to be mathematically equivalent [24]. Local transmitting boundaries are frequency independent and can therefore be used directly in time domain analyses. Unfortunately they are transmitting only for planar waves striking the boundary normally, while for non-normal incidence they allow reflection. To achieve high accuracy, a sufficiently large finite element mesh is therefore required, allowing the outgoing wave pattern to become polarised [57], at larger distances from a source the waves become more directional. Note that some experience is needed to assess the nature of the wave pattern when using the simplified techniques.

Consider the simplest frequency independent dashpot boundary designed to transmit dilatational waves. The viscosity, c, of this dashpot is given by

$$c = A\rho\sqrt{\frac{E}{\rho}} = A\sqrt{\rho E} \tag{2.1}$$

where A is the contributory area associated with each dashpot, E is the elastic (Young's) modulus of the soil and ρ is the mass density. The use of dashpots alone at the transmitting boundary will lead to permanent displacements. Introducing linear springs overcomes this problem but all existing local transmitting boundaries

require careful calibration.

The use of consistent rational transmitting boundaries holds further promise. The key step in developing rational transmitting boundaries is the approximation of the frequency domain solution by a rational system. Weber presents such an approach for the scalar wave problem of a structure dynamically interacting with an unbounded compressible fluid domain [54]. Equivalent solutions for the vector wave problem have yet to be developed.

2.1.5 Infinite Elements

As one of the most renowned methods for the modelling of unbounded domains, the technique of *Infinite Elements* must be mentioned. However, as is shown conceptually below their applicability to the area of truly transient loading regimes is limited.

Infinite elements [9] are an approximate approach to modelling infinite domains by special finite elements. These elements approximate the distribution of the variable beyond the truncated finite element mesh. As the technique is quite general the approximation will differ according to the physical problem being addressed. Therefore, when treating a specific problem knowledge as to the nature of the appropriate Green's function is required.

Infinite elements may be subdivided into two major categories according to their formulation

- decay function infinite elements
- mapped infinite elements

only the former are described. A further distinction is made as to whether the element developed is suitable for static or dynamic analysis.

Decay Function Infinite Elements

The finite element shape function is retained in the formulation of such elements, but is multiplied by a decay function. The decay function enforces the variables (displacements) to tend to the far field value (that is the radiation condition where displacements are equal to zero), in addition the rate of decay should be consistent with the physical problem. For example, given the standard finite element shape function, $P_i(\xi, \eta)$ and the decay function, $f_i(\xi, \eta)$ the following infinite element shape function is given

$$\underbrace{N_i(\xi,\eta) = P_i(\xi,\eta).f_i(\xi,\eta)}_{\textit{no summation on } i} \tag{2.2}$$

The decay function (to be compatible with standard finite elements) must take the value of unity at its own node

$$f_i(\xi_i,\eta_i) = 1 \tag{2.3}$$

The derivatives of the element shape functions can be found via the chain rule (given here for decay in both directions, for a 2-D element)

$$\frac{\partial N_i}{\partial \xi} = \frac{\partial P_i}{\partial \xi} f_i + P_i \frac{\partial f_i}{\partial \xi} \tag{2.4}$$

$$\frac{\partial N_i}{\partial \eta} = \frac{\partial P_i}{\partial \eta} f_i + P_i \frac{\partial f_i}{\partial \eta} \tag{2.5}$$

Decay Function Periodic Infinite Elements In the periodic problem, the behaviour to be modelled is that of a wave, travelling outwards and gradually decaying i.e. an extra component due to wave type behaviour must be added to the shape function.

$$N_i(\xi,\eta) = P_i(\xi,\eta)\, f_i(\xi,\eta)\, e^{jks} \tag{2.6}$$

where k is the wave number and s is a co-ordinate directly related to ξ (the radial co-ordinate). As a result of superposing the harmonic shape function, the model is transformed to a generalised co-ordinate system.

Dynamic soil-structure interaction problems in the frequency domain have been tackled successfully by many researchers [13] [45] [14] for instance, a more thorough review is presented in the book by Bettess [9].

2.2 Substructure Methods

In the substructure method the influence of the underlying soil conditions is modelled on the soil-structure interface, and is expressed at points (nodes) on the interface surface. The soil-structure interface may be placed arbitrarily, however it may typically lie closer to the structure than transmitting boundaries. All non-

linearities must be treated inside the interface as beyond this elastic behaviour is enforced by the substructure model. Due to the close proximity of the soil-structure interface, the unbounded medium in general needs to be modelled rigorously for sufficient accuracy.

An exact model of the unbounded medium will be global in space and time, and is formulated in terms of the interaction forces on the soil-structure interface. In the frequency domain, the interaction forces can be expressed as simple linear equations for each frequency of interest to the analyst

$$\{R(\omega)\} = [S^{\infty}(\omega)]\{u(\omega)\} \tag{2.7}$$

where $\{R(\omega)\}$ are the interaction forces, $\{u(\omega)\}$ are the displacements (mode shape) for the given frequency, and $[S^{\infty}(\omega)]$ is the *dynamic stiffness matrix.* In the time domain the interaction force-displacement relationship is calculated using a convolution integral

$$\{R(t)\} = \int_0^t [S^{\infty}(t-\tau)]\{u(\tau)\}\, d\tau \tag{2.8}$$

where $[S^{\infty}(t-\tau)]$ is the *unit impulse response matrix to displacement.* $[S^{\infty}(\omega)]$ and $[S^{\infty}(t-\tau)]$ form a Fourier transform pair

$$[S^{\infty}(t)] = \frac{1}{2\pi}\int_{-\infty}^{+\infty} [S^{\infty}(\omega)]\, e^{i\omega t} d\omega \tag{2.9}$$

Computationally, the consequences of this global formulation are that different dynamic stiffness matrices (or unit-impulse response matrices) need to be calculated for each frequency or time station. These matrices will be fully populated (global spatial coupling).

In the time domain the total response of a structure is calculated by dividing the input force-time history into a series of small individual pulses, and summating the response of each individual pulse (fig.2.3).

2.2.1 Boundary Integral Methods

The governing equations of physical phenomena are invariably expressed in terms of partial differential equations along with the corresponding boundary conditions, and in addition for a transient problem the initial conditions are required.

It is however, possible to reformulate these partial differential equations for many

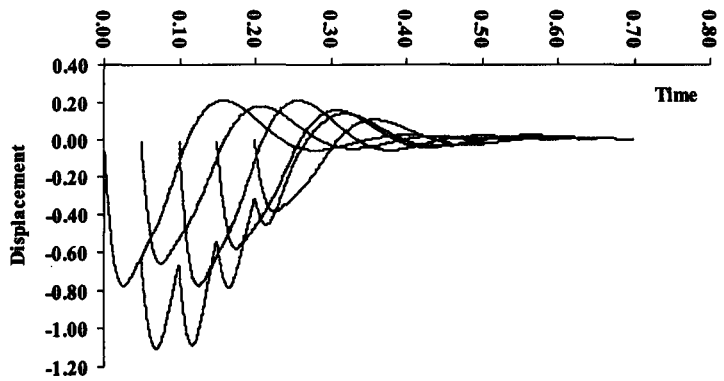

Figure 2.3: Total Response from the Summation of Individual Unit-Impulse Responses

problems in terms of integral equations using the dynamic reciprocal theorem, Green's functions, weighted residuals or variational principals. These integral representations can be used to form an expression for the field variable (displacements in elasto-dynamics) for a general point both spatially and in time. These will involve convolutions of the boundary values, initial values and the applied loading throughout the medium.

A set of integral equations are constructed involving only the boundary values, initial values, and the applied loading, with the only unknowns in the problem occurring on the boundary. Therefore, in a soil-structure interaction analysis, only the bounding surface of a 3-D problem needs to be discretised to describe the influence of the foundation.

The medium's dynamic behaviour is entirely represented by these equations, which are applicable to both bounded and unbounded domains. These *fundamental solutions* intrinsically include the radiation condition.

These integral formulations are well established, appearing in the literature almost a century ago, but analytical solutions to these resulting singular integrals may well be impossible to obtain for all but the simplest of soil strata. The mathematical techniques for solving singular integrals are generally unfamiliar to most engineers, which is a significant barrier to their general acceptance.

A review of the development of analytical solutions to the problem of wave propagation in semi-infinite media is given in the classic text book [43], four of the earliest and most important of which are briefly summarised here.

In the seminal paper [27], Lamb considers the problem of both an oscillator resting on the surface of an elastic half-space and at an internal point within the half-

space, both horizontally and vertically. The analytical solution to this *dynamic Boussinesq loading* is found in both two and three dimensions. The response to a single vertical pulse is then found by combining oscillating forces acting at different frequencies.

The condition of reciprocity of the deflections at two points is noted for the dynamic case, which is an extension of Maxwell's reciprocal theorem for statics. The work of Lamb was extended by Reissner [42] to the case the vertical displacement of a circular footing by integration of the fundamental solution. This leads to an approach whereby any shape of footing may theoretically be modelled. The effect of differing applied pressures over the surface area of the footing upon the vertical response, was developed simultaneously [41] [52].

The numerical solution of boundary integral equations is a relatively recent development (mid 1960s), and are carried out by discretising the integral equations in space and time. Much research into these solutions has been carried out since and the technique is generally referred to as the *Boundary Element Method* [31][3].

Much research has been carried out in order to benefit from the advantages of the Boundary Element Method to model infinite domains and couple such techniques with the more widely accepted and familiar Finite Element Method [19] [14] [1].

2.2.2 Similarity Based Methods

Finite Element methods, in contrast to the Boundary Integral Methods, use mathematics which the engineer is generally familiar with. Therefore it is desirable that an exact method of modelling unbounded media is formulated in compliance with the Finite Element method.

Such a method, based on *similar* soil-structure interfaces, was first proposed by Dasgupta [16] and has recently been investigated and considerably extended by Wolf and Song [59] with two different implementations proposed.

These *cloning* methods are all based on the simple concept that *geometrically similar* unbounded domains may be mathematically related to one another (fig.2.4).

Just as the geometry of the exterior interface, with characteristic length r_e, can be described in terms of the geometry on the interior interface r_i, the Unit-Impulse response matrices for the unbounded mediums beyond these interfaces may also be described in terms of one another

$$[S^{\infty}]_{r_e} = f\left([S^{\infty}]_{r_i}\right) \tag{2.10}$$

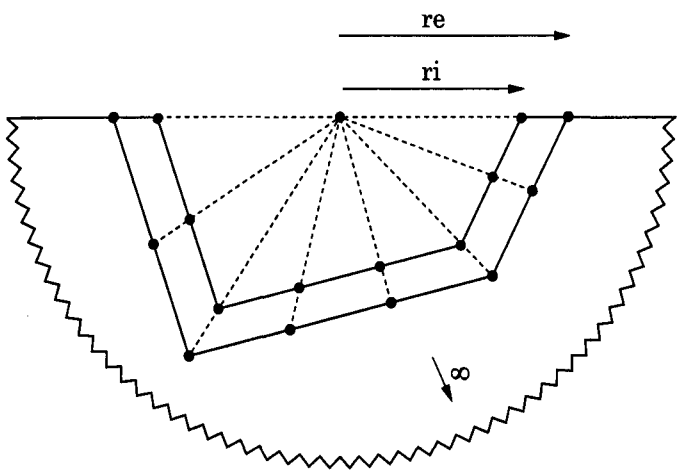

Figure 2.4: Similar Soil-Structure Interfaces

Wolf and Song show how the relationship between the unit-impulse response matrices is derived using dimensional analysis.

Forecasting

In the forecasting implementation of the cloning method, a small finite element region is introduced between the interior and exterior boundaries. With wave propagation at a finite velocity, the unit-impulse response matrix of the interior boundary can be calculated from the properties of the finite element region, and that of the exterior boundary from the interior boundary, using the relationship based on similarity.

Being based on a finite wave velocity this formulation (which updates the unit-impulse response matrices at each time station) leads to the drawback that many phenomena, where the entire unbounded domain is exited, cannot be modelled. This means that the forecasting method is unsuitable for modelling statics and dynamic analysis in the frequency domain. In addition, other phenomena outside of elasto-dynamics, for example, diffusion cannot be treated by this approach.

Consistent Infinitesimal Finite Element Cell Method

The disadvantage of the forecasting method, with it's inability to model actions upon the whole unbounded domain, are overcome in the Consistent Infinitesimal Finite Element Cell Method. The concept of similarity is used in conjunction with the concepts of assembling finite elements.

Addition of the finite element cell with the unbounded material beyond the exterior

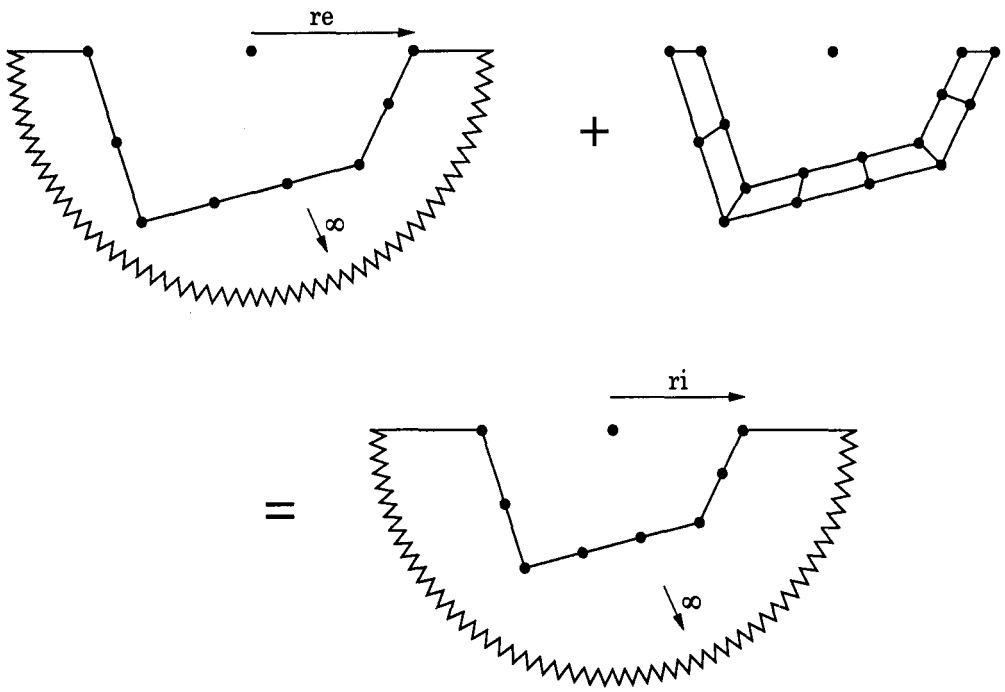

Figure 2.5: Assemblage

boundary is equivalent to the unbounded material beyond the interior boundary (fig.2.5)

$$[S^{\infty}]_{r_e} + [S]_{cell} = [S^{\infty}]_{r_i} \tag{2.11}$$

Eliminating the unit-impulse response matrix of the exterior boundary from the similarity equation (eqn.2.10) along with the assemblage equation (eqn.2.11), leaves one equation for the unit-impulse response matrix of the unbounded medium beyond the interior boundary, in terms of the properties of the finite element cell (i.e. static stiffness and mass)

$$f\left([S^{\infty}]_{r_i}\right) + [S]_{cell} = [S^{\infty}]_{r_i} \tag{2.12}$$

One cell of finite elements are constructed in the derivation. This cell characterises the unit-impulse response matrix of the unbounded medium beyond the interior boundary. The size (in the radial direction) of the cell is reduced, in the limit of the cell being infinitesimally small. This means that in the application of the method, only the soil-structure interface needs to be discretised, resulting in a spatial reduction by one, i.e. the soil-structure interface for a 3-D problem is modelled by a 2-D surface.

An alternative derivation based on the more familiar weighted residual technique has been derived, giving rise to an alternative name for the method of *The Scaled Boundary Method* [50].

2.2.3 Damping Solvent Extraction Method

The Damping Solvent Extraction method, like the Forecasting method, requires the use of a finite domain of the unbounded soil to calculate the unit impulse response functions of the site on the soil-structure interface. In contrast to the other substructure methods, this formulation is in general only approximate.

The finite domain beyond the soil-structure interface has an artificially large amount of material damping added to its properties. This acts to reduce the amplitudes of both the outgoing waves and any reflected waves at the exterior boundary. The effect of any reflected waves will, with a sufficiently high damping ratio, be negligible.

If there are no waves reflected back from the boundary to the soil-structure interface, then the dynamic stiffness of this bounded domain will be equal to that of the unbounded domain. Therefore, it is reasonable to assume that if the effect at the soil-structure interface is negligible, then the damped bounded domain can be considered to be approximately equal to the infinite extent of soil.

Finally, with unit-impulse response matrix of the unbounded domain now calculated, the effects of the artificial damping upon the outgoing waves must be removed.

2.3 Closure

A number of techniques for the modelling of unbounded media for use in time domain dynamics are described qualitatively above. A differentiation is made between direct and substructure methods. Direct methods may be straightforwardly applied within the usual finite element system matrices $[M]$, $[C]$ and $[K]$.

Despite the ease of implementation of the direct methods within existing finite element codes, much difficulty can be found in their application due to errors that will inevitable arise based upon the simplifying assumptions employed. The substructure methods by contrast are formulated rigourously in both time and space, and are simple to apply for the end user.

The complexity of the formulations of the substructure methods remains a large

obstacle to their general acceptance. A novel finite element based boundary element method, the Consistent Infinitesimal Finite Element Cell Method offers a serious alternative to the Boundary Integral Methods.

The formulation of the Consistent Infinitesimal Finite Element Cell Method is chosen for further study, along with its implementation within an existing finite element code.

Chapter 3

The Consistent Infinitesimal Finite Element Cell Method

The concept of this method has already been outlined in the review of existing methods. The formulation is presented here, which is based heavily on the book [59], in particular the sections 3.1 similarity, 5.2.1 coefficient matrices for 3-D vector waves, 5.2.7 assemblage, 5.2.8 CIFECM equation in the frequency domain, 5.2.9 CIFECM equation in the time domain, 5.3 time discretisation. The full formulation is developed here with appropriate references given for further exploration of selected components outside of the scope of this study.

The derivation begins with an introduction to unit-impulse response to acceleration matrices, as opposed to the more usual unit-impulse response to displacement. The following sections then describe the Consistent Infinitesimal Finite Element Cell Method for calculating the unit-impulse response to acceleration matrices.

Firstly, the coefficient matrices for a special semi-analytic finite element is developed. A number of these elements are assembled upon the boundary of a given problem. Each element varies outwards from the problem in a geometrically confined manner (similarity) (fig.3.1).

The effect of varying the width of these elements away from the bounding surface of the problem is then investigated. Relationships relating the frequency of excitation to the width of the element and its converse are determined.

The dynamic stiffness matrix of the special elements on the bounding surface is formulated and coupled with the dynamic stiffness matrix (as yet unascertained) of the unbounded media beyond these elements. The cumulative response of this coupled system can be equated to the dynamic stiffness of the unbounded system on the original bounding surface of the problem.

The cell width is now reduced in the limit to zero, leaving a single equation for the dynamic stiffness of the unbounded system from the bounding surface of the problem to infinity. This single equation is transformed to the time domain using the inverse Fourier transform and cast in terms of the unit-impulse response to accelerations.

The presentation is as dictated by the flow of the algorithm by considering only the case for three dimensional, compressible medium for use in time domain analysis.

3.1 Interaction Force-Acceleration Relationship

The effect of unbounded media upon the structure is given in terms of externally applied forces, calculated from the history of its excitation (convolution integral). It is more usual to calculate these forces from unit-impulse response to displacement functions. The Consistent Infinitesimal Finite Element Cell Method is cast in terms of the unit-impulse response to accelerations. Therefore, there is a need to convert interaction force-acceleration relationship from its complimentary displacement (eqn.2.8) relationship. The Interaction force-acceleration relationship is formulated analogously to those for displacement

$$\{R(t)\} = \int_0^t [M^\infty(t-\tau)]\{\ddot{u}(\tau)\}\,d\tau \tag{3.1}$$

converting to the frequency domain, and using the relationship

$$\{\ddot{u}(\omega)\} = \{i\omega\}^2\{u(\omega)\} \tag{3.2}$$

yields

$$\{R(\omega)\} = [M^\infty(\omega)](i\omega)^2\{\ddot{u}(\omega)\} \tag{3.3}$$

Comparing equations (eqn.2.7) and (eqn.3.3) gives the relationship between the dynamic stiffness to displacement and that to acceleration

$$[M^\infty(\omega)] = \frac{[S^\infty(\omega)]}{(i\omega)^2} \tag{3.4}$$

The interaction force-displacement relationship given in equation (eqn.2.8) is converted to accelerations.

3.2 Coefficient Matrices of the Finite Element Cell

In the Consistent Infinitesimal Finite Element Cell Method, the properties of the unit-impulse response to acceleration matrices are defined entirely in terms of a cell of finite elements formed on the exterior of the problem.

The exterior (unbounded) volume that will be represented is defined by a similarity centre. Lines extending from the similarity centre to the nodes on a bounding surface of a problem can be imagined to extend beyond the boundary, the volume encapsulated between these lines extending from the bounding surface to infinity is the domain of influence.

The coefficient matrices of the finite element cell are formulated next. The volume contained within the cell is defined in an identical manner as the domain of influence, but now with a finite width w. The finite element cell is an assemblage of a number of elements on a bounding surface of a problem, each possessing a finite domain of influence based upon geometric similarity. The geometry of the bounding surface is described in a local co-ordinate system with the similarity centre at the origin.

3.2.1 Formulation and Assemblage of the Finite Element Cell

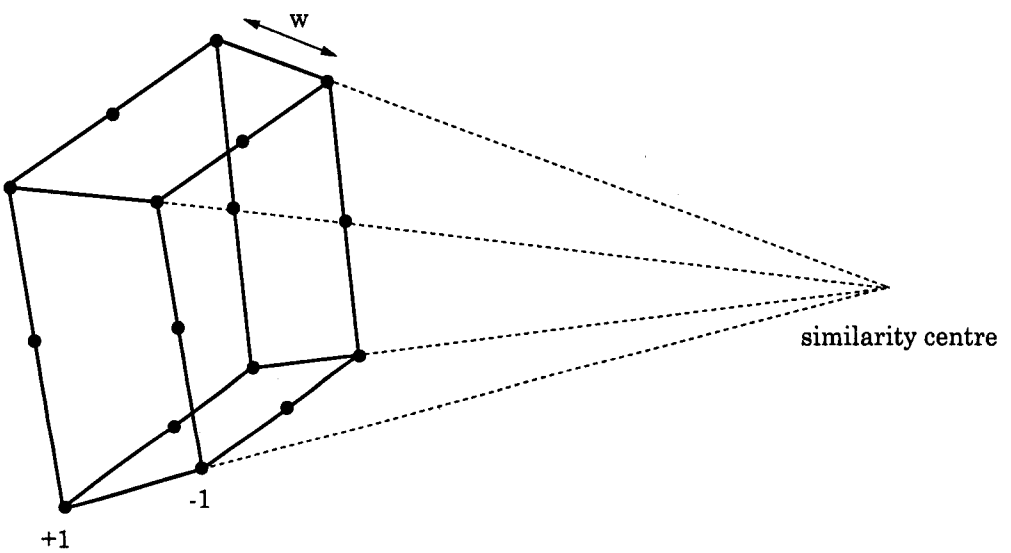

Figure 3.1: Similarity based Finite Element

A brick element is developed using two surface elements, denoted interior (subscript i) and exterior (subscript e) whose geometries are geometrically similar (fig.3.1). The shape functions relating to the direction between these surface elements are developed analytically.

3-D Isotropic Elasticity Matrix

The elastic constitutive matrix $[D]$ is formulated

$$[D] = \frac{E(1-\nu)}{(1+\nu)(1-2\nu)} \begin{bmatrix} 1 & \frac{\nu}{(1-\nu)} & \frac{\nu}{(1-\nu)} & 0 & 0 & 0 \\ & 1 & \frac{\nu}{(1-\nu)} & 0 & 0 & 0 \\ & & 1 & 0 & 0 & 0 \\ & \text{symmetric} & & \frac{1-2\nu}{2(1-\nu)} & 0 & 0 \\ & & & & \frac{1-2\nu}{2(1-\nu)} & 0 \\ & & & & & \frac{1-2\nu}{2(1-\nu)} \end{bmatrix} \tag{3.5}$$

given here in terms of Young's modulus as is the norm for structural mechanics, the shear modulus more often used in geomechanics is directly related by

$$G = \frac{E}{2(1+\nu)} \tag{3.6}$$

here the Isotropic form has been used, however, a more general elasticity matrix could be used. This is particularly useful in soil mechanics, where anisotropy is frequently encountered. Care must be taken in ensuring that the direction of anisotropy is as desired in the global co-ordinate system of a model, and not in the local co-ordinates employed in the formulation of the method.

Shape Functions

The surfaces parallel to the soil-structure boundary are defined for an 8-noded generally curved quadrilateral element or 4-noded element with linear interpolation. The numbering system employed is as shown (fig.3.2).

$$N_1(\eta,\zeta) = \frac{1}{4}(1-\eta)(1-\zeta) - \frac{1}{2}(N_8(\eta,\zeta) + N_5(\eta,\zeta)) \tag{3.7}$$

$$N_2(\eta,\zeta) = \frac{1}{4}(1+\eta)(1-\zeta) - \frac{1}{2}(N_5(\eta,\zeta) + N_6(\eta,\zeta)) \tag{3.8}$$

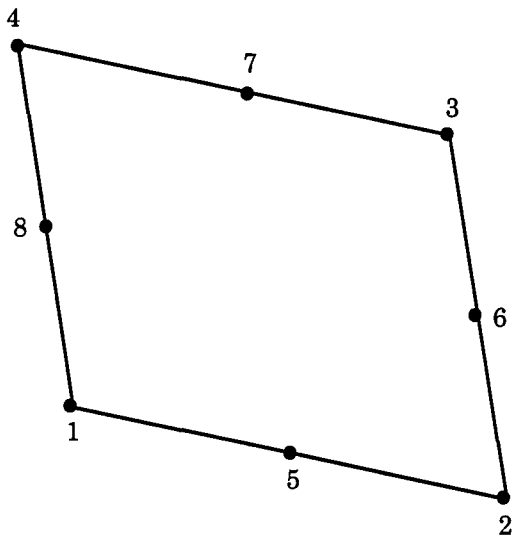

Figure 3.2: Surface Quadrilateral Element

$$N_3(\eta,\zeta) = \frac{1}{4}(1+\eta)(1+\zeta) - \frac{1}{2}(N_6(\eta,\zeta) + N_7(\eta,\zeta)) \tag{3.9}$$

$$N_4(\eta,\zeta) = \frac{1}{4}(1-\eta)(1+\zeta) - \frac{1}{2}(N_7(\eta,\zeta) + N_8(\eta,\zeta)) \tag{3.10}$$

$$N_5(\eta,\zeta) = \frac{1}{2}(1-\eta^2)(1-\zeta) \tag{3.11}$$

$$N_6(\eta,\zeta) = \frac{1}{2}(1+\eta)(1-\zeta^2) \tag{3.12}$$

$$N_7(\eta,\zeta) = \frac{1}{2}(1-\eta^2)(1+\zeta) \tag{3.13}$$

$$N_8(\eta,\zeta) = \frac{1}{2}(1-\eta)(1-\zeta^2) \tag{3.14}$$

Three Dimensional Parent Element

The three dimensional shape functions are now created by decomposing the three dimensional parent element into those components concerned with the interior boundary and those on the exterior boundary from the two dimensional parent element shape functions calculated above.

$$\left\{\hat{N}\right\} = \left\{\begin{array}{c}\left\{\hat{N}_i\right\} \\ \left\{\hat{N}_e\right\}\end{array}\right\} \tag{3.15}$$

with

$$\hat{N}_{jk} = \frac{1}{2}\left(1+\xi_j\xi\right)N_k \qquad j = i,e\ ;\ k = 1,2,\ldots \tag{3.16}$$

enforcing geometric similarity

$$\{x_e\} = (1+w)\{x_i\} \tag{3.17}$$

$$\{y_e\} = (1+w)\{y_i\} \tag{3.18}$$

$$\{z_e\} = (1+w)\{z_i\} \tag{3.19}$$

where w is the cell width (fig.3.1) or distance between the two surfaces. Therefore, the displacement at any point within the cell, can be calculated

$$x = \left\{\hat{N}\right\}^T\{\hat{x}\} = \left\{\hat{N}_i\right\}^T\{x_i\} + \left\{\hat{N}_e\right\}^T\{x_e\} \tag{3.20}$$

$$x = \{N_i\}^T\{x_i\} + \{N_e\}^T(1+w)\{x_i\} \tag{3.21}$$

$$x = \{N_i\}^T\{x_i\} + \{N_e\}^T\{x_i\} + w\{N_e\}^T\{x_i\} \tag{3.22}$$

We now substitute for the two dimensional shape functions. It is now possible to remove the subscript i as the actual application of CIFECM only uses the interior boundary as the two boundaries become coincident later when the infinitesimal limit of the cell width is performed. Thus, the exterior boundary is used only in the derivation as a convenience.

$$x = \frac{1}{2}\left(1+\xi_i\xi\right)N\{x\} + \frac{1}{2}\left(1+\xi_e\xi\right)N\{x\} + \frac{w}{2}\left(1+\xi_e\xi\right)N\{x\} \tag{3.23}$$

remembering that the local co-ordinates of the two surface elements are $\xi_i = -1$ and $\xi_e = +1$

$$\hat{x} = \left(1 + \frac{w}{2}(1+\xi)\right) \{N\}^T \{x\} \tag{3.24}$$

and similarly for the y and z directions

$$\hat{y} = \left(1 + \frac{w}{2}(1+\xi)\right) \{N\}^T \{y\} \tag{3.25}$$

$$\hat{z} = \left(1 + \frac{w}{2}(1+\xi)\right) \{N\}^T \{z\} \tag{3.26}$$

The Jacobian matrix of the Three Dimensional Finite Element

The local co-ordinate system (ξ, η, ζ) used for numerical integration is now related to the global (x, y, z) co-ordinates of the problem with the origin placed at the similarity centre (a further transformation would be required if a general similarity centre is preferred).

$$\left[\hat{J}\right] = \begin{bmatrix} \frac{\partial x}{\partial \xi} & \frac{\partial y}{\partial \xi} & \frac{\partial z}{\partial \xi} \\ \frac{\partial x}{\partial \eta} & \frac{\partial y}{\partial \eta} & \frac{\partial z}{\partial \eta} \\ \frac{\partial x}{\partial \zeta} & \frac{\partial y}{\partial \zeta} & \frac{\partial z}{\partial \zeta} \end{bmatrix} = \begin{bmatrix} \frac{w}{2} & & \\ & 1 + \frac{w}{2}(1+\xi) & \\ & & 1 + \frac{w}{2}(1+\xi) \end{bmatrix} [J] \tag{3.27}$$

Where the matrix $[J]$ is defined as

$$[J] = \begin{bmatrix} \{N\}^T \{x\} & \{N\}^T \{y\} & \{N\}^T \{z\} \\ \{N,\eta\}^T \{x\} & \{N,\eta\}^T \{y\} & \{N,\eta\}^T \{z\} \\ \{N,\zeta\}^T \{x\} & \{N,\zeta\}^T \{y\} & \{N,\zeta\}^T \{z\} \end{bmatrix} \tag{3.28}$$

The Determinant of the Jacobian Matrix

$$det\left[\hat{J}\right] = \frac{w}{2}\left(1 + \frac{w}{2}(1+\xi)\right)^2 [J] \tag{3.29}$$

with the nomenclature $det\,[J] = |J|$

The Inverse of the Jacobian Matrix

$$\left[\hat{J}\right]^{-1} = [J]^{-1} \cdot \begin{bmatrix} \frac{2}{w} & & \\ & \frac{1}{1+\frac{w}{2}(1+\xi)} & \\ & & \frac{1}{1+\frac{w}{2}(1+\xi)} \end{bmatrix} \tag{3.30}$$

The Derivatives of the Shape Functions

It is now convenient to define $[J]^{-1}$ as

$$[J]^{-1} = \begin{bmatrix} j_{11} & j_{12} & j_{13} \\ j_{21} & j_{22} & j_{23} \\ j_{31} & j_{32} & j_{33} \end{bmatrix} \tag{3.31}$$

the derivatives of the shape functions are then

$$\begin{Bmatrix} \hat{N}_{jk,\hat{x}} \\ \hat{N}_{jk,\hat{y}} \\ \hat{N}_{jk,\hat{z}} \end{Bmatrix} = \left[\hat{J}\right]^{-1} \begin{Bmatrix} \hat{N}_{jk,\xi} \\ \hat{N}_{jk,\eta} \\ \hat{N}_{jk,\zeta} \end{Bmatrix} \tag{3.32}$$

$$= \frac{\xi_i}{w} \begin{Bmatrix} j_{11} \\ j_{21} \\ j_{31} \end{Bmatrix} N_k + \frac{1+\xi_j\xi}{2\left(1+\frac{w}{2}\left(1+\xi\right)\right)} \left(\begin{Bmatrix} j_{21} \\ j_{22} \\ j_{23} \end{Bmatrix} N_{k,\eta} + \begin{Bmatrix} j_{13} \\ j_{23} \\ j_{33} \end{Bmatrix} N_{k,\zeta} \right) \tag{3.33}$$

[B1] and [B2] (3-D vector waves)

Arranging the strain vector as

$$[\varepsilon_x, \varepsilon_y, \varepsilon_z, \gamma_{yz}, \gamma_{xz}, \gamma_{xy}]^T \tag{3.34}$$

the strain-nodal displacement matrix equals

$$[B]_{jk} = \begin{bmatrix} \hat{N}_{jk,\hat{x}} & 0 & 0 \\ 0 & \hat{N}_{jk,\hat{y}} & 0 \\ 0 & 0 & \hat{N}_{jk,\hat{z}} \\ 0 & \hat{N}_{jk,\hat{z}} & \hat{N}_{jk,\hat{y}} \\ \hat{N}_{jk,\hat{z}} & 0 & \hat{N}_{jk,\hat{x}} \\ \hat{N}_{jk,\hat{y}} & \hat{N}_{jk,\hat{x}} & 0 \end{bmatrix} \tag{3.35}$$

substituting for the derivatives of the shape functions (eqn.3.33) in the above yields

$$= \frac{\xi_j}{w} \left[B^1\right]_k + \frac{1+\xi_j\xi}{2\left(1+\frac{w}{2}\left(1+\xi\right)\right)} \left[B^2\right]_k \tag{3.36}$$

where

$$[B^1]_k = \begin{bmatrix} j_{11} & 0 & 0 \\ 0 & j_{21} & 0 \\ 0 & 0 & j_{31} \\ 0 & j_{31} & j_{21} \\ j_{31} & 0 & j_{11} \\ j_{21} & j_{11} & 0 \end{bmatrix} N_k \tag{3.37}$$

$$[B^2]_k = \begin{bmatrix} j_{12} & 0 & 0 \\ 0 & j_{22} & 0 \\ 0 & 0 & j_{32} \\ 0 & j_{32} & j_{22} \\ j_{32} & 0 & j_{12} \\ j_{22} & j_{12} & 0 \end{bmatrix} N_{k,\eta} + \begin{bmatrix} j_{13} & 0 & 0 \\ 0 & j_{23} & 0 \\ 0 & 0 & j_{33} \\ 0 & j_{33} & j_{23} \\ j_{33} & 0 & j_{13} \\ j_{23} & j_{13} & 0 \end{bmatrix} N_{k,\zeta} \tag{3.38}$$

Assembling these coefficient matrices for all k nodes in the element gives the total $[B^1]$ and $[B^1]$ coefficient matrices which are independent of the radial direction. The full strain-displacement matrix, including the radial direction, is determined using decomposition with respect to the interior and external boundaries

$$[B] = [[B_i]\,[B_e]] \tag{3.39}$$

with

$$[B]_j = \frac{\xi_j}{w}[B^1] + \frac{1+\xi_j\xi}{2\left(1+\frac{w}{2}(1+\xi)\right)}[B^2] \quad (j = i, e) \tag{3.40}$$

Element Static Stiffness Matrix

The static stiffness of a three dimensional finite element is defined as

$$[K] = \int_V [B]^T [D]\,[B]\,dV \tag{3.41}$$

with integration over the volume V, to be performed numerically and the elastic constitutive relationship (fig.3.5). Constructing the static stiffness matrix of the finite element cell, with decomposition with respect to the interior and exterior boundaries

$$[K]_{j,l} = \int_V [B]_j^T [D]\,[B]_l\,dV = \int_{-1}^{+1}\int_{-1}^{+1}\int_{-1}^{+1} [B]_j^T [D]\,[B]_l \left|\hat{J}\right| d\xi d\eta d\zeta \tag{3.42}$$

substituting (eqn.3.40) and (eqn.3.29) into (eqn.3.42) gives a polynomial in ξ which can be integrated analytically. Decomposing with respect to the dimensionless cell width w

$$[K]_{jl} = \frac{1}{w}[K^0]_{jl} + [K^1]_{jl} + w[K^2]_{jl} \tag{3.43}$$

where

$$[K^0]_{jl} = \xi_j \xi_l [E^0] \tag{3.44}$$

$$[K^1]_{jl} = \xi_j \xi_l [E^0] + \frac{\xi_l}{2}[E^1] + \frac{\xi_j}{2}[E^1]^T \tag{3.45}$$

$$[K^2]_{jl} = \frac{\xi_j \xi_l}{3}[E^0] + \left(\frac{\xi_l}{4} + \frac{\xi_j \xi_l}{12}\right)[E^1] + \left(\frac{\xi_j}{4} + \frac{\xi_j \xi_l}{12}\right)[E^1]^T + \left(\frac{1}{4} + \frac{\xi_j \xi_l}{12}\right)[E^2] \tag{3.46}$$

$$[E^0] = \int_{-1}^{+1}\int_{-1}^{+1}[B^1]^T [D][B^1]|J|\, d\eta d\zeta \tag{3.47}$$

$$[E^1] = \int_{-1}^{+1}\int_{-1}^{+1}[B^2]^T [D][B^1]|J|\, d\eta d\zeta \tag{3.48}$$

$$[E^2] = \int_{-1}^{+1}\int_{-1}^{+1}[B^2]^T [D][B^2]|J|\, d\eta d\zeta \tag{3.49}$$

with the coefficient matrices in (eqn.3.47),(eqn.3.48),(eqn.3.49), are determined by numerical integration and are dependant upon the discretisation of the soil-structure interface.

Element Mass Matrix

The mass matrix of a general three dimensional finite element is

$$[M] = \int_V \rho \left[\hat{N}\right]^T \left[\hat{N}\right] dV \tag{3.50}$$

Constructing the mass matrix of the finite element cell, with decomposition with respect to the interior and exterior boundaries, using the nomenclature (j=i,e; l=i,e)

$$[M]_{jl} = \int_V \rho \left[\hat{N}\right]_j^T \left[\hat{N}\right]_l dV = \int_{-1}^{+1}\int_{-1}^{+1}\int_{-1}^{+1} \rho \left[\hat{N}\right]_j^T \left[\hat{N}\right]_l \left|\hat{J}\right| d\xi d\eta d\zeta \tag{3.51}$$

where

$$\left[\hat{N}\right]_j = \frac{1}{2}\left(1 + \xi_j \xi\right)[N] \quad (j = i, e) \tag{3.52}$$

Substituting in the determinant of the jacobian matrix (eqn.3.29) in (eqn.3.51). Integration in the radial direction is performed analytically, and, neglecting terms in w higher than 1 (which become negligible upon performing the limit of the cell width $w \rightarrow 0$)

$$[M]_{jl} = w\left[M^2\right]_{jl} + O\left(w^2\right) = \frac{w}{4}\left(1 + \frac{\xi_j \xi_l}{3}\right)\left[M^0\right] + O\left(w^2\right) \tag{3.53}$$

with the positive definite coefficient matrix

$$\left[M^0\right] = \int_{-1}^{+1}\int_{-1}^{+1} \rho [N]^T [N] |J| \, d\eta d\zeta \tag{3.54}$$

Supplementary Relationships

Supplementary relationships from (eqns.3.47,3.48 and 3.49) are given here for use later in the derivation of the Consistent Infinitesimal Finite Element Cell equation in the frequency domain

$$\left[K_{ii}^0\right] = -\left[K_{ie}^0\right] = -\left[K_{ei}^0\right] = \left[K_{ee}^0\right] = \left[E^0\right] \tag{3.55}$$

$$\left[K_{ie}^1\right] + \left[K_{ee}^1\right] = -\left(\left[K_{ii}^1\right] + \left[K_{ie}^1\right]\right)^T = \left[E^1\right] \tag{3.56}$$

$$\left[K_{ii}^2\right] + \left[K_{ie}^2\right] + \left[K_{ei}^2\right] + \left[K_{ee}^2\right] = \left[E^2\right] \tag{3.57}$$

$$\left[M_{ii}^2\right] + \left[M_{ie}^2\right] + \left[M_{ei}^2\right] + \left[M_{ee}^2\right] = \left[M^0\right] \tag{3.58}$$

3.3 Assemblage of the Finite Element Cell and Unbounded Media

The assemblage of the finite element cell and the unbounded media is carried out in the frequency domain. The force-displacement relationship of the **finite element cell** is formulated as

$$[S(\omega)]\{d(\omega)\} = \{P(\omega)\} \tag{3.59}$$

where the dynamic stiffness for the bounded finite element cell $[S(\omega)]$ is defined as

$$[S(\omega)] = [K] - \omega^2 [M] \tag{3.60}$$

with the static stiffness of cell $[K]$ and the mass matrix of cell $[M]$. The force displacement relationship of the finite element cell can be rewritten in terms of the interior and exterior boundary nodes

$$\begin{bmatrix} [S_{ii}(\omega)] & [S_{ie}(\omega)] \\ [S_{ei}(\omega)] & [S_{ee}(\omega)] \end{bmatrix} \begin{Bmatrix} \{d_i(\omega)\} \\ \{d_e(\omega)\} \end{Bmatrix} = \begin{Bmatrix} \{P_i(\omega)\} \\ \{P_e(\omega)\} \end{Bmatrix} \tag{3.61}$$

The force-displacement relationships at the interior boundary of the unbounded medium is now formulated

$$\{R_i(\omega)\} = [S_i^{\infty}(\omega)]\{d_i(\omega)\} \tag{3.62}$$

and similarly at the exterior boundary exterior

$$\{R_e(\omega)\} = [S_e^{\infty}(\omega)]\{d_e(\omega)\} \tag{3.63}$$

To ensure compatibility, the correct displacement amplitudes at the respective boundaries are used. Note the dynamic stiffnesses act directly upon their corresponding frequency dependant displacements, i.e. no cross coupling as required for the cell (eqn.3.61). Stating equilibrium at both the interior and exterior boundaries

$$[P_i(\omega)] = [R_i(\omega)] \tag{3.64}$$

$$[P_e(\omega)] = -[R_e(\omega)] \tag{3.65}$$

on substituting into these equilibrium equations the force-displacement relationships, of the cell (eqn.3.61) and the unbounded medium (eqn.3.64) (eqn.3.65) gives

$$\begin{bmatrix} [S_{ii}(\omega)] & [S_{ie}(\omega)] \\ [S_{ei}(\omega)] & [S_{ee}(\omega)] \end{bmatrix} \begin{Bmatrix} \{d_i(\omega)\} \\ \{d_e(\omega)\} \end{Bmatrix} = \begin{bmatrix} [S_i^{\infty}(\omega)] & \\ & -[S_e^{\infty}(\omega)] \end{bmatrix} \begin{Bmatrix} \{d_i(\omega)\} \\ \{d_e(\omega)\} \end{Bmatrix} \tag{3.66}$$

The similarity relationship is obtained by eliminating $\{d_e(\omega)\}$ from the above equation. Restating (eqn.3.61) into its upper and lower components

$$[S_{ii}(\omega)]\{d_i(\omega)\} + [S_{ie}(\omega)]\{d_e(\omega)\} = [S_i^{\infty}(\omega)]\{d_i(\omega)\} \tag{3.67}$$

$$[S_{ei}(\omega)]\{d_i(\omega)\} + [S_{ee}(\omega)]\{d_e(\omega)\} = -[S_e^{\infty}(\omega)]\{d_e(\omega)\} \tag{3.68}$$

rearranging the upper component (eqn.3.67)

$$([S_i^{\infty}(\omega)] - [S_{ii}(\omega)])\{d_i(\omega)\} = [S_{ie}(\omega)]\{d_e(\omega)\} \tag{3.69}$$

and similarly the lower component (eqn.3.68)

$$-([S_e^{\infty}(\omega)] + [S_{ee}(\omega)])\{d_e(\omega)\} = [S_{ei}(\omega)]\{d_i(\omega)\} \tag{3.70}$$

and now solving in terms of $\{d_e(\omega)\}$

$$\{d_e(\omega)\} = -([S_e^{\infty}(\omega)] + [S_{ee}(\omega)])^{-1}[S_{ei}(\omega)]\{d_i(\omega)\} \tag{3.71}$$

substituting for $\{d_e(\omega)\}$ back into (eqn.3.67)

$$\left([S_i^{\infty}(\omega)] - [S_{ii}(\omega)] + [S_{ie}(\omega)]([S_e^{\infty}(\omega)] + [S_{ee}(\omega)])^{-1}[S_{ei}(\omega)]\right)\{d_i(\omega)\} = 0 \tag{3.72}$$

the above equation can be satisfied for any (arbitrary) $[d_i(\omega)]$, therefore

$$\left([S_i^{\infty}(\omega)] - [S_{ii}(\omega)] + [S_{ie}(\omega)]([S_e^{\infty}(\omega)] + [S_{ee}(\omega)])^{-1}[S_{ei}(\omega)]\right) = 0 \tag{3.73}$$

and thus

$$[S_i^{\infty}(\omega)] = [S_{ii}(\omega)] - [S_{ie}(\omega)]\left([S_e^{\infty}(\omega)] + [S_{ee}(\omega)]\right)^{-1}[S_{ei}(\omega)] \tag{3.74}$$

3.4 Similarity

Wolf and Song show how the relationship between the unit-impulse response matrices is derived using dimensional analysis, investigating the dependance of the unit impulse response matrix and the dynamic stiffness matrix on the characteristic length r, which is related to the cell width.

Poisson's ratio	ν	dimensionless
characteristic length(radial distance)	r	$[L]$
shear modulus	G	$[L]^{-1}[M][T]^{-2}$
mass density	ρ	$[M][L]^{-3}$
frequency of excitation	ω	$[T]^{-1}$

The product of dynamic stiffness and all of it's dependant variables must be dimensionless

$$[S^{\infty}]^{n_1}[r]^{n_2}[G]^{n_3}[\rho]^{n_4}[\omega]^{n_5} = [L]^{(s-3)n_1+n_2-n_3-3n_4}[M]^{n_1+n_3+n_4}[T]^{-2n_1-2n_3-n_5} \tag{3.75}$$

leading to

$$(s-3)n_1 + n_2 - n_3 - 3n_4 = 0 \tag{3.76}$$

$$n_1 + n_3 + n_4 = 0 \tag{3.77}$$

$$-(2n_1 + 2n_3 + n_5) = 0 \tag{3.78}$$

This yields 3 equations with 5 unknowns, however we may choose values for the two unknowns arbitrarily $n_1 = 1$; $n_5 = 0$. Substituting these values into (eqn.3.76), (eqn.3.77) and (eqn.3.78)

$$(s-3) + n_2 - n_3 - 3n_4 = 0 \tag{3.79}$$

$$1 + n_3 + n_4 = 0 \tag{3.80}$$

$$-2 - 2n_3 - 0 = 0 \tag{3.81}$$

from equation (eqn.3.81) we get

$$n_3 = -1 \tag{3.82}$$

substituting for n_3 in equation (eqn.3.80)

$$n_4 = 0 \tag{3.83}$$

now substituting these two results into equation (eqn.3.79), yields

$$n_2 = 2 - s \tag{3.84}$$

finally putting the results from (eqn.3.82),(eqn.3.83),(eqn.3.84) along with the original assumed values (eqn.3.4) into (eqn.3.75), gives the first dimensionless variable

$$[S^{\infty}]\, r^{2-s} G^{-1} = 0 \tag{3.85}$$

The second dimensionless variable is derived in the same manner, choosing another 2 arbitrary constants

$$n_1 = 0 \;\; ; \;\; n_5 = 1 \tag{3.86}$$

again, substituting these values into equations (eqn.3.76), (eqn.3.77) and (eqn.3.78)

$$n_2 - n_3 - 3n_4 = 0 \tag{3.87}$$

$$n_3 + n_4 = 0 \tag{3.88}$$

$$-2n_3 - 1 = 0 \tag{3.89}$$

from (eqn.3.89) $n_3 = -0.5$, substituting for n_3 in (eqn.3.88) $n_4 = 0.5$ and substituting both results into (eqn.3.87) gives $n_2 = 1$, which by substituting back into equation (eqn.3.75) again, yields the second dimensionless variable

$$rG^{-0.5}\rho^{0.5} \tag{3.90}$$

This second dimensionless variable is called the dimensionless frequency

$$a_0 = \omega r\sqrt{\frac{\rho}{G}} = \frac{\omega r}{c_s} \quad where\ c_s = \sqrt{\frac{G}{\rho}} \tag{3.91}$$

The first dimensionless variable will be a function $\left[\bar{S}^{\infty}\right]$, of the second

$$\left[S^{\infty}(r,\omega)\right] = Gr^{s-2}\left[\bar{S}^{\infty}(a_0)\right] \tag{3.92}$$

Relationship Between the Dynamic Stiffness Matrices of Similar Structure Interfaces

The derivative of the dimensionless frequency dynamic-stiffness matrix with respect to the dimensionless frequency may be performed by variation in either the radial distance r or the actual frequency ω, whilst the other remains constant, yielding

$$\left[\bar{S}^{\infty}(a_0)\right]_{,a_0} = \frac{c_s}{\omega}\left[\bar{S}^{\infty}(a_0)\right]_{,r} \tag{3.93}$$

$$\left[\bar{S}^{\infty}(a_0)\right]_{,a_0} = \frac{c_s}{r}\left[\bar{S}^{\infty}(a_0)\right]_{,\omega} \tag{3.94}$$

Setting the right hand sides of equation (eqn.3.93) equal

$$r\left[\bar{S}^{\infty}(a_0)\right]_{,r} = \omega\left[\bar{S}^{\infty}(a_0)\right]_{,\omega} \tag{3.95}$$

Now, the partial derivatives with respect to r and ω can be performed

$$\left[\bar{S}^{\infty}(a_0)\right]_{,r} = \frac{1}{Gr^{s-2}}\left(-\frac{s-2}{r}\left[S^{\infty}(r,\omega)\right] + \left[\bar{S}^{\infty}(r,\omega)\right]_{,r}\right) \tag{3.96}$$

$$r\left[S^{\infty}(a_0)\right]_{,\omega} = \frac{1}{Gr^{s-2}}\left[S^{\infty}(r,\omega)\right] \tag{3.97}$$

substituting (eqn.3.96) and (eqn.3.97) into (eqn.3.95)

$$r\left[S^{\infty}(r,\omega)\right]_{,r} = (s-2)\left[S^{\infty}(r,\omega)\right] + \omega\left[S^{\infty}(r,\omega)\right]_{,\omega} \tag{3.98}$$

$\left[S^{\infty}(r,\omega)\right]_{,\omega}$ in above equation becomes $\left[S^{\infty}(\omega)\right]_{,\omega}$ when a specific soil-structure interface is addressed. This is because characteristic length is fixed, thus only the frequency ω is variable.

3.5 The Consistent Infinitesimal Finite Element Cell Equation in the Frequency Domain

The dynamic stiffness matrices similarity relationship (eqn.3.98) and the relationship based on assemblage (eqn.3.74) are now used to derive the Consistent Infinitesimal Finite Element Cell Equation in the frequency domain. Reformulating (eqn.3.74)

$$\left(\left[S_e^{\infty}(\omega)\right] + \left[S_{ee}^{\infty}(\omega)\right]\right)\left[S_{ie}(\omega)\right]^{-1}\left(\left[S_i^{\infty}(\omega)\right] - \left[S_{ii}^{\infty}(\omega)\right]\right) + \left[S_{ei}^{\infty}(\omega)\right] = 0 \tag{3.99}$$

and invoking the definition of the dynamic-stiffness matrix

$$\left[S(\omega)\right] = [K] - \omega^2[M] \tag{3.100}$$

each of the submatrices in (eqn.3.99) can be formulated using $[K]$ specified in (eqn.3.43) and $[M]$ from (eqn.3.53)

$$\left[S_{ii}(\omega)\right] = \frac{1}{w}\left[K_{ii}^0\right] + \left[K_{ii}^1\right] + w\left[K_{ii}^2\right] - w\omega^2\left[M_{ii}^2\right] + O\left(w^2\right) \tag{3.101}$$

with $\left[K_{ii}^0\right]$ substituted by $[E]^0$ from the first supplementary relationship (eqn.3.55)

$$\left[S_{ii}(\omega)\right] = \frac{1}{w}\left[E^0\right] + \left[K_{ii}^1\right] + w\left(\left[K_{ii}^2\right] - \omega^2\left[M_{ii}^2\right]\right) + O\left(w^2\right) \tag{3.102}$$

and analogously the remaining submatrices are formulated using the supplementary relationships (eqn.3.55), (eqn.3.56) and (eqn.3.57)

$$\left[S_{ie}(\omega)\right] = -\frac{1}{w}\left[E^0\right] + \left[K_{ie}^1\right] + w\left(\left[K_{ie}^2\right] - \omega^2\left[M_{ie}^2\right]\right) + O\left(w^2\right) \tag{3.103}$$

$$[S_{ei}(\omega)] = -\frac{1}{w}[E^0] + [K^1_{ei}] + w\left([K^2_{ei}] - \omega^2[M^2_{ei}]\right) + O(w^2) \tag{3.104}$$

$$[S_{ee}(\omega)] = \frac{1}{w}[E^0] + [K^1_{ee}] + w\left([K^2_{ee}] - \omega^2[M^2_{ee}]\right) + O(w^2) \tag{3.105}$$

The inverse term in (eqn.3.99) can now be equated to the inverse of (eqn.3.103), and is expressed now as a polynomial in w, with the as yet unknown coefficient matrices $[A]$, $[B]$ and $[C]$

$$[S_{ie}(\omega)]^{-1} = -w[A]^{-1} + w^2[B] + w^3[C] + O(w^2) \tag{3.106}$$

From (eq,3.103), the coefficient matrix $[A]$ is the inverse of $[E^0]$. $[B]$ and $[C]$ are determined from

$$[I] = [S_{ie}][S_{ie}]^{-1} \tag{3.107}$$

On substituting for $[S_{ie}]$ from (eqn.3.103) and $[S_{ie}]^{-1}$ from (eqn.3.106) and setting the coefficient matrices in term of w and w^2 to zero gives

$$[A] = [E^0]$$

$$[B] = -[E^0]^{-1}[K^{-1}_{ie}][E^0]^{-1}$$

$$[C] = -[E^0]^{-1}\left([K^1_{ie}][E^0]^{-1}[K^1_{ie}] - \left([K^2_{ie}] - \omega^2[M^2_{ie}]\right)\right)[E^0]^{-1} \tag{3.108}$$

All of the terms in (eqn.3.99) in terms of the bounded cell are now known, so substituting for $[S_{ii}(\omega)]$ from (eqn.3.102), $[S_{ei}(\omega)]$ from (eqn.3.104), $[S_{ee}(\omega)]$ from (eqn.3.105) and $[S_{ie}(\omega)]^{-1}$ from (eqn.3.106), along with the coefficient matrices $[A]$, $[B]$ and $[C]$ (eqn.3.108) yields

$$\underbrace{[K^1_{ii}] + [K^1_{ie}] + [K^1_{ei}] + [K^1_{ee}]}_{1}$$

$$-w\underbrace{\left(\left[S_e^{\infty}(\omega)\right]+\left[K_{ie}^{1}\right]+\left[K_{ee}^{1}\right]\right)\left[E^{0}\right]^{-1}\left(\left[S_i^{\infty}(\omega)\right]-\left[K_{ii}^{1}\right]-\left[K_{ie}^{1}\right]\right)}_{2}$$

$$+\underbrace{\left[S_e^{\infty}(\omega)\right]-\left[S_i^{\infty}(\omega)\right]}_{3}$$

$$+w\underbrace{\left[K_{ii}^{2}\right]+\left[K_{ie}^{2}\right]+\left[K_{ei}^{2}\right]+\left[K_{ee}^{2}\right]}_{4}$$

$$+w^{2}\underbrace{\left[M_{ii}^{2}\right]+\left[M_{ie}^{2}\right]+\left[M_{ei}^{2}\right]+\left[M_{ee}^{2}\right]}_{4}=O\left(\omega^{2}\right) \tag{3.109}$$

In the above equation term (1) vanishes from consideration of equilibrium. (eqn.3.56) is substituted into (2), terms (4) and (5) are transformed by (eqn.3.57) and (eqn.3.58) and dividing (eqn.3.109) by w gives

$$\left(\left[S_e^{\infty}(\omega)\right]+\left[E^{1}\right]\right)\left[E^{0}\right]^{-1}\left(\left[S_i^{\infty}(\omega)\right]+\left[E^{1}\right]^{T}\right)$$

$$\frac{\left[S_e^{\infty}(\omega)\right]-\left[S_i^{\infty}(\omega)\right]}{w}-\left[E^{2}\right]+\omega^{2}\left[M^{0}\right]=O(w) \tag{3.110}$$

The limit of the cell width w tending towards zero can now be made

$$\lim_{w\to 0}\frac{\left[S_e^{\infty}(\omega)\right]-\left[S_i^{\infty}(\omega)\right]}{w}=\lim_{w\to 0}\frac{\left[S_e^{\infty}(\omega)\right]-\left[S_i^{\infty}(\omega)\right]}{r_e-r_i}$$

$$=r\left[S^{\infty}(\omega)\right]_{,r} \tag{3.111}$$

$$\left(\left[S^{\infty}(\omega)\right]+\left[E^{1}\right]\right)\left[E^{0}\right]^{-1}\left(\left[S^{\infty}(\omega)\right]+\left[E^{1}\right]^{T}\right)-r\left[S^{\infty}(\omega)\right]_{,r}-\left[E^{2}\right]+\omega^{2}\left[M^{0}\right]=O(w) \tag{3.112}$$

finally substituting for the similarity relationship (eqn.3.98), we arrive at The Consistent Infinitesimal Finite Element Cell Equation in the Frequency Domain

$$\left([S^{\infty}(\omega)]+[E^1]\right)[E^0]^{-1}\left([S^{\infty}(\omega)]+[E^1]^T\right)$$

$$-(s-2)[S^{\infty}(\omega)]-\omega[S^{\infty}(\omega)]_{,\omega}-[E^2]+\omega^2[M^0]=0 \tag{3.113}$$

This is a system of non-linear, first order differential equations in ω.

3.6 The Consistent Infinitesimal Finite Element Cell Equation in the Time Domain

In the time domain the consistent infinitesimal finite element cell method is constructed in terms of the unit-impulse response to acceleration. To derive the consistent infinitesimal finite element cell equation in the time domain the corresponding equation in the frequency domain is reformulated in terms of the dynamic-stiffness to acceleration using the relationship in (eqn.3.4) and dividing (eqn.3.113) by $(i\omega)^4$

$$[M^{\infty}(\omega)][E^0]^{-1}[M^{\infty}(\omega)]+[E^1][E^0]^{-1}\frac{[M^{\infty}(\omega)]}{(i\omega)^2}+[E^0]^{-1}[E^1]^T-$$

$$s\frac{[M^{\infty}(\omega)]}{(i\omega)^2}+\frac{1}{\omega}[M^{\infty}(\omega)]_{,\omega}-\frac{1}{(i\omega)^4}\left([E^2]-[E^1][E^0]^T\right)-\frac{1}{(i\omega)^2}[M^0]=0 \tag{3.114}$$

applying the inverse Fourier transform

$$\int_0^t[M^{\infty}(t-\tau)][E^0]^{-1}[M^{\infty}(\tau)]\,d\tau+\left([E^1][E^0]^{-1}-\frac{s+1}{2}\right)\int_0^t\int_0^{\tau}[M^{\infty}(\tau')]\,d\tau'd\tau$$

$$+\int_0^t\int_0^{\tau}[M^{\infty}(\tau')]\,d\tau'd\tau\left([E^0]^{-1}[E^1]^T-\frac{s+1}{2}\right)+t\int_0^t[M^{\infty}(\tau)]\,d\tau$$

$$-\frac{t^3}{6}\left([E^2]-[E^1][E^0]^{-1}[E^1]^T\right)H(t)-t[M^0]H(t)=0 \tag{3.115}$$

this transform is performed using the relationship

$$F^{-1}\left\langle\frac{1}{\omega}[M^{\infty}(\omega)]_{,\omega}\right\rangle=\int_0^t\tau[M^{\infty}(\tau)]\,d\tau=t\int_0^t[M^{\infty}(\tau)]\,d\tau-\int_0^t\int_0^{\tau}[M^{\infty}(\tau')]\,d\tau'd\tau \tag{3.116}$$

Equation (eqn.3.115) can be expressed in a more concise manner by decomposing

$[E^0]$, which is positive definite, by Cholesky's method as

$$[E^0] = [U]^T [U] \tag{3.117}$$

where $[U]$ is an upper triangular matrix. Substituting (eqn.3.117) in (eqn.3.115), which is premultiplied by $\left([U]^{-1}\right)^T$,and postmultiplied by $[U]^{-1}$. Giving the consistent infinitesimal finite element cell equation in the time domain

$$\int_0^t [m^\infty (t-\tau)]\,[m^\infty (\tau)]\,d\tau + [e^1] \int_0^t \int_0^\tau [m^\infty (\tau')]\,d\tau' d\tau + \int_0^t \int_0^\tau [m^\infty (\tau')]\,d\tau' d\tau\,[e^1]^T$$

$$+t \int_0^t [m^\infty (\tau)]\,d\tau - \frac{t^3}{6}[e^2]\,H(t) - t\,[m^0]\,H(t) = 0 \tag{3.118}$$

with the coefficient matrices

$$[e^1] = \left([U]^{-1}\right)^T [E^1]\,[U]^{-1} - \frac{s+1}{2}[I] \tag{3.119}$$

$$[e^2] = \left([U]^{-1}\right)^T \left([E^2] - [E^1]\,[E^0]^{-1}\,[E^1]^T\right)[U]^{-1} \tag{3.120}$$

$$[m^0] = \left([U]^{-1}\right)^T [M^0]\,[U]^{-1} \tag{3.121}$$

and

$$[m^\infty (t)] = \left([U]^{-1}\right)^T [M^\infty (t)]\,[U]^{-1} \tag{3.122}$$

3.7 Time Discretisation

Equation (eqn.3.118) is discretised with respect to time, giving an equation for the acceleration unit-impulse response matrix at each discrete time station n. The integral terms in (eqn.3.118) are discretised as

$$[I]_n = \int_0^{n\Delta t} [m^\infty (\tau)]\,d\tau = [I]_{n-1} + \Delta t\,[m^\infty]_n \tag{3.123}$$

$$[J]_n = \int_0^{n\Delta t} \int_0^\tau [m^\infty (\tau')]\,d\tau' d\tau = [J]_{n-1} + \Delta t\,[I]_{n-1} + \frac{\Delta t^2}{2}[m^\infty]_n \tag{3.124}$$

$$\int_0^t [m^\infty(t-\tau)]\,[m^\infty(\tau)]\,d\tau = \Delta t \sum_{j=1}^{n} [m^\infty]_{n-j+1}\,[m^\infty]_j \tag{3.125}$$

3.7.1 1st Time Step

The convolution term leads to a quadratic equation in the unknown matrix for the first time step. Substituting equations (eqn.3.123), (eqn.3.124) and (eqn.3.125) with n=1 in (eqn.3.118) yields

$$[m^\infty]_1^2 + \frac{\Delta t}{2}\left([e^1] + [I]\right)[m^\infty]_1 + [m^\infty]_1 \frac{\Delta t}{2}\left([e^1]^T + [I]\right) - \frac{\Delta t^2}{6}[e^2] - [m^0] = 0 \tag{3.126}$$

This is in the form of the algebraic **Riccati** equation. Details on the numerical solution of this equation is briefly described by Wolf and Song [59] from a method described by Laub [28].

3.7.2 nth Time Step

The convolution integral term in (eqn.3.118) results in linear terms for the unknown matrix for all but the first time step. Discretising (eqn.3.118) for the nth time step

$$\begin{aligned}\left([m^\infty]_1 + \frac{\Delta t}{2}[e^1]\right)[m^\infty]_n + [m^\infty]_n\left([m^\infty]_1 + \frac{\Delta t}{2}[e^1]\right) + t\,[m^\infty]_n = \\ -\sum_{j=2}^{n-1}[m^\infty]_{n-j+1}\,[m^\infty]_j - [e^1]\left(\frac{[J]_{n-1}}{\Delta t} + [I]_{n-1}\right) \\ -\left(\frac{[J]_{n-1}}{\Delta t} + [I]_{n-1}\right)[e^1]^T + \frac{t^3}{6\Delta t}[e^2] + \frac{t}{\Delta t}\left([m^0] - [I]_{n-1}\right)\end{aligned} \tag{3.127}$$

this is in the form of the **Lyapunov** equation, a technique for the matrix solution of this equation can be found in [4].

3.8 Closure

The solution of the Riccati and Lyapunov equations is beyond the scope of this work, and have been treated here as relative black box routines. The Lyapunov equation is solved dependant upon the previous steps, thus to solve the n^{th} equation

all previous solutions must have been found.

Following the solution of the Riccati and Lyapunov equations in terms of $[m^{\infty}(t)]$ the unit-impulse response matrices to acceleration can be calculated from (eqn.3.118) by

$$[M^{\infty}(t)] = [U]^T [m^{\infty}(t)] [U] \tag{3.128}$$

The implementation of the interaction force-acceleration relationship within the dynamic force equilibrium equation is discussed in the following chapter for both directly applied loading and transmitted loading.

Chapter 4

Non-Linear Dynamic Framework

4.1 Introduction

This chapter describes the FE code into which the CIFECM is introduced[1]. The dynamic time integration scheme and non-linear material model (subsequently used in chapter 5) are outlined. The dynamic equation of force equilibrium for directly applied loading and transmitted loads are given.

4.2 The Implicit Code *ya*FE*c*

The implicit non-linear dynamic Finite Element code *ya*FE*c*[2] was created by Crouch in 1998 [15] and subsequently modified by him and fellow researchers working in the Computational Mechanics Unit within the Department of Civil and Structural Engineering at Sheffield University.

The code was developed using many of the Fortran 90 FE library routines published by Smith and Griffiths [46]. It is able to handle large 3-D non-linear dynamic structural analysis problems in the time-domain. A FORTRAN 77 version of the Smith and Griffiths (SG) FE library was first released in 1982. This very useful set of routines enabled an FE developer to rapidly assemble a programme which could be tailored to specific needs. Fifty-six complete FE programmes appeared in the book. This modular approach is highly attractive and the SG routines did much to spread the wider user of FE analysis (particularly in the field of geomechanics). In 1998 the new (3^{rd} edition) Fortran 90 version of the routines

[1]The text describing *ya*FE*c* represents a synthesis of internal notes and ideas produced by fellow workers in the Computational Mechanics Unit at Sheffield University)

[2]*y* et *a* nother *F* inite *E* lement *c* ode

appeared. Several addition capabilities were included (for example, an iterative solver). While many other numerical libraries exist which are of real value to the FE developer (LINPACK, EISPACK, BLAS, NAG and Numerical Recipes) as well as public domain FE codes (for example DLEARN [23] and FEAP [61], it appears that it is only the SG library which offers Fortran 90 routines (including 3-D capabilities), written in a clear, compact way. The codes are not only useful for researchers but they also provide an excellent basis for understanding the Finite Element method and learning to programme.

Specific features of *ya*FE*c* which extend the work of Smith and Griffiths include

(*i*) use of the Hilber-Hughes-Taylor time stepping scheme to suppress amplification of the high frequency response

(*ii*) use of *consistent lumped* or standard consistent mass matrices

(*iii*) use of inclined boundary conditions

(*iv*) use of an advanced non-symmetric element-by-element iterative solver to enable large FE problems to be tackled without imposing excessive restrictions on the computer memory required

(*v*) choice of two advanced non-linear constitutive models for concrete [40] and [53]. The elasto-plastic material model offers a rigorous closest point projection to return the trial stress onto the yield surface and a consistent tangent modulus to speed-up convergence.

(*vi*) ability to introduce a strain-rate dependency on the material response [33]

(*vii*) use of a smeared membrane approach to represent the reinforcing steel in concrete. This technique enables a layer of stiffer material to be embedded at any location within the element (normal to the local co-ordinate directions), providing it with uniaxial properties in any direction within that membrane

(*viii*) ability to model dynamic (compressible) fluid-structure interaction [60]

(*ix*) ability to report on the evolution of the acoustic tensor as a means of identifying localisation in concrete

(*x*) ability to transfer nodal pressures on element faces to consistent nodal forces and apply gravity body forces

(*xi*) incorporation of a transparent non-linear solution technique based on the Newton-Raphson procedure

(*xii*) ability to extrapolate and smooth Gauss point data (for example, stresses and strains) to nodes to enable 3D post-processing contour plots to be drawn and error estimation to be performed. The routines also enable determination of the principal values of second-order tensor quantities.

4.2.1 HHT Time Integration Scheme

As noted in the introductory chapter, a time domain approach is required when dealing with non-linear dynamic problems. In direct time integration methods, a finite difference approximation is used to replace the time derivatives $\{\ddot{d}\}$ and $\{\dot{d}\}$. This procedure forms a relationship between the three unknown updated vectors $\{\ddot{d}\}$, $\{\dot{d}\}$ and $\{d\}$. Both linear and non-linear dynamic problems can be treated in the same manner using a time domain approach. The only difference being that an iterative non-linear solution strategy is required to be nested within an implicit time-stepping scheme when solving non-linear problems.

The dynamic equation of motion

$$\overbrace{[M]\{\ddot{d}\}}^{\text{inertial forces}} + \overbrace{[C]\{\dot{d}\}}^{\text{damping forces}} + \overbrace{[K]\{d\}}^{\text{internal (\textit{stiffness}) forces}} = \underbrace{\{f(t)\}}_{\text{applied loads}} \tag{4.1}$$

can be re-expressed in terms of the updated values based on an assumption of how the response varies within a time-step. At a selected time instance, if the solution is based on the previous time t, the method is classed as an *explicit* method. If it is based on the new time $t + \Delta t$, the method is known as an *implicit* method.

Explicit schemes compute the nodal accelerations, velocities and displacements at the new time step, based on their values at previous time steps. This follows because the solution at the new time step is given from the equilibrium conditions at the previous time step. The matrix operations required during one time step are minimal in the explicit method if the structural mass and damping matrices are diagonal. In these cases a computationally expensive linear solver (of the form $[K^*]\{\delta d\} = \{\delta f^*\}$) is not required. However, the explicit scheme remains conditionally stable. This stability is dependent upon the size of the time-step used. If a too large time-step is employed the process will *blow-up* numerically, leading to meaningless results. The critical time step size depends on the particular form of the explicit algorithm and the stiffness of the stiffest finite elements used in the mesh. This will impose a severe computational penalty on the analysis if a long duration dynamic analysis is to be performed as a very large number of

time steps will be required. If the dynamic problem involves a very short duration excitation and response, then this method is highly efficient. A number of widely used commercial FE codes (for example DYNA and ABAQUS-EXPLICIT) operate with an explicit time stepping scheme. The most commonly used algorithm is the central difference approach.

Implicit methods compute the nodal accelerations, velocities and displacements at each new step based on satisfying equilibrium at the new time step. Use of a linear equation solver is *always* required in implicit schemes. However, implicit methods can be unconditionally stable (for linear systems). This implies that large time-step sizes may be used. It is relevant to note that while stability may be met, accuracy could still be poor. Therefore, the user should select the time step size to ensure that the characteristics of the external excitation and structural motion are captured properly. Many implicit schemes have been developed over the last 35 years. These include the Wilson θ [55], Newmark [36], Hilber-Hughes-Taylor [20] and the second and third order ZWTH algorithms [21].

The following notes describe the attractive Hilber-Hughes-Taylor scheme. The HHT algorithm offers a family of unconditionally stable one step methods. It has been recognised that in many structural dynamic applications only the lower frequency responses are of interest. In these cases, it is often advantageous for the time stepping algorithm to possess some form of numerical dissipation to damp out participation of the higher modes. Hilber *et al* [20] and Hughes [23] noted that numerical damping cannot be introduced into the familiar Newmark algorithm without degrading the order of accuracy. The HHT algorithm was specially developed to address this difficulty. It is widely known that the Newmark method allows the amount of numerical dissipation to be controlled by the parameters β and γ. However, the dissipation achievable with this scheme is considered to be inferior to both the Houbolt and Wilson methods since the lower structural modes are affected too strongly. The HHT method provides a new family of approaches which can give a more accurate simulation of the lower modes while damping out the unwanted higher frequency response.

Consider the standard equation of dynamic equilibrium at time $t + \Delta t$ for a linear system

$$[M]\{^{t+\Delta t}\ddot{d}\} + [C]\{^{t+\Delta t}\dot{d}\} + [K]\{^{t+\Delta t}d\} = \{^{t+\Delta t}f\} \tag{4.2}$$

In order to solve (eqn.4.2) for new accelerations, velocities and displacements, the initial conditions $\{d_0\}$, $\{\dot{d}_0\}$ and $\{\ddot{d}_0\}$ are required.

The HHT equation of equilibrium is given by the following modification to (eqn.4.2)

$$\begin{aligned}[M]\{^{t+\Delta t}\ddot{d}\} + (1+\alpha)[C]\{^{t+\Delta t}\dot{d}\} - \alpha[C]\{^{t}\dot{d}\} \\ +(1+\alpha)[K]\{^{t+\Delta t}d\} - \alpha[K]\{^{t}d\} \;&=\; (1+\alpha)]\{^{t+\Delta t}f\} - \alpha\{^{t}f\}\end{aligned} \tag{4.3}$$

where α is a new algorithm parameter which controls the numerical dissipation. Clearly when $\alpha = 0$, (eqn.4.2) is recovered. As α is decreased, so greater numerical dissipation occurs. Using the Newmark approximation for displacements and velocities at time $t + \Delta t$, gives

$$\{^{t+\Delta t}d\} = \{^{t}d\} + \Delta t\{^{t}\dot{d}\} + \frac{(\Delta t)^2}{2}\left\{(1-2\beta)\{^{t}\ddot{d}\} + 2\beta\{^{t+\Delta t}\ddot{d}\}\right\} \tag{4.4}$$

and

$$\{^{t+\Delta t}\dot{d}\} = \{^{t}\dot{d}\} + \Delta t\left\{(1-\gamma)\{^{t}\ddot{d}\} + \gamma\{^{t+\Delta t}\ddot{d}\}\right\} \tag{4.5}$$

where β and γ are the familiar Newmark parameters which govern the stability of the algorithm.

Using (eqn.4.4) and rearranging to solve for $\{^{t+\Delta t}\ddot{d}\}$, gives

$$\{^{t+\Delta t}\ddot{d}\} = \frac{1}{\beta(\Delta t)^2}\left\{\{^{t+\Delta t}d\} - \{^{t}d\} - \Delta t\{^{t}\dot{d}\}\right\} - \frac{(1-2\beta)}{2\beta}\{^{t}\ddot{d}\} \tag{4.6}$$

hence (eqn.4.5) becomes

$$\begin{aligned}\{^{t+\Delta t}\dot{d}\} = \;& \{^{t}d\} + \Delta t\left\{(1-\gamma)\{^{t}\ddot{d}\} + \tfrac{\gamma}{\beta(\Delta t)^2}\left\{\{^{t+\Delta t}d\} - \{^{t}d\} - \Delta t\{^{t}\dot{d}\}\right\}\right\} \\ & -\tfrac{\gamma(1-2\beta)\Delta t}{2\beta}\{^{t}\ddot{d}\}\end{aligned} \tag{4.7}$$

It is always possible to rewrite the dynamic equilibrium equations in the form

$$[K^*]\{d\} = \{f^*\} \tag{4.8}$$

Thus a form similar to a non-linear static problem is recovered. Substituting (eqn.4.6) and (eqn.4.7) into (eqn.4.3), and collecting terms, one obtains

$$\begin{aligned}
&[M]\left\{\tfrac{1}{\beta(\Delta t)^2}\left\{\{^{t+\Delta t}d\} - \{^t d\} - \Delta t\{^t\dot{d}\}\right\} - \tfrac{(1-2\beta)}{2\beta}\{^t\ddot{d}\}\right\} + \\
&(1+\alpha)[C]\left\{\{^t d\} + \Delta t(1-\gamma)\{^t\ddot{d}\}\right\} + \\
&+(1+\alpha)[C]\left\{\tfrac{\gamma}{\beta(\Delta t)^2}\left\{\{^{t+\Delta t}d\} - \{^t d\} - \Delta t\{^t\dot{d}\}\right\} - \tfrac{\gamma(1-2\beta)}{2\beta}\{^t\ddot{d}\}\right\} - \\
&\alpha[C]\{^t\dot{d}\} + (1+\alpha)[K]\{^{t+\Delta t}d\} - \alpha[K]\{^t d\} \\
&= (1+\alpha)\{^{t+\Delta t}f\} - \alpha\{^t f\}
\end{aligned} \tag{4.9}$$

If Rayleigh damping is applied, (using $[C] = A[M] + B[K]$) and all terms on the left hand side are collected, one has

$$\left[\overbrace{\left(\frac{1 + A\gamma\Delta t(1+\alpha)}{\beta(\Delta t)^2}\right)}^{c_1}[M] + \overbrace{\left(\frac{B\gamma(1+\alpha) + \Delta t\beta(1+\alpha)}{\beta\Delta t}\right)}^{c_2}[K]\right]\{^{t+\Delta t}d\} \tag{4.10}$$

On the right hand side of (eqn.4.9), that is $\{f^*\}$, one similarly gets

$$\begin{aligned}
&\left[\overbrace{\left(\frac{1 + A\gamma\Delta t(1+\alpha)}{\beta(\Delta t)^2}\right)}^{c_1}[M] + \overbrace{\left(\frac{B\gamma(1+\alpha) + \Delta t\alpha\beta}{\beta\Delta t}\right)}^{c_3}[K]\right]\{^t d\} + \\
&\left[\overbrace{\left(\frac{1 - A\Delta t(\beta - \gamma(1+\alpha))}{\beta\Delta t}\right)}^{c_4}[M] - \overbrace{\left(\frac{B(\beta - \gamma(1+\alpha))}{\beta}\right)}^{c_5}[K]\right]\{^t\dot{d}\} + \\
&\left[\overbrace{\left(\frac{(1-2\beta) + A\Delta t(1+\alpha)(\gamma - 2\beta)}{2\beta}\right)}^{c_6}[M] + \overbrace{\left(\frac{B\Delta t(1+\alpha)(\gamma - 2\beta)}{2\beta}\right)}^{c_7}[K]\right]\{^t\ddot{d}\} + \\
&\overbrace{(1+\alpha)}^{c_8}\{^{t+\Delta t}f\} - \overbrace{\alpha}^{c_9}\{^t f\}
\end{aligned} \tag{4.11}$$

The coefficients c_1 to c_9 may be calculated in advance of entering the time-stepping algorithm. The standard Newmark scheme recovers the widely used average acceleration (or trapezoidal) method when $\beta = 0.25$ and $\gamma = 0.5$. The linear acceleration

and central difference versions are obtained when $\beta = 0.167^r$, $\gamma = 0.5$, $\beta = 0$ and $\gamma = 0.5$, respectively. α must lie in the range $-\frac{1}{3} \leq \alpha \leq 0$ while γ and β should take the values $\frac{1}{2} - \alpha$ and $\frac{1}{4}(1-\alpha)^2$ respectively to achieve unconditional stability for linear systems (for non-linear analyses, such as considered in this thesis, the issue of guaranteed stability remains a topic of research investigation).

4.2.2 Bi-pccgSTAB Element-By-Element Linear Solver

Given that the core solution algorithm consumes a large part of the total Finite Element computer run time, a suitable method needs to be selected carefully. There are two basic approaches used to solve (eqn.4.9) for the iterative nodal displacements. These are the direct and indirect (or iterative) methods. The latter technique has become popular when solving large systems of equations. In general, standard direct solvers, based on some form of Gaussian elimination, are considered efficient when solving problems with up to approximately 1000 degrees of freedom (DoF). This limit depends on the available computer core memory. Over the past 15 years, iterative techniques have become the main tools for solving sets of FE equations. A range of black box iterative solvers now appears in established matrix algorithm packages such as MATLAB [32] (or numerical routines such as NAG and numerical recipes [38]. Smith and Griffiths [46] describe and code the basic pre-conditioned conjugate gradient method.

Running large 3-D dynamic soil-structure simulations (with highly non-linear, strain-softening structures) calls for a very efficient solver algorithm. This can be achieved by using an element-by-element iterative approach and controlling the complete array space through allocating and deallocating the variables to preserve computer memory.

The use of the Microplane constitutive model (discussed in subsection 4.2.4), leads to a non-symmetric tangent stiffness matrix. If the full Newton-Raphson non-linear solution method is to be used, then a non-symmetric solver is required. Initial studies with a pre-conditioned bi-conjugate gradient scheme (BiCG) showed poor convergence characteristics [15]. The code used in *ya*FE*c* provides a more general, element-by-element version of the algorithm presented by Smith [47]. In this approach, a local residual vector is repeatedly minimized (using a GMRES, Generalised Minimum Residual, method) leading to smoother convergence characteristics than techniques such as the Conjugate Gradient Squared. Simple diagonal pre-conditioning is used in all analyses described here.

4.2.3 *ya*FEc Element Library

*ya*FEc uses 8-noded and 20-noded 3-D (hexahedral) isoparametric elements. The following notes identify the 20-noded element stiffness, mass and damping matrices.

Element Stiffness Matrix

The standard definition of the element stiffness matrices follows from applying the Galerkin weighted residual approach to the weak form of the governing partial differential equation of dynamic equilibrium. This results in

$$[K^e] = \int_{V_e} [B^e]^T [D][B^e] dV \tag{4.12}$$

where $[B^e]$ represents the spatial derivatives of the element shape functions and $[D]$ is the constitutive matrix. It is standard practice to operate with a local co-ordinate system when generating the elemental stiffness matrices. Thus use of local co-ordinates ξ, η and ζ leads to

$$[K^e] = \int_{-1}^{+1} \int_{-1}^{+1} \int_{-1}^{+1} [B]^T [D][B] det[J] d\xi d\eta d\zeta \tag{4.13}$$

where $det[J]$ is the determinant of the Jacobian matrix, discussed below.

The quadratic shape functions for the 20-noded isoparametric elements are given by

$$\{N\} = \left\{ \begin{array}{c} N_1^e \\ N_2^e \\ N_3^e \\ N_4^e \\ N_5^e \\ N_6^e \\ N_7^e \\ N_8^e \\ N_9^e \\ N_{10}^e \\ N_{11}^e \\ N_{12}^e \\ N_{13}^e \\ N_{14}^e \\ N_{15}^e \\ N_{16}^e \\ N_{17}^e \\ N_{18}^e \\ N_{19}^e \\ N_{20}^e \end{array} \right\} = \left\{ \begin{array}{c} \frac{1}{8}(1+\xi)(1+\eta)(1+\zeta)(\xi+\eta+\zeta-2) \\ \frac{1}{4}(1+\xi)(1+\eta)(1-\zeta^2) \\ \frac{1}{8}(1+\xi)(1+\eta)(1+\zeta)(\xi+\eta+\zeta-2) \\ \frac{1}{4}(1-\xi^2)(1+\eta)(1+\zeta) \\ \frac{1}{8}(1+\xi)(1+\eta)(1+\zeta)(\xi+\eta+\zeta-2) \\ \frac{1}{4}(1+\xi)(1+\eta)(1-\zeta^2) \\ \frac{1}{8}(1+\xi)(1+\eta)(1+\zeta)(\xi+\eta+\zeta-2) \\ \frac{1}{4}(1-\xi^2)(1+\eta)(1+\zeta) \\ \frac{1}{4}(1+\xi)(1-\eta^2)(1+\zeta) \\ \frac{1}{4}(1+\xi)(1-\eta^2)(1+\zeta) \\ \frac{1}{4}(1+\xi)(1-\eta^2)(1+\zeta) \\ \frac{1}{4}(1+\xi)(1-\eta^2)(1+\zeta) \\ \frac{1}{8}(1+\xi)(1+\eta)(1+\zeta)(\xi+\eta+\zeta-2) \\ \frac{1}{4}(1+\xi)(1+\eta)(1-\zeta^2) \\ \frac{1}{8}(1+\xi)(1+\eta)(1+\zeta)(\xi+\eta+\zeta-2) \\ \frac{1}{4}(1-\xi^2)(1+\eta)(1+\zeta) \\ \frac{1}{8}(1+\xi)(1+\eta)(1+\zeta)(\xi+\eta+\zeta-2) \\ \frac{1}{4}(1+\xi)(1+\eta)(1-\zeta^2) \\ \frac{1}{8}(1+\xi)(1+\eta)(1+\zeta)(\xi+\eta+\zeta-2) \\ \frac{1}{4}(1-\xi^2)(1+\eta)(1+\zeta) \end{array} \right\} \tag{4.14}$$

These shape functions possess the usual properties ($N_1^e(-1,-1,-1) = 1$ whereas $N_2^e = N_3^e = N_4^e = N_5^e = N_6^e = N_7^e = N_8^e = 0$ at the same location, $\xi = -1$, $\eta = -1$, $\zeta = -1$).

Using the chain rule, one has

$$\left\{ \begin{array}{c} dx \\ dy \\ dz \end{array} \right\} = \left[\begin{array}{ccc} \frac{\partial x}{\partial \xi} & \frac{\partial x}{\partial \eta} & \frac{\partial x}{\partial \zeta} \\ \frac{\partial y}{\partial \xi} & \frac{\partial y}{\partial \eta} & \frac{\partial y}{\partial \zeta} \\ \frac{\partial z}{\partial \xi} & \frac{\partial z}{\partial \eta} & \frac{\partial z}{\partial \zeta} \end{array} \right] \left\{ \begin{array}{c} d\xi \\ d\eta \\ d\zeta \end{array} \right\} \tag{4.15}$$

where the array

$$\left[\begin{array}{ccc} \frac{\partial x}{\partial \xi} & \frac{\partial x}{\partial \eta} & \frac{\partial x}{\partial \zeta} \\ \frac{\partial y}{\partial \xi} & \frac{\partial y}{\partial \eta} & \frac{\partial y}{\partial \zeta} \\ \frac{\partial z}{\partial \xi} & \frac{\partial z}{\partial \eta} & \frac{\partial z}{\partial \zeta} \end{array} \right] \tag{4.16}$$

is the Jacobian matrix $[J]$. Solving for $\{d\xi\, d\eta\, d\zeta\}^T$, one has

$$\begin{Bmatrix} d\xi \\ d\eta \\ d\zeta \end{Bmatrix} = [J]^{-1} \begin{Bmatrix} dx \\ dy \\ dz \end{Bmatrix} \tag{4.17}$$

It can be show that (for example see Wu [60])

$$dV = \|det[J]\| \, d\xi d\eta d\zeta \tag{4.18}$$

Analytical integration of (eqn.4.13) would be highly tedious, thus numerical integration is performed using Gaussian quadrature such that

$$[K^e] \approx \sum_{i=1}^{n} [B]^T [D][B] det[J] w(i) \tag{4.19}$$

where n represents the number of integration points and w is the Gaussian weight parameter.

The $2 \times 2 \times 2$ reduced Gaussian integration scheme places the sampling points at $\xi, \eta, \zeta = \pm 1/\sqrt{3}$, whereas in the $3 \times 3 \times 3$ scheme, they lie at $\xi, \eta, \zeta = \pm 1/\sqrt{0.6}, 0$. Despite the high computational cost, it is recommended that full integration should be used whenever possible, except when the material approaches incompressible behaviour [5]. The latter point is not of concern here as concrete appears (in a macroscopic sense) strongly dilative as *failure* is approached.

As noted (section 4.2), an embedded, smeared approach is adopted for modelling the steel reinforcement in the concrete. The stiffness (and internal forces in a non-linear analysis) associated with the reinforcement are added to the concrete, resulting in a combined stiffness (and internal forces) for the hexahedral elements. This approach is considered reasonable for many situations, although it does not allow completely arbitrary positioning of the membrane inside the element. The reinforcement is categorised by (i) the definition of the plane it is acting in with respect to the local co-ordinate system, (ii) the depth of the reinforcing layer away from an element face, (iii) the direction of the reinforcing bars (providing uniaxial stiffness) in the reinforcing plane (using local co-ordinates x^r and y^r), defined by the angle between the x^r axis and the direction of the reinforcing bars and (iv) the equivalent thickness of the membrane layer. The latter is calculated as follows. Given the total cross-sectional area of the bars acting in that element (A_r) and the width of the element normal to the axes of the bars in the plane of the membrane (w), the equivalent thickness is simply given by

$$t_r = \frac{A_r}{w} \tag{4.20}$$

Note that the node numbering which defines the element topology also defines the local co-ordinate directions for each element. For example, the direction of first three nodes define the local positive ζ direction, the third, fourth and fifth nodes define the positive ξ direction and the positive η direction follows from the right-hand rule. A second local 2-D Cartesian co-ordinate system (x^r, y^r) must be set up in the reinforcement membrane. This is achieved by first identifying the local co-ordinate direction (ξ, η and ζ) which is normal to the plane of the reinforcement. Then the relative position of this plane (in the range -1 to $+1$) is given.

Element Mass Matrix

Although the consistent matrix appears the most logical definition for the finite element, it is widely recognised that there are some real advantages in lumping the masses at the element nodes. In most early FE attempts to deal with dynamic problems, the mass of the elements was invariably lumped at the nodes, resulting in a diagonal matrix even though no such concentrated masses actually exist in the structure.

Consider the following the lumping scheme. The total mass M_t^e is given by one-third of the sum of all mass terms appearing in the consistent mass matrix given below

$$[M^e] = \int_{-1}^{+1}\int_{-1}^{+1}\int_{-1}^{+1} [N]^T \rho [N] det[J] d\xi d\eta d\zeta \tag{4.21}$$

where ρ is the mass density of the element.

Let the sum of the diagonal terms in the mass matrix be defined as M_d^e. Thus, a scaling factor, f_M, can be defined as

$$f_M = \frac{M_t^e}{M_d^e} \tag{4.22}$$

such that the final lumped mass matrix is given by the product of this scaling factor and the diagonal terms appearing in the consistent mass matrix (with all off-diagonal terms set equal to zero). It is clear that when using a lumped mass matrix, less storage space is required. This leads to a reduced run-time with no real loss in accuracy provided a sufficient number of elements are used. The above form of mass lumping was first presented by Hinton *et al* [22]. *ya*FE*c* allows the

option of using either the fully consistent mass matrices, or the *consistently* lumped mass matrices as described above.

Element Damping Matrix

The element damping matrix $[C^e]$ may be constructed in a similar manner as the consistent mass matrix.

$$[C^e] = \int_{-1}^{+1} \int_{-1}^{+1} \int_{-1}^{+1} [N]^T \mu [N] det[J] d\xi d\eta d\zeta \tag{4.23}$$

where μ represents a viscous damping parameter. For linear systems, μ is treated as a constant. For non-linear systems, μ may be a function of the material velocity. The real difficulty in constructing $[C^e]$ lies in choosing an appropriate value for μ. Rayleigh damping is often used to express the damping effects in an engineering structure. This form of damping is available in *ya*FE*c* although it should be remembered that the code has the ability to directly model material hysteresis (through the path-dependent microplane model, discussed in the following section) and of course far field radiation damping (through the CIFECM).

4.2.4 Non-Linear Material Model for Concrete

Reinforced concrete represents the most common building material in a wide range of safety critical civil engineering structures. This material is relatively cheap to produce, is easily adapted to a variety of geometric forms and offers an almost inert material which exhibits high durability over many years if properly designed and carefully constructed. Concrete can appear to behave either as a highly brittle, weak material (under purely tensile loading) or a moderately ductile, very strong material (under high levels of multi-axial confinement [35]). Thus the multiaxial stress state should be taken into consideration in structures where moderate confinement exists. Unfortunately, a constitutive model for concrete which is able to capture accurately all the main deformation mechanisms (such as, pre-peak non-linearity, hysteresis and damage under cyclic loading, compaction, dilation, Mode I, II and III fracturing and the associated, induced anisotropy) under arbitrary, non-proportional multi-axial paths throughout strain space has yet to emerge. Recent work at Sheffield University has involved the detailed examination of two classes of constitutive models which claim to offer fairly complete descriptions of the material response.

The models examined at Sheffield include (i) a smooth isotropic elasto-plasticity

model where material softening is based on the specific fracture-energy concept [53] and (ii) an explicit microplane model (now referred to as the M2 formulation [40]). The latter provides a means of capturing the evolving anisotropy in the material by means of a series of pre-defined planes acting through a material point, upon which simplified stress-strain relations hold.

Note that for any standard constitutive model which includes a softening response, there exists the difficulty that FE solutions can be shown to be inobjective with respect to the mesh alignment (and mesh density in some cases). This serious limitation is the subject of detailed investigation world-wide, yet falls outside the scope of this thesis. Interested readers could refer to the study by Mesmar ([33] and the references cited within) for further details.

Returning to the basic microplane model, it is relevant to point out that it represents a real improvement over the constitutive formulations currently found in almost all the general purpose FE codes (such as ANSYS, ABAQUS, DIANA and LUSAS).

Although the main thrust of this thesis is not to provide a detailed critique of all the available constitutive models for concrete (of which there are many), it is argued that the realism provided by the microplane model allows a meaningful damage simulation under dynamic soil-structure interaction to be performed in chapter 5.

Bažant *et al* [8] noted that the majority of existing constitutive models for concrete exhibit a tensorial character, in the sense that they establish a direct relationship between the nine-component strain tensor and the nine-component stress tensor. Such relationships must satisfy certain requirements of frame indifference (that is, independence of the choice of the co-ordinate system). However, an alternative framework can be constructed based on the microplane concept, itself motivated by the slip theory of metals. Microplane models operate with stress and strain vectors on a set of planes with pre-defined orientations (the so-called *microplanes*). The basic constitutive laws are defined on the level of the microplane. The microplane stresses must then be transformed back to the generalised macroscopic stresses using a virtual work expression relating the tensorial and vectorial components.

The original idea of this technique can be attributed to Taylor, who in 1938 proposed that the stress-strain relationships could be characterised independently on different slip planes. A chronological summary of earlier microplane models is given by Mesmar [33]. Here attention is restricted to the M2 version of the model first proposed by Carol *et al* [10]. Unlike previous versions, this explicit formulation was cast in terms of the total stresses and strains. The work reported in this thesis takes advantage of work done by Qiu [40] and Mesmar [33] who coded the M2

model within *ya*FE*c*. The following notes provide a summary of the model.

A *microplane* is defined as an arbitrary plane which cuts through the material at a pre-defined point. The plane is identified by the three directional cosines, n_i, which describe the orientation of a normal unit vector. Any number of microplanes may be considered to exist at a point. On each microplane, resolved components of stress and strain are considered. These are normal stress and normal strain, which are further decomposed into volumetric, and deviatoric components. A set of simplified stress-strain relations on the microplane are then defined. These include expressions which describe both the monotonic and the unloading/reloading response. The relationships, together with a scheme transforming the stresses back to their the macroscopic measures, constitute the material model. The $M2$ microplane model is based on three core hypotheses which are required to develop the final constitutive relationships.

Hypothesis I. The three microplane strains (ε_V, ε_D and ε_{T_r}) are the resolved components of the macroscopic strain tensor, ε_{ij}. This decomposition provides a tensorial kinematic constraint.

Hypothesis II. The microplane stresses ($\bar{\sigma}_V$, $\bar{\sigma}_D$ and $\bar{\sigma}_{T_r}$) are each functions of their corresponding strains alone. Thus the responses on each microplane are mutually independent. This approach ensures that the associated products give directly the work done on the microplane.

Hypothesis III. The relationship between the microplane stresses and the macroscopic stresses tensor, σ_{ij}, is obtained by applying the virtual work principle and enforcing the equivalence of virtual work on both micro and macro scales when a field of arbitrary virtual strain variations $\delta\varepsilon_{ij}$ is prescribed.

Notice that ε_V, ε_D and ε_{T_r} are the volumetric, deviatoric and shear strains respectively. The following subsections provide the mathematical derivation involved in formulating the microplane equations. Full details are give by Carol *et al* [10].

Decomposition of the Macroscopic Strains, ε_{ij}

Consider the microplane normal defined by the direction cosines n_i. The components of the strain acting (in the global direction) on the microplane, are given by (*Hypothesis I*)

$$\varepsilon_j^n = n_k \varepsilon_{jk} \tag{4.24}$$

This strain component can be decomposed into a normal strain vector ε_{N_i} and two orthogonal shear strain vectors ε_{T_r}. The normal strain magnitude is given by

$$\varepsilon_N = n_j \varepsilon_j^n = n_j n_k \varepsilon_{jk} \tag{4.25}$$

with individual components

$$\varepsilon_{N_i} = n_i n_j n_k \varepsilon_{jk} \tag{4.26}$$

The normal strain magnitude may be further split into the volumetric and deviatoric components

$$\varepsilon_V = \varepsilon_{kk}/3, \qquad \varepsilon_D = \varepsilon_N - \varepsilon_V \tag{4.27}$$

Thus, the first-order shear strain tensor is given by

$$\varepsilon_{T_r} = \varepsilon_r^n - \varepsilon_{Nr} = (\delta_{ri} - n_r n_i) n_j \varepsilon_{ij} \tag{4.28}$$

where once again δ_{ij} is the Kronecker delta tensor. In (eqn.4.28), the entity forming a product with ε_{ij} is the third-order tensor

$$a_{ijk} = (\delta_{ij} - n_i n_j) n_k \tag{4.29}$$

Note that a_{ijk} is non-symmetric with respect to j and k, that is $a_{ijk} \neq a_{ikj}$. Because the strain tensor ε_{ij} is symmetric, the non-symmetric part of the tensor a_{ijk} will have no effect on the value of ε_{T_i}. This means that only a_{ijk}^{sym} $(= (a_{ijk} + a_{ikj})/2)$, the symmetric part of the tensor a_{ijk} with respect to j and k, is active in (eqn.4.28). Hence, the shear strain components in (eqn.4.28) may finally be expressed as

$$\varepsilon_{T_i} = \frac{1}{2}(n_j \delta_{ik} + n_k \delta_{ij} - 2 n_i n_j n_k) \varepsilon_{jk} \tag{4.30}$$

The shear strain magnitude is therefore calculated as

$$\begin{aligned} \varepsilon_T &= \sqrt{\varepsilon_{T_i} \varepsilon_{T_i}} = \sqrt{(n_k \varepsilon_{ik} - n_i n_j n_k \varepsilon_{jk})(n_r \varepsilon_{ir} - n_i n_m n_r \varepsilon_{mr})} \\ &= \sqrt{n_k n_r \varepsilon_{ik} \varepsilon_{ir} - n_i n_m n_r n_k \varepsilon_{ik} \varepsilon_{mr} - n_i n_j n_k n_r \varepsilon_{jk} \varepsilon_{ir} + n_i n_i n_j n_k n_m n_r \varepsilon_{mr} \varepsilon_{jk}} \end{aligned} \tag{4.31}$$

Noticing that $n_i n_i = 1$ the second term and the fourth term cancel, leaving

$$\varepsilon_T = \sqrt{n_k n_r \varepsilon_{ik} \varepsilon_{ir} - n_i n_j n_k n_r \varepsilon_{jk} \varepsilon_{ir}} \tag{4.32}$$

or

$$\varepsilon_T = \sqrt{n_k \varepsilon_{ir} n_r (\varepsilon_{ik} - n_i n_j \varepsilon_{jk})} \tag{4.33}$$

Microplane Stresses, $\bar{\sigma}_V$, $\bar{\sigma}_D$, and $\bar{\sigma}_{T_r}$

According to Hypothesis II, the secant moduli for each microplane can be considered as a function of the current strains and stresses only for monotonic loading. The decoupled relations are of the form

$$\begin{aligned} \bar{\sigma}_V &= C_V(\varepsilon_V)\,\varepsilon_V \\ \bar{\sigma}_D &= C_D(\varepsilon_D)\,\varepsilon_D \\ \bar{\sigma}_{T_r} &= C_T(\varepsilon_T, \varepsilon_V)\,\varepsilon_{T_r} \end{aligned} \tag{4.34}$$

where C_V, C_D and C_T are the *secant* moduli. C_V depends only on ε_V, C_D depends only on ε_D, however C_T depends on both ε_{T_r} and ε_V.

The explicit microplane stress-strain relations used by Carol *et al* [Carol *et al*, 1992] are as follows

(*i*) *Volumetric law.* This relationship directly reproduces the macroscopic behavior of the material when purely hydrostatic (that is, no deviatoric) stresses are present. The following law has been obtained by direct curve fitting of experimental data from a hydrostatic test

$$\bar{\sigma}_V = \begin{cases} E_V^0 \varepsilon_V [(1 + \frac{|\varepsilon_V|}{a})^{-p} + (\frac{|\varepsilon_V|}{b})^q] & \text{for } \bar{\sigma}_V < 0 \\ \\ E_V^0 \varepsilon_V e^{-(\frac{|\varepsilon_V|}{a_0})^{p_0}} & \text{for } \bar{\sigma}_V \geq 0 \end{cases} \tag{4.35}$$

where E_V^0 is the initial volumetric elastic modulus and a, b, p and q are the material constants obtained by fitting a hydrostatic compression curve and a_0 and p_0 are obtained from a hydrostatic tension test (extremely rarely performed because of the difficulties in delivering well defined multi-axial tensile loads). Once again note that tension is considered positive here while compression is negative.

(*i*) *Deviatoric law.* This relationship is based on the same form of exponential stress-strain curve used for the tensile volumetric behavior. However two different sets of material constants are used, one for tension and the other for compression

$$\bar{\sigma}_D = \begin{cases} E_D^0 \varepsilon_D e^{-(\frac{|\varepsilon_D|}{a_1})^{p_1}} & \text{for } \bar{\sigma}_D < 0 \\ \\ E_D^0 \varepsilon_D e^{-(\frac{|\varepsilon_D|}{a_2})^{p_2}} & \text{for } \bar{\sigma}_D \geq 0 \end{cases} \tag{4.36}$$

where E_D^0 is the initial deviatoric elastic modulus and a_1, p_1, a_2 and p_2 are further material constants.

(*i*) *Shear law.* Although this is the most complicated among the three microplane constitutive relationships, a simplified law offering a reasonable compromise between performance and computational cost is obtained using the *'parallel tangential hypothesis'* which assumes that the shear stress vector on a microplane, $\bar{\sigma}_{T_r}$, remains always parallel to the corresponding shear strain vector, ε_{T_r}. This means that

$$\bar{\sigma}_{T_r} = \frac{\tau}{\gamma}\varepsilon_{T_r} \tag{4.37}$$

where $\tau = \sqrt{\bar{\sigma}_{T_r}\bar{\sigma}_{T_r}}$ and $\gamma = \sqrt{\varepsilon_{T_r}\varepsilon_{T_r}}$. Then the problem reduces to establishing a one-dimensional relation between the shear stress and strain measures τ and γ. An exponential curve similar to that adopted for the other microplane relationships has been used for this purpose

$$\tau = E_T^0 \gamma e^{-(\frac{\gamma}{a_3})^{p_3}} \tag{4.38}$$

where E_T^0 is the initial shear elastic modulus and p_3 is a further material constant. a_3 requires careful attention as it depends on the macroscopic confinement. In Carol *et al*'s $M2$ model, the variable ε_V has been used as the measure of the external confinement. It is this assumption which makes this model fully kinematically constrained and hence explicit. A linear variation is assumed for the dependence of a_3 on ε_V

$$a_3 = a_3^0 + k_a \varepsilon_V \tag{4.39}$$

where a_3^0 and k_a are the final two material constants.

Macroscopic Stresses, σ_{ij}, by Integration

To move from the microplane to macroscopic stresses, the principle of virtual work is employed. By assuming an arbitrary strain variation $\delta\varepsilon_{ij}$, the following equation is obtained

$$\frac{4\pi}{3}\sigma_{ij}\delta\varepsilon_{ij} = 2\int_\Omega (\sigma_V \delta\varepsilon_V + \sigma_D \delta\varepsilon_D + \sigma_{T_r}\delta\varepsilon_{T_r})\, f(n).d\Omega \tag{4.40}$$

where the symbol δ denotes virtual variations and Ω defines the surface of a unit hemisphere. The integral on the right-hand side of (eqn.4.40) is determined over all possible directions (represented by unit vectors with end points touching the surface of a sphere of unit radius). $f(n)$ is a weight function operating on the

normal directions n_i. This function can introduce anisotropy in the material in its initial state. Concrete can be reasonably considered to be as an isotropic material prior to loading, in which case $f(n) = 1$.

The virtual variations with respect to (eqn.4.25), (eqn.4.27) and (eqn.4.30) are

$$\delta\varepsilon_D = (n_i n_j - \frac{\delta_{ij}}{3})\delta\varepsilon_{ij} \tag{4.41}$$

where $\delta\varepsilon_V = \frac{\delta_{ij}}{3}\delta\varepsilon_{ij}$ is the virtual volumetric strain and

$$\delta\varepsilon_{T_r} = \frac{1}{2}(n_i\delta_{rj} + n_j\delta_{ri} - 2n_r n_i n_j)\varepsilon_{ij} \tag{4.42}$$

Substituting (eqn.4.41) and (eqn.4.42) into (eqn.4.40) and rearranging yields

$$\sigma_{ij}\delta\varepsilon_{ij} = \frac{3}{2\pi}\int_\Omega [\sigma_V\frac{\delta_{ij}}{3} + \sigma_D(n_i n_j - \frac{\delta_{ij}}{3}) + \sigma_{T_r}\frac{1}{2}(n_i\delta_{rj} + n_j\delta_{ri} - 2n_r n_i n_j)]\delta\varepsilon_{ij}.d\Omega \tag{4.43}$$

Recognising that the integral of the invariant σ_V over Ω is 2π, the first term in (eqn.4.43) becomes

$$\frac{3}{2\pi}\int_\Omega \sigma_V\frac{\delta_{ij}}{3}d\Omega = \sigma_V\delta_{ij} \tag{4.44}$$

Finally, the macroscopic stress-strain relation can be written as

$$\sigma_{ij} = \sigma_V\delta_{ij} + \frac{3}{2\pi}\int_\Omega \sigma_D(n_i n_j - \frac{\delta_{ij}}{3})d\Omega + \frac{3}{2\pi}\int_\Omega \frac{\sigma_{T_r}}{2}(n_i\delta_{rj} + n_j\delta_{ri} - 2n_r n_i n_j)d\Omega \tag{4.45}$$

Numerical Integration of the Microplane Stresses

The microplane model trades conceptual simplicity of the stress-strain relations on a microplane against the need for considerable computational effort, as a sufficiently large number of microplanes need to be considered in order to achieve an acceptable level of realism. Because of this, numerical efficiency becomes important in the development of the constitutive algorithm. To speed things up, the tensorial expressions $n_i n_j$ and $\frac{1}{2}(n_i\delta_{rj} + n_j\delta_{ri} - 2n_i n_j n_r)$ should be calculated prior to calling the constitutive model and stored in arrays in the computer memory.

The integrals over the unit hemisphere (eqn.4.45) need to be evaluated numerically. This typically must be done a great many times in every loading step, within every global non-linear (Newton-Raphson) iteration of the step, and at every integration point within each Finite Element. Suitable Gaussian-type formulae for integrating over a unit hemisphere are listed by Stroud [51]. Some further formulae, which

are more efficient, have been derived by Bažant and Oh [6]. All such formulae approximate the integral as follows

$$\int_{\Omega} F \, d\Omega \approx 4\pi \sum_{\alpha=1}^{N} w_\alpha F_\alpha \tag{4.46}$$

in which subscript α refers to a discrete microplane (belonging to the set of size N) characterized by the orientation of its unit normal. w_α are the corresponding weights (or numerical integration coefficients) for each of these directions. Table 4.1 lists values for the microplane normal co-ordinates and weights for a 21-point rule.

α	n_1^α	n_2^α	n_3^α	w_α
1	1.	0.	0.	0.0265214244093
2	0.	1.	0.	0.0265214244093
3	0.	0.	1.	0.0265214244093
4	0.707106781187	0.707106781187	0.	0.0199301476312
5	0.707106781187	-0.707106781187	0.	0.0199301476312
6	0.707106781187	0.	0.707106781187	0.0199301476312
7	0.707106781187	0.	-0.707106781187	0.0199301476312
8	0.	0.707106781187	0.707106781187	0.0199301476312
9	0.	0.707106781187	-0.707106781187	0.0199301476312
10	0.387907304067	0.387907304067	0.836095596749	0.0250712367487
11	0.387907304067	0.387907304067	-0.836095596749	0.0250712367487
12	0.387907304067	-0.387907304067	0.836095596749	0.0250712367487
13	0.387907304067	-0.387907304067	-0.836095596749	0.0250712367487
14	0.387907304067	0.836095596749	0.387907304067	0.0250712367487
15	0.387907304067	0.836095596749	-0.387907304067	0.0250712367487
16	0.387907304067	-0.836095596749	0.387907304067	0.0250712367487
17	0.387907304067	-0.836095596749	-0.387907304067	0.0250712367487
18	0.836095596749	0.387907304067	0.387907304067	0.0250712367487
19	0.836095596749	0.387907304067	-0.387907304067	0.0250712367487
20	0.836095596749	-0.387907304067	0.387907304067	0.0250712367487
21	0.836095596749	-0.387907304067	-0.387907304067	0.0250712367487

Table 4.1: Microplane normal co-ordinates and weights for the 21-point rule

Numerically integrating (eqn.4.45) gives

$$\sigma_{ij} = \sigma_V \delta_{ij} + 6 \sum_{\alpha=1}^{N} \sigma_D (n_i^\alpha n_j^\alpha - \frac{\delta_{ij}}{3}) w_\alpha + 6 \sum_{\alpha=1}^{N} \frac{\sigma_{T_r}}{2} (\delta_{ri} n_j^\alpha + \delta_{rj} n_i^\alpha - 2 n_r^\alpha n_i^\alpha n_j^\alpha) w_\alpha \tag{4.47}$$

It is important to recognise that a significant number of internal memory variables need to be stored for each microplane in this model. Table 4.2 lists the internal variables associated with the $M2$ for 6 to 61 microplanes. ε_V^{max} and ε_V^{min} are the maximum and minimum volumetric strains attained during the analysis. These two scalar variables are shared by all microplanes. ε_D^{max}, ε_D^{min} and γ^p are the maximum and minimum deviatoric strains and plastic shear strain attained by each individual microplane during the analysis.

microplanes	6	16	21	28	61
ε_V^{max}, ε_V^{min}	2	2	2	2	2
ε_D^{max}, ε_D^{min}	12	32	42	56	122
γ^p	6	16	21	28	61
Total	20	50	65	86	185

Table 4.2: $M2$ internal variables required for different microplane rules

Qiu and Crouch [39] proposed a new adaptive integration scheme to allow the number of microplanes active at a point to change dynamically during a Finite Element analysis (see also Qiu [40]). They gave examples of switching in the pre-peak and post-peak regions and commented on the useful efficiency gains.

It has been noticed by Qiu and Crouch [39] that while the model appears to handle anisotropy in a simple, attractive, manner it can not simulate properly the strongly anisotropic behaviour whereby tensile softening followed by compressive loading either in the same direction or orthogonal to the original tensile load leads to very different experimental responses in the material. In addition, there remains considerable difficulty in calibrating each of the material constants as their contributions can not be uncoupled and their cause-effect can not be isolated within one particular experimental load path.

Note that in the original $M2$ model proposed by Carol *et al* [10] the integration was performed over the normal and shear microplane stresses, which resulted in the absence of the term $(-\frac{\delta_{ij}}{3})$ in (eqn.4.45). Thus, this earlier version used

$$\sigma_{ij} = \sigma_V \delta_{ij} + \frac{3}{2\pi}\int_\Omega \sigma_D n_i n_j d\Omega + \frac{3}{2\pi}\int_\Omega \frac{\sigma_{T_r}}{2}(n_i\delta_{rj} + n_j\delta_{ri} - 2n_r n_i n_j)d\Omega \quad (4.48)$$

rather than (eqn.4.45).

Carol and co-workers appear to have been the first to notice this omission [11]. Subsequently (eqn.4.45) was proposed as being the appropriate thermodynamically

consistent expression. Mesmar [33] used (eqn.4.45) in place of (eqn.4.48) the model stability improved in the unaxial mixed control simulations. However, using the original set of material constants resulted in completely unrealistic biaxial envelopes in the combined tension-compression region. Despite considerable trial and error, no satisfactory set of material constants were found which recovered a reasonable biaxial envelope. Clearly, this point needs further investigation. For the purpose of this research the original $M2$ formulation (without the $(-\frac{\delta_{ij}}{3})$ term, that is (eqn.4.48)) has been used henceforth as it appears to lead to more realistic material simulations. The author should point out that the very recently published $M4$ version [8] of the model may have overcome this difficulty yet its investigation falls outside the time-frame of this particular study.

The macroscopic tangential stiffness derivation is given in full by Mesmar [33]. The resulting expression may be written as

$$\begin{aligned} D^{tan}_{ijkl} = \; & \frac{E^{tan}_V}{3}\delta_{ij}\delta_{kl} + \frac{3}{2\pi}\int_\Omega E^{tan}_D n_i n_j (n_k n_l - \frac{\delta_{kl}}{3}) d\Omega \\ & + \frac{3}{2\pi}\int_\Omega \frac{H^{tan}_{rs}}{4}(n_i\delta_{rj} + n_j\delta_{ri} - 2n_r n_i n_j)(n_k\delta_{sl} + n_l\delta_{sk} - 2n_s n_k n_l) d\Omega \end{aligned} \tag{4.49}$$

The three initial moduli (E^0_V, E^0_D and E^0_T) of the microplane stress-strain relationships (which carry no obvious macroscopic physical meaning) may be related to the more familiar elastic constants as follows.

$$\begin{aligned} E^0_V &= \frac{E}{1-2\nu} \\ E^0_D &= \eta_0 E^0_V \\ E^0_T &= \frac{1}{3}\left[\frac{5(1-2\nu)}{1+\nu} - 2\eta_0\right] E^0_V \end{aligned} \tag{4.50}$$

where once again, E is Young's modulus, ν is Poisson's ratio and the additional parameter η_0 distributes the elastic contribution between the volumetric and deviatoric responses. It has been found by Bažant and Prat [7] that good fits with established experimental data are obtained when $0.25 \leq \eta_0 \leq 1$.

Finally, Table 4.3 gives values for each of the 15 material constants used in the analyses of chapter 5. Details of how to calibrate the model are provided by Qiu [40].

4.2.5 Non-Linear Solution Strategy

The non-linear solution strategy represents a crucial part of the overall Finite Element code. There exist no general analytical solution techniques able to cope

Material constants	Values
$E(\times 10^6 N/m^2)$	20
ν	0.17
a	0.005
b	0.225
p	0.25
q	2.25
η_0	1.0
a_0	0.000085
a_1	0.000085
a_2	0.003
a_3	0.005
k_a	0
p_1	0.5
p_2	1.5
p_3	1.5

Table 4.3: Microplane material constants for the concrete simulated in chapter 5. Note that all constants except Young's modulus are dimensionless

with highly non-linear multi-degree of freedom problems, thus numerical, iterative, schemes are required. However, one such iterative method may be efficient for one type of problem yet be inefficient for another. Unfortunately, the selection of a solution algorithm for a particular problem is often based on experience rather than a clear set of rules. In the case of non-linear dynamic FE codes, the task is to find the consistent set of displacements, velocities and accelerations such that equilibrium is met within a pre-defined tolerance. Incremental-iterative schemes represent the only practical approaches which can be used in complex problems. Whichever method is chosen, the user is required to take small enough time-steps to ensure that the path dependent material behaviour is properly captured and the initial approximation to the solution lies with the region of convergence.

Material non-linearity causes $[K^*]$ (eqn.4.8) to become an indirect function of $\{d\}$. $[K^*]$ typically changes during each time-step. The standard Newton-Raphson procedure consists of determining the incremental displacements iteratively such that equilibrium is satisfied while $[K^*]$ changes during each iteration.

Consider a structure in a state of equilibrium where the effective applied loads are $\{f_0^*\}$ and the corresponding displacements $\{d_0\}$. When the load is increased to $\{f_1^*\}$ by applying a new effective load increment $\{\Delta f\}$, the trial displacement increment $\{\Delta d_1\}$ is given by solving

$$[K^*]\{\Delta d_1^{(1)}\} = \{\Delta f_1^{*(1)}\} \tag{4.51}$$

This first estimate for $\{\Delta d_1\}$ ($\{\Delta d_1^{(1)}\}$) is given is by using the effective tangent stiffness matrix $[K^*]$ corresponding to the displacements $\{d_0\}$. $[K^*]$ is assembled using contributions from each element. The mass and damping elements will remain unchanged, however the tangent stiffness matrix may change. Having solved for $\{\Delta d_1\}$ the new displacement vector is determined as

$$\{d_1^{(1)}\} = \{d_0\} + \{\Delta d_1^{(1)}\} \tag{4.52}$$

Given this new set of displacements, strains are determined at the element integration points which are then passed to the constitutive model to calculate the corresponding stresses, *internal variables* (such as maximum and minimum microplane strains) and tangent matrices. The material point stresses are then numerically integrated over the element volume to calculate the internal nodal forces ($\{f_{int}\} = \int [B]\{\sigma\}dV \approx \sum [B]^T\{\sigma\}w$).

In order to decide whether equilibrium has been met, a stopping criterion has to be determined. There are a number of such criteria, including displacement-based, out-of-balance-force-based or energy-based. If the stopping criterion has not been met, then the remaining out-of balance equivalent force is applied to the system to solve for the next iterative displacement.

$$[K^*]\Big|_{d_1^{(1)}} \{\delta d_1^{(2)}\} = \{\delta f_1^{*(2)}\} \tag{4.53}$$

Note that the superscripts refer to the iteration number, whereas the subscripts refer to the increment (or time-step) number. Once $\{\delta d_1^{(2)}\}$ have been determined, the displacements are updated

$$\{d_1^{(2)}\} = \{d_1^{(1)}\} + \{\delta d_1^{(2)}\} \tag{4.54}$$

and the process of calculating the internal forces repeated. This iterative loop continues until the stopping criterion has been met.

Recall that in the full Newton-Raphson method the element stiffness matrices are recalculated during each iteration. This is expensive computationally, but it can lead to very rapid convergence. In the modified Newton-Raphson method, $[K]$ is updated only at the beginning of each increment (or time-step). The initial stiffness method operates entirely with the linear elastic $[K]$. This is calculated at the beginning of the analysis and then used throughout the run. Despite saving a great deal of time within one iteration loop, the initial stiffness method is very slow to converge. Although one additional advantage of the initial stiffness method

is that even through the material non-linearity might imply a non-symmetric $[D]$ matrix, an efficient symmetric linear solver can be used as the non-linear $[D]$ matrix is never directly employed. Experience within the Computational Mechanics Group at Sheffield University has shown that for the range of problems analysed, the full Newton-Raphson (NR) approach always results in a quicker run-time than modified NR methods.

4.2.6 Pre and post-processing

*ya*FE*c* exports `*.dp` files to the public domain post-processing package *Danplot4*. Crouch [15] added routines to *ya*FE*c* to extrapolate Gauss point values (such as stress, strain and microplane variables) to the element nodes. The technique employs the same shape functions as used in the element matrix calculations and weights (and hence smooths) the nodal contributions from adjacent elements with respect to the Gauss point effective volume. The whole process of `*.dp` result file generation is integrated within *ya*FE*c*.

Danplot4 enables deformed contour plots to be produced and exported as high quality *Postscript* files. These files may be subsequently edited within standard vector-graphic drawing packages such as Adobe Illustrator or Corel Draw. Examples of such post processing are given in chapter 5.

4.3 Coding the CIFECM

Song [49] coded the CIFECM in a general form including the 2-D and 3-D scalar and vector wave solutions for both bounded and unbounded media in the static, time and frequency domains [49]. This programme supplied the set of $[M^{\infty}]$ (unit-impulse response to acceleration) matrices (one corresponding to each time-step), given basic geometric and topological information defining the CIFECM surface elements together with the material properties (E, μ and ρ) identifying the stiffness and density.

Starting from this algorithm, the author retained only those sections needed for unbounded compressible 3-D vector wave problems. The programme was then completely rewritten in a free format style encompassing Fortran 90 features such as allocation and deallocation of array spaces (to save on computer memory requirements), neater unlabelled `do loops`, and the use of the implied array handling capabilities. All common blocks from the original code were replaced by transferring variables between subroutines using an argument list. Real numbers were

defined as double precision throughout the code. This rewriting of the code was also necessary in order that it is consistent with the main routine calling it, this is of most importance for memory handling.

Many of the techniques used in computational mechanics require extensive and repetitive use of standard matrix algebra routines. Wherever possible, use should be made of existing, proven numerical libraries. This is the case here where LAPACK [2] routines have been used. LAPACK (an acronym for **L**inear **A**lgebre **PACK**age) provides a set of FORTRAN 77 routines for solving the most commonly occurring operations in linear algebra. The well known BLAS (**B**asic **L**inear **A**lgebra **S**ubroutines) library represent a subset of the LAPACK package. These two libraries are updates of LINPACK and EISPACK, which were developed in the 1970s (and are extensively employed by MATLAB).

Versions of LAPACK are now available in Fortran 90, C and C++, taking advantage of many different computer architectures. The source code can be downloaded from the NETLIB website by `ftp` or by `e-mail`. This source code may be compiled along with the user developed code (as has been the case in this or alternatively a static library may be created by the user for linking with many successive applications that make use of the subroutines.

4.4 Implementation of the CIFECM within the Dynamic Equation of Force Equilibrium

The following section identifies how the interaction force-acceleration relationship is implemented within an implicit time integration scheme. The approach extends the Newmark integration scheme to include the more general Hilber-Hughes-Taylor method. Implementation of the Consistent Finite Element Cell Method within the dynamic equation of force equilibrium is discussed next. A distinction between directly applied loads and loads transmitted through the underlying soil towards the structure is now made.

4.4.1 Dynamic Equation of Force Equilibrium for Directly Applied Loading

The equation of motion for directly applied loading is now developed. The nodes within the finite element model are substructured into two groups. Those nodes within the structure (this will also include any soil modelled explicitly by finite

elements) are denoted by the subscript s. Those nodes on the boundary of the finite element model are denoted here by subscript b, these nodes are identical to those on the interior boundary, subscript i, in the derivation of the CIFECM.

$$\begin{bmatrix}[K_{ss}] & [K_{sb}]\\ [K_{bs}] & [K_{bb}]\end{bmatrix}\begin{Bmatrix}\{d_s\}\\ \{d_b\}\end{Bmatrix}+\begin{bmatrix}[C_{ss}] & [C_{sb}]\\ [C_{bs}] & [C_{bb}]\end{bmatrix}\begin{Bmatrix}\{\dot{d}_s\}\\ \{\dot{d}_b\}\end{Bmatrix}+\begin{bmatrix}[M_{ss}] & [M_{sb}]\\ [M_{bs}] & [M_{bb}]\end{bmatrix}\begin{Bmatrix}\{\ddot{d}_s\}\\ \{\ddot{d}_b\}\end{Bmatrix}=\begin{Bmatrix}\{f_s\}\\ -\{f_b\}\end{Bmatrix} \tag{4.55}$$

The forces on the right hand side above represent the externally applied loading upon the structure f_s, and f_b are the reaction forces from the underlying soil.

The calculation of the reaction forces from the interaction-force equation is now developed. The interaction forces $\{R_b\}$ are now discretised for the piecewise *constant* acceleration unit-impulse response matrix at time $t+\Delta t$, for conciseness of the notation of the convolution integral this corresponds in the following as time step subscript n, and similarly the time t is denoted as time step $n-1$.

$$\{R\}_n=\sum_{j=1}^{n}[M^{\infty}]_{n-j+1}\int_{(j-1)\Delta t}^{j\Delta t}\{d(\tau)\}\,d\tau \tag{4.56}$$

$$\{R\}_n=[M^{\infty}]_1\left(\left\{\dot{d}\right\}_n-\left\{\dot{d}\right\}_{n-1}\right)+\sum_{j=1}^{n-1}[M^{\infty}]_{n-j+1}\left(\left\{\dot{d}\right\}_j-\left\{\dot{d}\right\}_{j-1}\right) \tag{4.57}$$

The displacements and corresponding velocities are now approximated according to the Hilber-Hughes-Taylor time integration scheme (section 4.2.1)

Inserting the approximations for the displacements (eqn.4.4) and velocities (eqn.4.5) into the interaction force equation (eqn.4.56) yields

$$\{R_b\}_n=\gamma\Delta t\,[M^{\infty}]_1\left\{\ddot{d}\right\}_n+(1-\gamma)\,\Delta t\,[M^{\infty}]_1\left\{\ddot{d}\right\}_{n-1}+\sum_{j=1}^{n-1}[M^{\infty}]_{n-j+1}\left(\left\{\dot{d}\right\}_j-\left\{\dot{d}\right\}_{j-1}\right) \tag{4.58}$$

Those terms relating to the *current* time step are now distinguished from the *lingering* response (occurring from the actions at previous time steps) by splitting the interaction force equation into two parts. Thus the part of the interaction forces relating to the current time step are now able to be included on the left hand side of the equation of dynamic force equilibrium (eqn.4.55).

$$\{R_b\}_n = \gamma \Delta t [M^\infty]_1 \left\{\ddot{d}\right\}_n \tag{4.59}$$

The following *lingering* contribution $\{\hat{R}_b\}$ appears on the right hand side of (eqn.4.55)

$$\left\{\hat{R}_b\right\}_n = (1-\gamma)\,\Delta t [M^\infty]_1 \left\{\ddot{d}\right\}_{n-1} + \sum_{j=1}^{n-1} [M^\infty]_{n-j+1} \left(\left\{\dot{d}\right\}_j - \left\{\dot{d}\right\}_{j-1}\right) \tag{4.60}$$

Compatibility of the displacements of the substructure containing the internal nodes of the structure at interface nodes and those from the unbounded media substructure representing the underlying soil is expressed by

$$\{d_b\}_n = \{d\}_n \tag{4.61}$$

Force equilibrium between the two substructures is formulated as

$$\{f_b\}_n = -\{R\}_n \tag{4.62}$$

Finally, the substructure dynamic equation of equilibrium is given as

$$\begin{bmatrix} [K_{ss}] & [K_{sb}] \\ [K_{bs}] & [K_{bb}] \end{bmatrix} \begin{Bmatrix} \{d_s\}_n \\ \{d_b\}_n \end{Bmatrix} + \begin{bmatrix} [M_{ss}] & [M_{sb}] \\ [M_{bs}] & [M_{bb}] + \gamma \Delta t [M^\infty]_1 \end{bmatrix} \begin{Bmatrix} \left\{\ddot{d}_s\right\}_n \\ \left\{\ddot{d}_b\right\}_n \end{Bmatrix} = \begin{Bmatrix} \{f_s\}_n \\ -\left\{\hat{R}\right\}_n \end{Bmatrix} \tag{4.63}$$

It is evident from the above equation that the consequence of including the dynamic far field is felt on either side of the equilibrium equation. Substitution and rearrangement in the form of (eqn.4.8) follows in an analagous manner as shown earlier (section 4.2.1).

4.4.2 Dynamic Equation of Force Equilibrium for Transmitted Loading

When the loading upon the structure is assumed to have been transmitted through the (unbounded) underlying soil to the structure the loading regime needs to be established first from the free field response of the soil. The free field response of the soil is the response of the soil without the presence of the structure. The dynamic equation of force equilibrium is simply stated here, the implementation

within a time integration scheme follows from that shown in the above section for direct loading.

$$\begin{bmatrix} [M_{ss}] & [M_{sb}] \\ [M_{bs}] & [M_{bb}] \end{bmatrix} \begin{Bmatrix} \{\ddot{d}_s\} \\ \{\ddot{d}_b\} \end{Bmatrix} + \begin{bmatrix} [C_{ss}] & [C_{sb}] \\ [C_{bs}] & [C_{bb}] \end{bmatrix} \begin{Bmatrix} \{\dot{d}_s\} \\ \{\dot{d}_b\} \end{Bmatrix} + \begin{bmatrix} [K_{ss}] & [K_{sb}] \\ [K_{bs}] & [K_{bb}] \end{bmatrix} \begin{Bmatrix} \{d_s\} \\ \{d_b\} \end{Bmatrix} + \begin{Bmatrix} \{0\} \\ \int_0^t [M^g_{bb}(t-\tau)] \left\{\ddot{d}^t_b(\tau)\right\} d\tau \end{Bmatrix} = \begin{Bmatrix} \{0\} \\ \{f_b\} \end{Bmatrix} \tag{4.64}$$

where

$$\{f_b\} = \left\{ \int_0^t \left[S^f_{bb}(t-\tau)\right] \left\{d^f_b(\tau)\right\} d\tau \right\} \tag{4.65}$$

given that

$$\int_0^t \left[S^f_{bb}(t-\tau)\right] \left\{d^f_b(\tau)\right\} d\tau = \int_0^t [S^g_{bb}(t-\tau)] \left\{d^f_b(\tau)\right\} d\tau + \int_0^t [S^e_{bb}(t-\tau)] \left\{d^f_b(\tau)\right\} d\tau \tag{4.66}$$

The superscripts t, g and f refer to the total motion, the ground motion and the free field motion respectively. As can be seen from (eqn.4.64) with (eqn.4.65) and (eqn.4.66) the influence of the unbounded media is apparent in both the free field forcing function on the right hand side and reaction of the soil included by means of the convolution integral appearing on the left hand side.

In the current implementation within *ya*FE*c* the nodes which lie on the soil-structure interaction boundary are entered last in the input co-ordinate list. This simplifies the matrix partitioning scheme in the element-by-element solver. The far field CIFECM elements are collectively treated a one *super element* in the code.

4.4.3 Pre-Storage of Unit-Impulse Response Matrices

The FE code provides the option of ether calculating the unit-impulse response matrices or reading them from storage prior to entering the time stepping loop. The latter approach enables different non-linear structure analyses (changing the applied loads, or structural stiffnesses, for example) to be performed using common far field matrices, or conversely the properties of the unbounded substructure may be altered whilst keeping the structural model fixed. This is attractive since the calculation of $[M^\infty]$ for each time step consumes a significant part of the total CPU time.

4.5 Closure

The main features of the the FE code have been described with particular emphasis given to the time integration scheme and the non-linear material model that are subsequently applied in chapter 5. The coupling of the CIFECM with finite elements in the dynamic equation of force equilibrium is given. The framework is now set for the analysis of non-linear concrete structures with account for dynamic soil-structure interaction.

Chapter 5

FE Simulations Using the New Code

Two simulations have been performed using the new code. Firstly, a simple single element structure is examined, with the influence of a number of input parameters studied. This is followed by a more practical engineering example of a reinforced concrete containment vessel subjected to an aircraft impact.

5.1 Simple Single Element Structure

As the simplest possible numerical example to qualitatively demonstrate the effects of radiation damping, the response of a single ($1m \times 1m \times 10m$) 8-noded brick element coupled with a single 4-noded CIFECM element is examined. The similarity centre for the CIFECM element is chosen at the middle of the top surface of the finite element (that is 10m above the CIFECM element). Figure (fig.5.1) shows the finite element on the left, together with 20 elements representing an extended mesh arrangement on the right.

The systems are subjected to both extremities of load duration, that is a short term impulse of one time step (0.005s) in duration (fig.5.2a) and a step function (fig.5.2b). In both cases the loading is applied normal to the top surface of the finite element, The material properties of the control system are mass density $1850kg.m^{-3}$, Young's modulus $10MPa$ and Poisson's ratio 0.3.

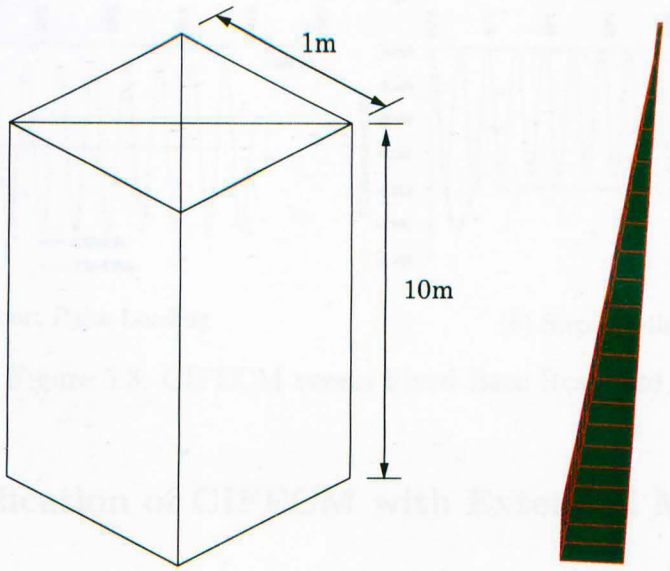

Figure 5.1: Single Element Model

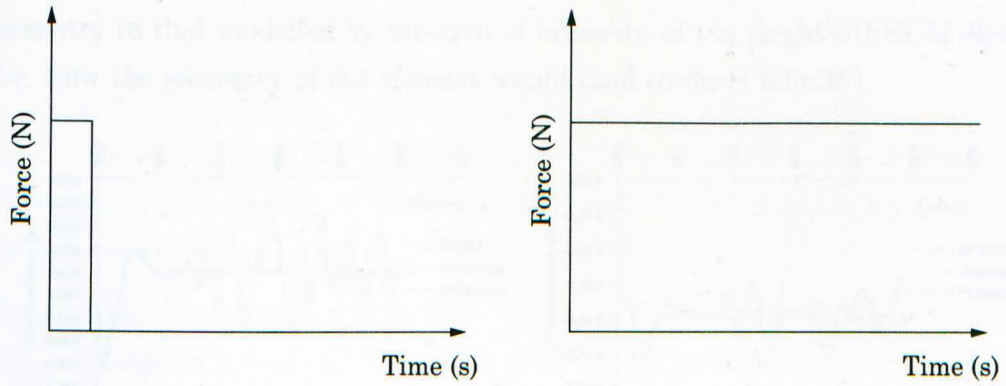

(a) Short Pulse Loading (b) Step Loading

Figure 5.2: Loading Functions

5.1.1 Unbounded Versus Fixed Base Response

The two extremities of founding conditions are first examined. The response of the finite element fully fixed at one end is compared to that of the unbounded system of the finite element coupled with a CIFECM element.

The damping out of the waves from the system can clearly be seen by comparing the fixed base response of the finite element with that founded upon a CIFECM element (fig.5.3). With the long duration step loading (fig.5.3b) the total displacement converges (after dissipation of the stress waves) to a value greater than the fixed base illustrating the reduced elastic stiffness effect upon the system.

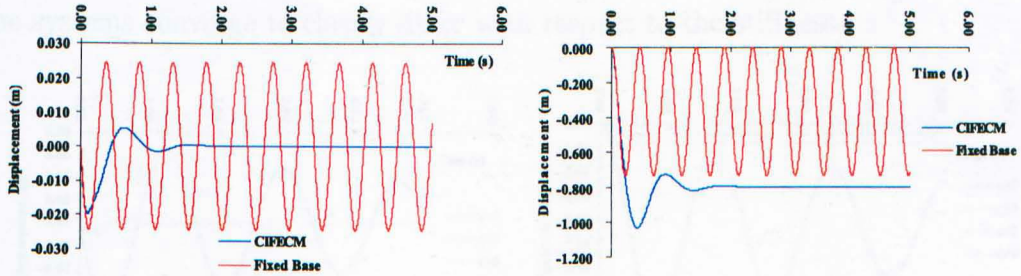

(a) Short Pulse Loading (b) Step Loading

Figure 5.3: CIFECM versus Fixed Base Response

5.1.2 Verification of CIFECM with Extended Mesh

In order to verify the new code, the response of the single FE coupled with a single CIFECM element system is now compared with those results obtained using an extended FE mesh. The mesh of elements extending outwards have identical geometry to that modelled by the area of influence of the single CIFECM element (i.e. how the geometry of the element would tend towards infinity).

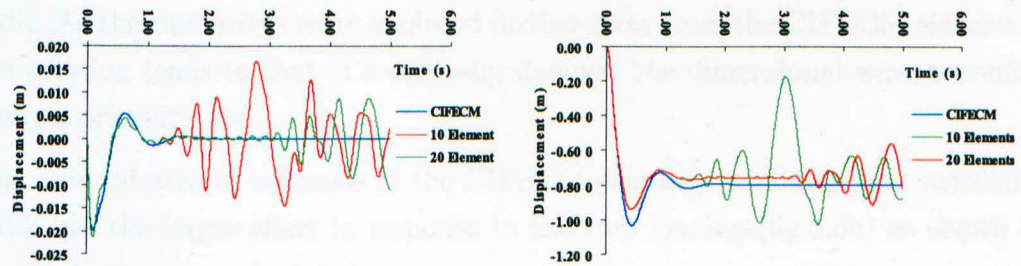

(a) Short Pulse Loading (b) Step Loading

Figure 5.4: CIFECM versus Extended Mesh

The results of these analyses shows initially good agreement between the responses. However, the effect of stress reflections can clearly be seen (fig.5.4). This wave reflection is further highlighted and verified by using two different extended meshes of 10 and 20 finite elements, where the time before the wave reflections occur in the later case is doubled from that of the former.

5.1.3 Variation of Material Properties

The elastic stiffnesses of both the finite element and CIFECM element are now varied. Damping of the systems is quicker with increasing stiffness (fig.5.5) in both cases. Note that in the case of the step loading the static displacements at which

the systems converge to clearly differ with respect to the stiffness.

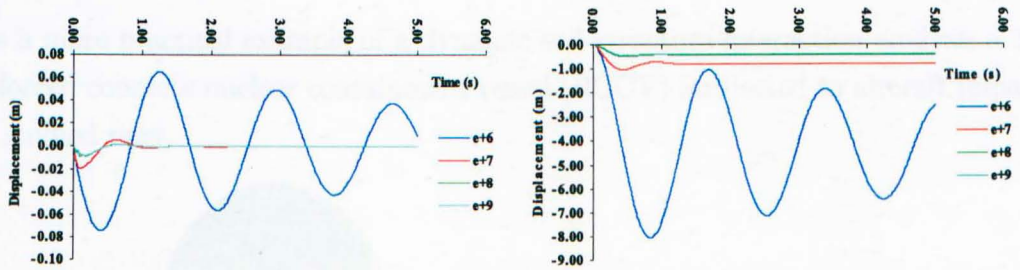

(a) Short Pulse Loading (b) Step Loading

Figure 5.5: Effects of Variation of Material Stiffness upon the Response

5.1.4 Variation of Distance to Similarity Centre

The distance of the similarity centre from the CIFECM element is considered next. The effects of damping govern the behaviour of the response of the system excited by the short pulse loading (fig.5.6a) with the greater effects observed with larger radii. As the similarity centre is placed further away from the CIFECM element so the solution tends to that of a critically damped one dimensional wave travelling along a prismatic rod.

The reduced area of influence of the CIFECM element to infinity with increasing radii, has the larger effect in response to the step loading (fig.5.6b) as shown by the final responses calculated.

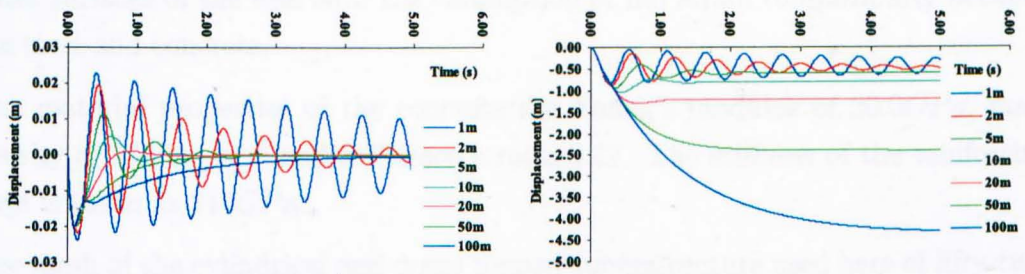

(a) Short Pulse Loading (b) Step Loading

Figure 5.6: Effects of Variation of Similarity Centre on the Response

5.2 Nuclear Reactor Containment Vessel

As a more practical example of a dynamic soil-structure interaction analysis a reinforced concrete nuclear containment vessel (RCCV) Subjected to aircraft impact is studied next.

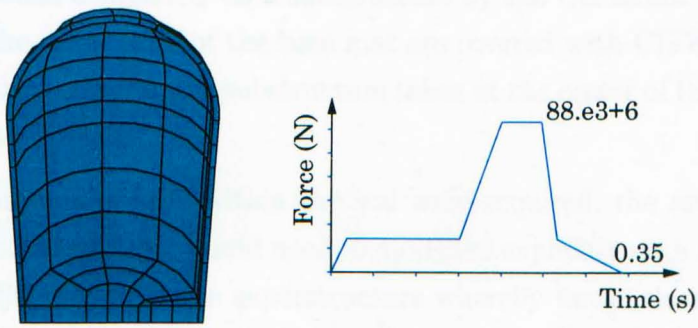

Figure 5.7: Finite Element Mesh and Force Time History

The containment vessel is the outer protective shell of a nuclear reactor installation. The shell is subjected to a horizontal load from an aircraft impact (Boeing 707-320) striking the structure diametrically, enabling exploitation of half-symmetry in the modelling of the structure. The idealised impact load time-history has a maximum force level of 88.3MN (fig.5.7).

The structure is in total $61m$ high and $42m$ wide, with wall thicknesses of $1.2m$. Within the concrete is contained $40mm$ diameter steel reinforcing bars, this are modelled as equivalent membranes $16mm$ thick, $6mm$ inside both the inner and outer surfaces of the wall with the assumption of full strain compatibility between the steel and concrete.

The material properties of the concrete are Young's modulus of $20.0GPa$, mass density of $2450kg.m^{-3}$ and a Poisson's ratio 0.17. The stiffness of the reinforcing steel is taken as $210GPa$.

The mesh of the cylindrical and dome topped superstructure used here of fifty-two, 20-noded brick elements. This arrangement is reproduced here from previous work carried out by Cervera *et al* [12] using shell elements. The mesh is locally refined close to the impact zone, and is considered adequate to capture the pertinent features.

The analysis is performed for $0.5s$ using 400 time steps of $0.00125s$, which is approximately $\frac{1}{200^{th}}$ of the elastic fundamental period ($T \approx 0.23s$). A total of four analyses have been carried out. Considered first are two analyses assuming a fixed base, with linear elastic and non-linear (microplane) material behaviour. The anal-

ysis is then extended to include the effects of dynamic soil-structure interaction. A basemat has been added to the superstructure and is embedded to a depth of $5m$ in the soil. The founding soil is here assumed to behave as drained linear elastic (no two-phase influence of the pore water considered), with Young's modulus of $100MPa$, mass density of $1850kg.m^{-3}$ and Poisson's ratio of 0.3. This allows the soil to be modelled completely as a substructure by the CIFECM. The surface of the base and the outer sides of the base mat are covered with CIFECM elements, with the similarity center of the substructure taken at the center of the containment vessel at ground level.

If non-linear material effects within the soil were required, the area where such effects are expected to occur would need to modelled explicitly with finite elements up to such a distance from the superstructure whereby linear elasticity can once again be assumed. The new bounding surface of this non-linear soil region can then be wrapped in CIFECM elements.

5.2.1 Linear Elastic Response with Fixed Base

The linear elastic response of the superstructure alone is studied first. The displacement plots (fig.5.8) are used in order to give an intuitive feeling of the dynamics of the system with time. As can be observed, the global vibration of the structure is still within the first cycle of its fundamental oscillation. The local deformation of the impact zone occurs within the first $0.275s$, beyond this point in time the global oscillation of the system dominates.

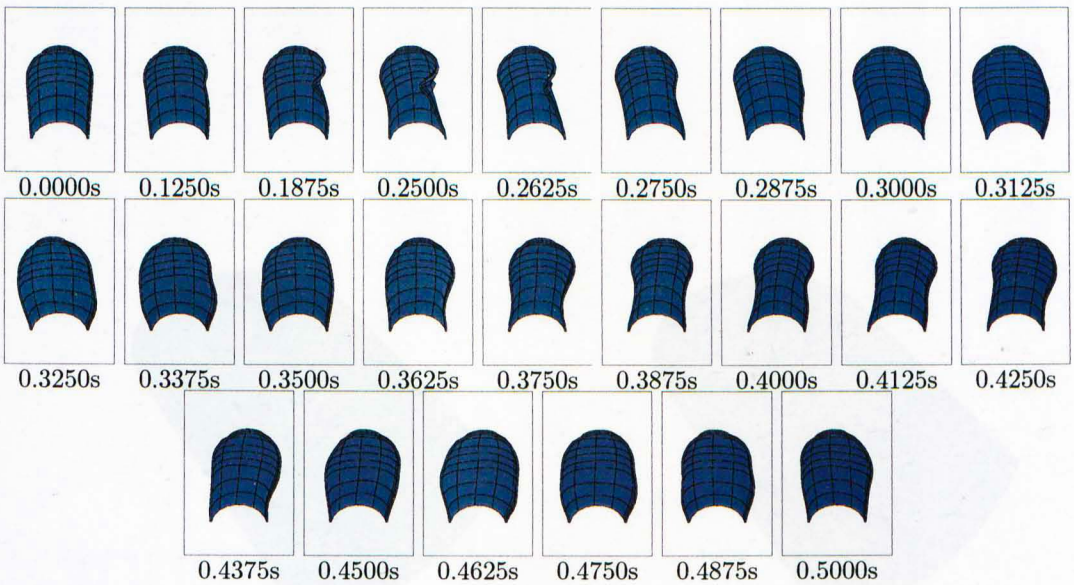

Figure 5.8: Displacements of RCCV with linear Material and Fixed Base

The highest observed principal strains ϵ_1 within the concrete are shown next, (fig.5.9a). The contour plots are given at $0.225s$, from the force-time history (fig.5.7) this can be seen to occur when the loading has reached its peak. The highest tensile (positive) strains of $750\mu\epsilon$ occur within the impact zone. This strain corresponds to a maximum principal stress σ_1 of $14.42MPa$ (fig.5.9b). Clearly this stress level exceeds the tensile strength of concrete which might typically be $3-4MPa$.

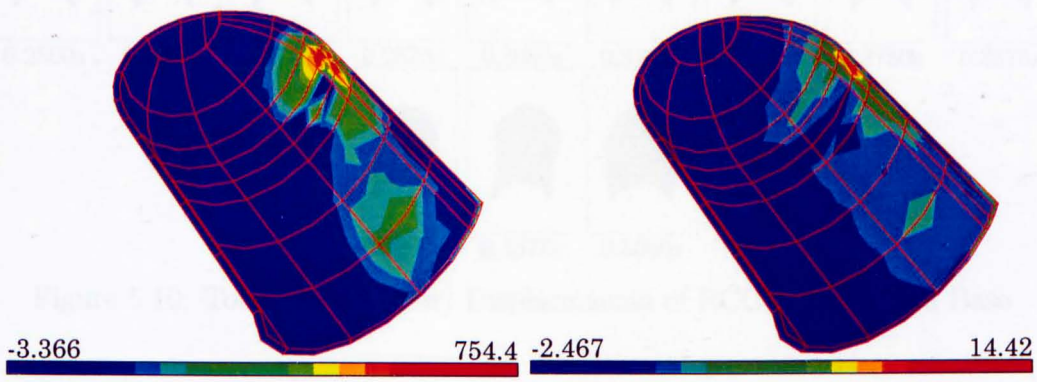

(a) Principal Strains (b) Principal Stresses

Figure 5.9: Major Principal Strains and Stresses of RCCV with Fixed Base

5.2.2 Non-Linear Model Response with Fixed Base

The non-linear response of the super structure is now examined. From the displacement plots (fig.5.10), it is evident that there is a greater deformation in the impact zone due to the yielding of the concrete compared with the elastic response. The long term oscillatory response follows in a similar manner to that seen in the elastic case.

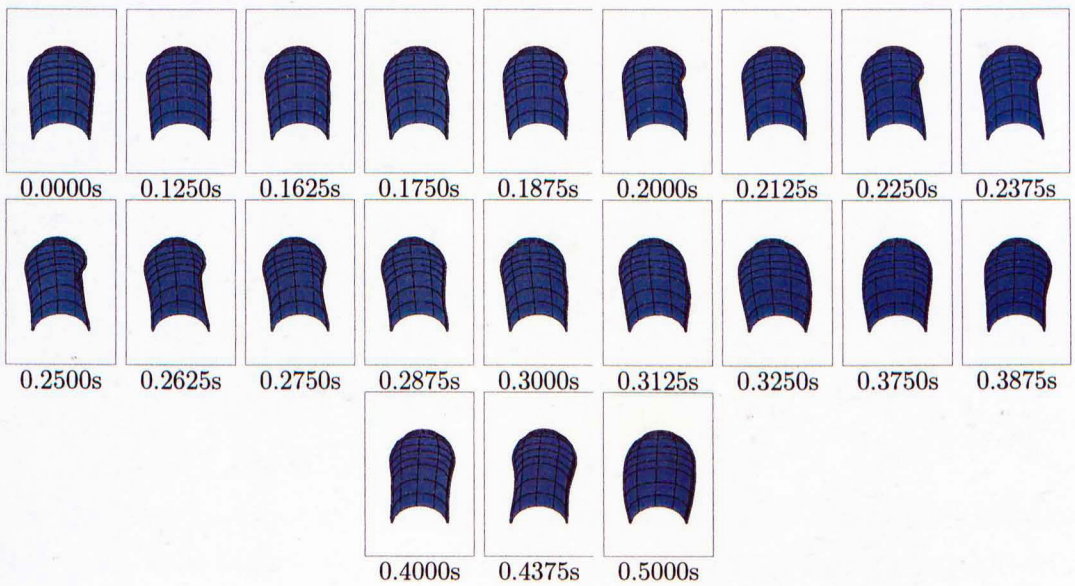

Figure 5.10: Total (Non-Linear) Displacements of RCCV with Fixed Base

The highest observed major principal strain (fig.5.11a) is again seen at the 180^{th} time step (0.225s). The strains are, as expected, much greater due to the non-linear material behaviour, with a maximum tensile strain of $1252\mu\epsilon$.

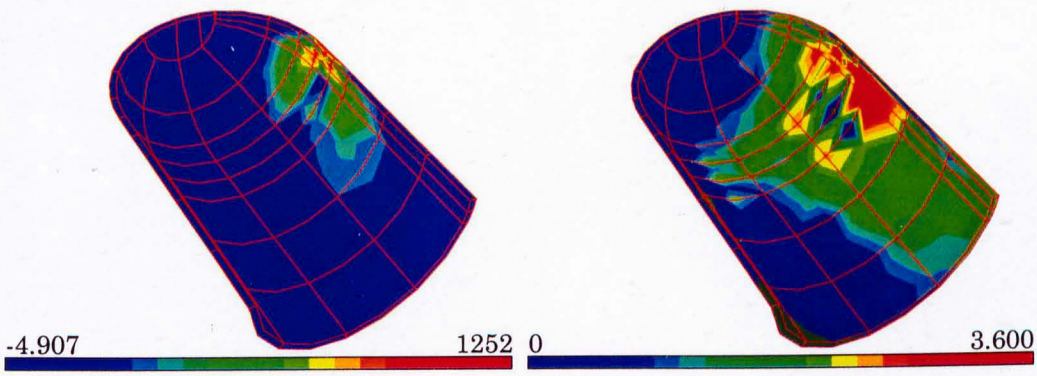

(a) Principal Strains (b) Principal Stresses

Figure 5.11: Non-Linear Principal Strains and Stresses of RCCV with Fixed Base

The effects of the material behaviour are best observed on inspection of the contour plot of the stresses (fig.5.11b). A marked contrast with the linear elastic response

(fig.5.9b) is evident, as maximum possible stress is limited to the tensile strength of concrete. The concentration of higher stresses in the impact zone is not seen now, with the stresses distributed over a much wider region around the shell. In figure (fig.5.11b), only the tensile regions are contoured to give a better resolution, the uncontoured regions are in compression.

5.2.3 Linear Elastic Response with DSSI Effects

In the following two analyses, the base mat is now added to the superstructure, with its external surface wrapped with CIFECM elements to simulate embedment within an elastic halfspace. The effects of inclusion of the foundation response in comparison with the fixed base superstructure can then be ascertained.

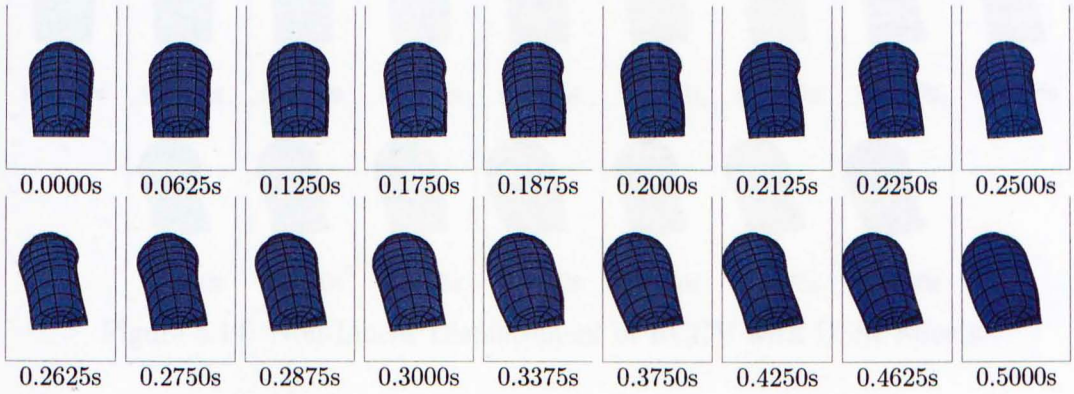

Figure 5.12: Displacement of RCCV with DSSI Effects

The displacement plots show the global rotation of the containment vessel upon its base mat. This motion is still within its first cycle associated with the fundamental frequency. The response of the superstructure does not appear to be greatly affected by this rocking. A local deformation in the impact zone is again observed.

The tensile strains are contoured (fig.5.13a), the major principal strain also happens at the same time ($0.225s$) as seen in both of the fixed base responses. The highest tensile strain of $760\mu\epsilon$ is almost identical (within 1 percent) to that seen in the linear elastic fixed base response (fig.5.9a). The principal stresses are also plotted (fig.5.13b).

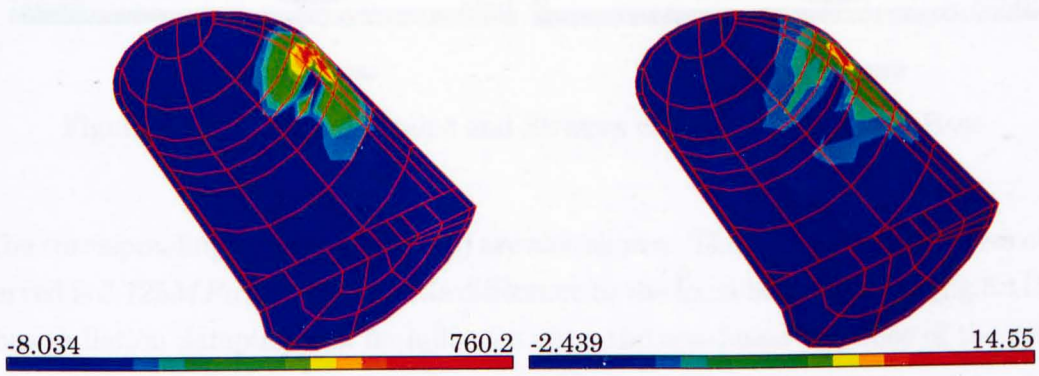

(a) Principal Strains (b) Principal Stresses

Figure 5.13: Major Principal Strains and Stresses of RCCV with Fixed Base

5.2.4 Non-Linear Model Response with DSSI Effects

The combined effects of non-linear material properties and the embedment within the elastic half-space are finally considered.

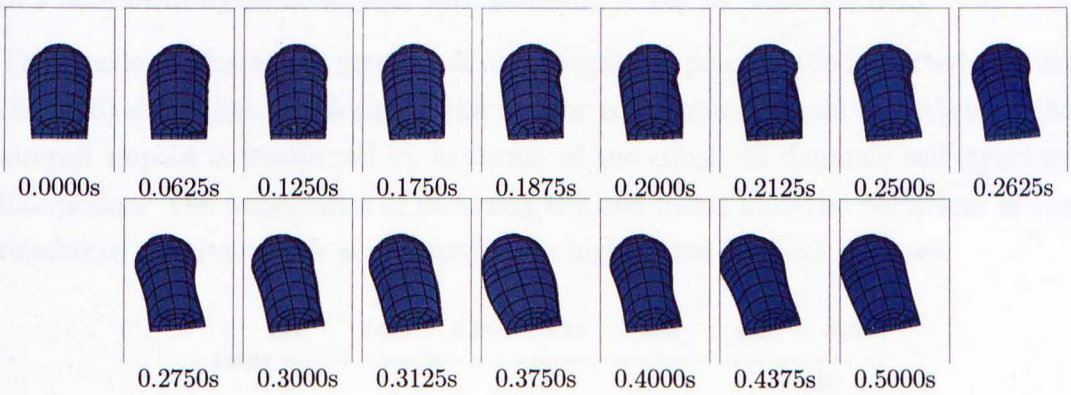

Figure 5.14: Non-Linear Displacement of RCCV with DSSI Effects

The maximum principal strain (fig.5.15a) $1230\mu\epsilon$ is just two percent lower than seen with the fixed base (fig.5.11a). Clearly, the difference is negligble and hence would not effect the design of the containment vessel, in terms of its resistance to the initial impact.

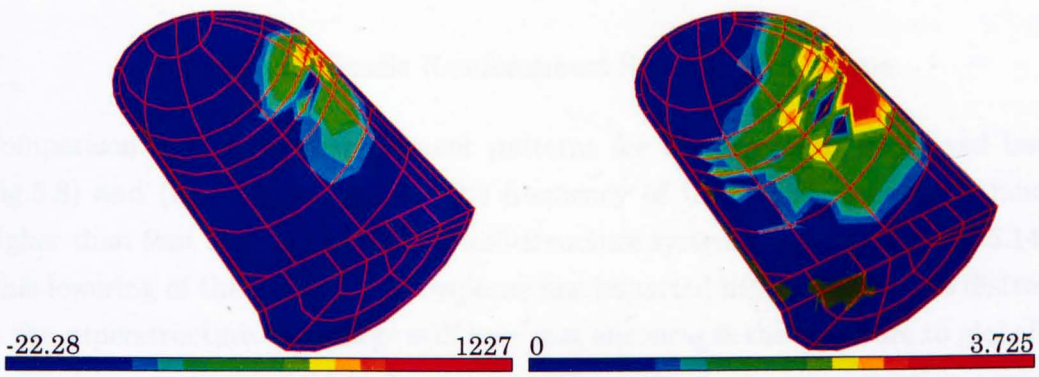

(a) Principal Strains (b) Principal Stresses

Figure 5.15: Principal Strains and Stresses of RCCV with Fixed Base

The corresponding stresses (fig.5.15b) are also shown. The highest tensile stress observed is $3.725MPa$ displaying little difference to the fixed base response (fig.5.11b) thus radiation damping is of no influence upon the non-linear response of the containment vessel.

5.2.5 Discussion of Results

A series of analyses simulating the effects of an aircraft impacting upon a containment vessel have been performed in ascending order of sophistication, culminating in a non-linear dynamic system with inclusion of the dynamic far field.

The tensile reinforcement stresses at one integration point in the impacted element (fig.5.16) show that the design of the reactor containment vessel to withstand the aircraft impact is unaffected by inclusion of the effects of dynamic soil-structure interaction. The importance of including the non-linear material behaviour of the reinforced concrete dome is undisputed, as highlighted in these analyses.

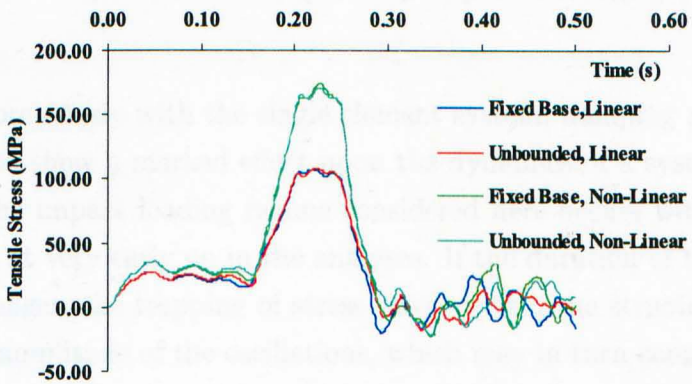

Figure 5.16: Tensile Reinforcement Stresses versus Time

Comparison of the the displacement patterns for the structure with fixed base (fig.5.8) and (fig.5.10), show that the frequency of the global response is much higher than that seen in the coupled soil-structure system (fig.5.12) and (fig.5.14). This lowering of the frequency of response has imparted little effect on the distress in the superstructure. The large stiff base mat encourages the structure to globally respond in an almost rigid body manner. The main design consideration here is the need to ensure that there is the strength within the impact zone.

As well as the ultimate limit state, the serviceability limit state must be considered in the design of engineering structures. The global rocking mode enabled by the underlying soil may have an adverse effect upon the safe functioning of the facility within the containment vessel. The displacements of the non-linear soil-structure system at the last time step considered in this analysis show the global movement horizontally (fig.5.17a), and vertically (fig.5.17b).

Furthermore a possible ultimate limit state failure due to rupture of service piping may become important, this effect can, from such an analyses, be ascertained and accounted for at the design stage in the life cycle of such a safety critical structure.

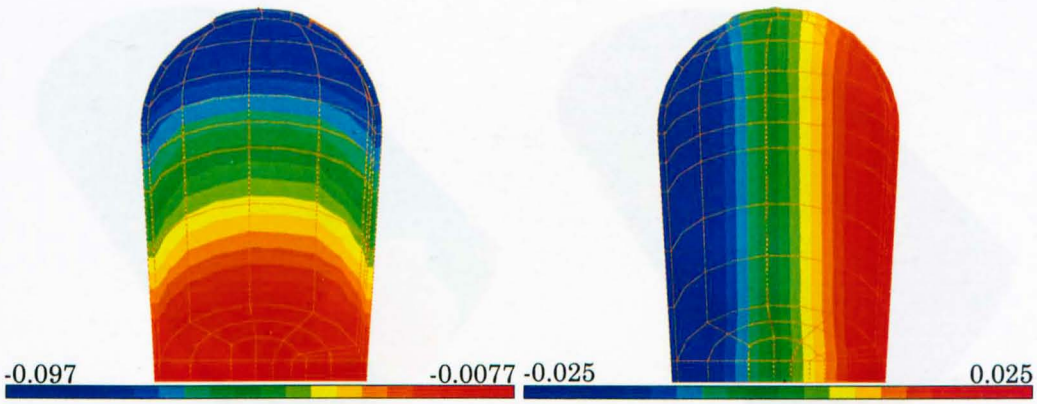

(a) Horizontal (b) Vertical

Figure 5.17: Final (t=0.5s) Displacements (m)

As observed previously with the single element system, damping mechanisms can require time to show a marked effect upon the dynamics of a system. The major response to the impact loading regime considered here occurs within the vicinity of the impact at very early on in the analyses. If the duration of the loading were to be much longer, the trapping of stress waves within the structure will serve to maintain the amplitude of the oscillations, which may in turn cause cyclic damage of the structure. Inspection of the tensile strains in the two non-linear systems at the final time step considered in this analysis, show the effects of radiation damping (fig.5.18). The highest strains in the fixed base response are 50 per cent higher than those corresponding in the soil-structure system.

Inspection of the reinforcement stresses under the relatively slow impact loading regime that the containment vessel has been subjected to, shows that the response under loading is essentially quasi-static. At the end of the applied loading vibration of the system can be seen (fig.5.16).

The system may have, with hindsight, been adequately described by a simpler lumped parameter model with just a few degrees of freedom. With such small embedment of the structure within the founding soil and the stiff base mat acting rigidly, an approximate discrete model may have been adequate. Such a model would employ a rotational spring with a stiffness corresponding to the static rotational resistance appropriate to the site. However, a protective containment vessel of such safety critical importance requires that confidence in the accuracy justifies the costs of the rigourous time domain analyses. Experience gained from the use of rigourous accurate models will also feed into the formulation and construction of cheaper (both in terms of implementation and computation costs) more simplified models, and give valuable insight in to their range of applicability.

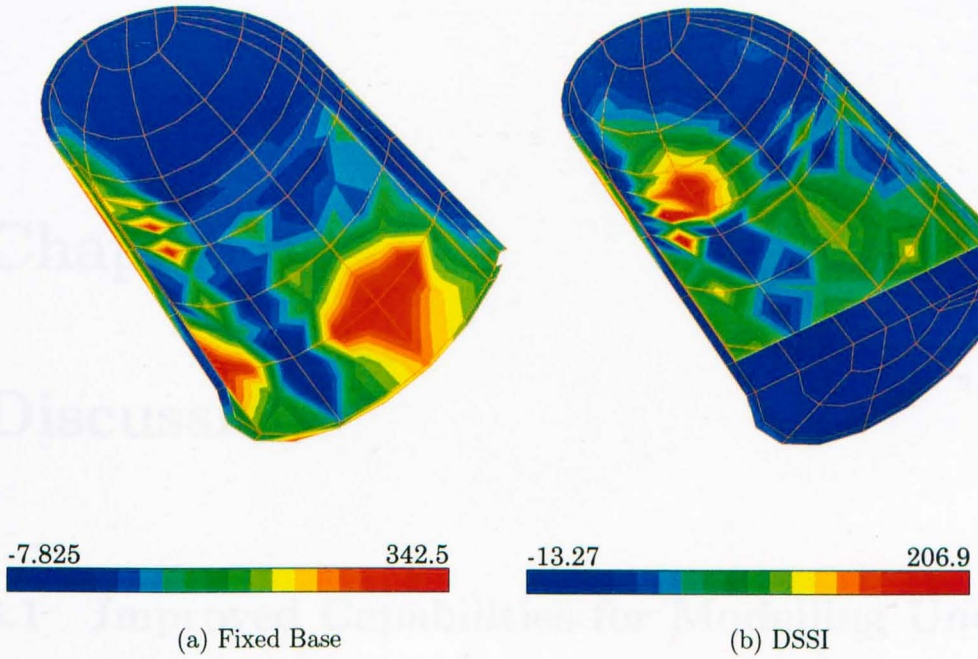

(a) Fixed Base (b) DSSI

Figure 5.18: Principal Strains (t=0.5s)

The inability to perform a preliminary eigenvalue analysis due to the infinite number of natural modes of vibration an unbounded system can exhibit, dictates that frequency domain analyses are an invaluable tool to investigate the dynamics. Simple frequency domain models derived from the experience gained from rigourous models (in both the time and frequency domains), can be used to determine whether the effects of dynamic soil structure interaction need to be included within a full non-linear dynamic analysis.

Chapter 6

Discussion

6.1 Improved Capabilities for Modelling Underlying Soil Conditions

The greatest limitation of using boundary elements to model unbounded media is the necessity to find its fundamental solution. The more complex the geometry the more difficult (or even possible) this becomes to formulate.

The reliance of the Consistent Infinitesimal Finite Element Cell Method on geometric similarity leads to some difficulties in modelling of horizontally layered strata. This could be negated somewhat by simply moving the boundary further away from the similarity centre. However, uncertainties are introduced as to the errors that will result in attempting to approximate the area of influence geometrically. Furthermore, a computational cost is incurred from having to represent a larger near field with finite elements.

Development of a 2-D element for a horizontal layer is shown by Wolf and Song by moving the similarity centre to a point at infinity. Thus it is possible that the bounding surface of a problem could be modelled with a mixture of elements with different similarity centres (fig.6.1), in order to better replicate the physical problem.

This may be performed in two ways, the most simple to develop would use a number of substructures with different similarity centres to one another (including infinite radius). The corresponding possibility in boundary element terms could be seen as using more than one substructure of dynamic boundary elements to model the far field using differing fundamental solutions, for example, layers lying upon a halfspace. This will of course lose the global spatial coupling, which could

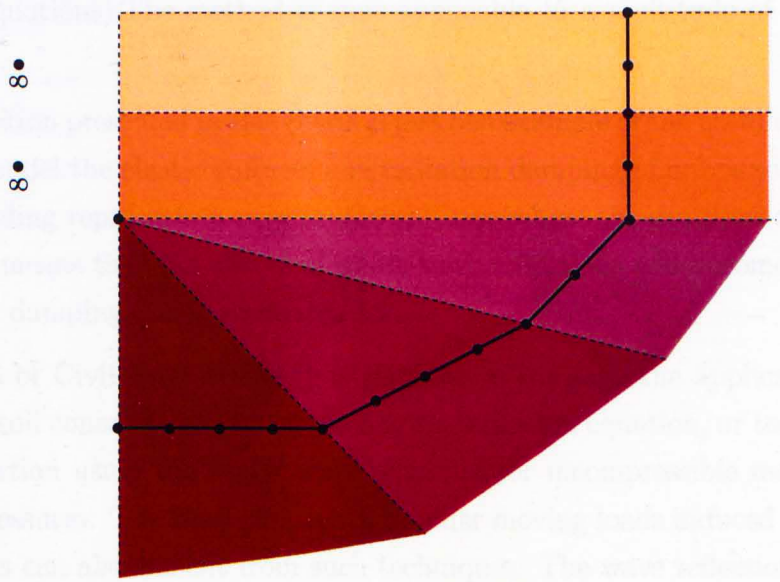

Figure 6.1: Improving the Modelling of Soil Geometry

be maintained by developing the capability to handle multiple similarity centres within a single substructure. This idea of multiple similarity centres within a single fully spatially coupled substructure remains a subject of debate.

The possibility to offer additional geometric flexibility adds to the analysts tool kit. Differing substructures derived from a boundary element or similarity perspective could even be used with one another where the geometric constraints of either method is convenient. The errors incurred by failing to maintain the global spatial coupling are very much problem dependant, and beyond the scope of this work.

The modelling of incompressible media is important for the modelling of fluids, for instance in a fluid-structure interaction problem, or in soil-structure interaction where the surrounding soil can be considered to be fully saturated. Wolf and Song demonstrate an approach to achieve this by taking the analytical limit as Poisson's ratio tends to 1/2.

6.2 Generality of Method to Model other Unbounded Problems

The Consistent Infinitesimal Finite Element Cell Method has been presented by Wolf and Song in a very comprehensive manner for different geometries (2-D, 3-D and axisymetric cases), temporal domains (time, frequency and statics), for scalar and vector variables and for different governing differential equations (wave and

diffusion equations).The method is thus applicable to a multitude of unbounded problems.

The application presented in this thesis is just one example of the usefulness of techniques to model the elastic stiffness and radiation damping of unbounded systems. Seismic loading represents a very important case where the duration of the event considered means that the effects of stress wave reflections will become significant if radiation damping is not accounted for.

In the area of Civil Engineering it is possible to envisage the application of the method to soil consolidation by employing the diffusion equation, or to fluid structure interaction using the scalar wave equation for incompressible media cast in terms of pressures. The wave propagation under moving loads induced due to high speed trains can also benefit from such techniques. The wave reflections observed in a two dimensional analyses [17], may be significantly reduced due to the three dimensional nature of the wave propagation. The non-reflection of such induced waves will thus need to be accounted for in any rigourous model of the system.

6.3 Rayleigh Waves and Love Waves

The formulation of the consistent infinitesimal finite element cell method cannot model the waves produced due to free boundary conditions (Rayleigh Waves) or those arising due to variation in material properties (Love waves). The consequence of this upon the accuracy of a model is problem dependant. The amount of energy dissipated due to Rayleigh waves has traditionally been thought to be significant [43], Wolf in justification of the validity of cone models [58], as approximate design tools, discusses this point further. The oft quoted figure of 66 per cent of the total energy transmitted by Rayleigh waves is shown to be only applicable in the limiting case of the dimensionless frequency tending to zero, i.e. static. The importance of capturing the features of Rayleigh waves diminishes in practical application of the method, further study of this phenomenon is required.

6.4 The Need for Rigour

As an engineer it is appropriate to question the need for such rigor in addressing the problem of dynamic soil-structure interaction. The inherent assumption of linearity used in combining substructures, the specification of the input motion (particularly in earthquake analyses) and input parameters such as the material

properties provide many uncertainties.

With the above limitations in mind the existing approximate methods already may already be sufficiently accurate. However, issues such as the ease of modelling and the interpretation of the results may counteract. For example, the use of decay function infinite elements for statics is dependant upon selecting the correct of decay for the problem being addressed. The important factors in this being the physics and the geometry of the problem, both of which are incorporated within the Green's functions used in the boundary element method. Therefore, the use of such infinite elements may be viewed as a way in which to approximate the Green's function, thus requiring a requisite amount of skill and judgement on the part of the analyst.

In the dynamic case, the application of viscous dampers again tries to approximate the Green's function by placing different damping levels around the boundary accordingly. A further extent of surrounding medium may also be required in order that the wave pattern becomes more uniform in order to select the different damping levels. The inclusion of a greater extent of bounding medium being modelled by finite elements also has the appealing feature of increasing the time delay till waves reflected at the boundary will reach the structure and if other sources of damping are taken into account within the model then the amplitude of any reflected waves may become insignificant.

6.5 Efficient Application of the Method

If the need for such rigour is justified then improvement in the efficiency of the method in terms of both storage and computation needs to be addressed. A number of approaches towards reaching this goal are briefly discussed

6.5.1 Reduced Spatial Coupling

Treating the boundary of a given problem as a number of substructures, the number degrees of freedom coupled with one another may be significantly reduced. This will have a considerable effect upon both the computational and storage requirement. The limiting case being each bounding element constituting a substructure of its own. The reduction in costs must of course be balanced against the greater degree of uncertainty introduced into the model.

6.5.2 Temporal Approximation

The variation of the unit-impulse response coefficients with time may be represented by a smaller number of calculated time steps, with interpolation between these to provide the coefficients at intermediate times applicable with the time step increment employed in the direct time integration scheme. The consistent infinitesimal finite element cell method is an explicit dynamic technique and thus becomes unstable when too large time steps are used, consequently the calculation of the unit-impulse response matrices must take place at small time increments. However, the storage will be significantly reduced.

6.5.3 Realisations

The conversion (realisation) from direct to substructure methods via transfer functions is applied routinely in control systems. The inverse operation however is not so trivial, but has been the focus of recent research [37][54] employing the concepts of linear systems theory. Though in its infancy these methods seem to offer an attractive method of modelling unbounded systems in a more efficient manner resulting in the addition of extra degrees of freedom in the dynamic force equilibrium equation to model the far field.

Realisations are possible from both unit-impulse response and dynamic stiffness matrices to continuous and discrete 1st and 2nd order systems [37]. The choice of best strategy is as yet unclear, and will most probably remain application specific depending upon whether accuracy or efficiency is of highest priority. Due to the method of approximation that need to be employed in order to convert from substructure to direct methods issues of stability also arise.

6.5.4 Parallel Processing

The solution of large finite element problems is now succesfully been tackled by researchers with the use of parallel processing. Computational aerodynamics grids with elements in the 10 to 20 million range and electromagnetic wave scattering problems modelled with 50 to 100 million elements required are been tackled [44]. Extended mesh calculations for dynamic soil-structure interaction analyses may thus becoming viable following the same approach.

The use of substructure methods could also be tackled making use of different computer architectures. For example, calculation of the unit-impulse response matrices may be performed as an ongoing process in tandem with solution of the

dynamic equation of equilibrium. However, the greatest reduction in computational costs are potentially achievable in the calculation of the convolution integral where many of the calculations for a given time step may be performed in advance as the required input (e.g. past velocities) and unit-impulse response matrices are already known.

With all applications of parallel processing applications issues concerning the performance of the parallel algorithm are very much architecture dependant. The ability to efficiently speed up analyses compared to extra computing power required, is limited by the ability to balance the workload on the individual processors and the increase in communication time between processors. In addition the design of the parallel algorithm is also dependant upon the storage scheme, whether shared by all processors or distributed across all of the processors (and the nature of the distribution).

Chapter 7

Conclusions and Further Work

7.1 Conclusions

A review of the current methods of analysing the problem of dynamic soil-structure interaction has been conducted. A number of limitations in the current state of the art (highlighted below) remain, the treatment of the dynamic far field amongst them.

The use of the correct soil material properties, which are naturally highly variable and non-homogeneous is possibly the greatest limitation. Advances in the area of laboratory and in-situ testing of the properties can give the engineer greater confidence and knowledge of the underlying founding material, alongside the use of better constitutive models.

Many advances have been made in the areas of non-linear material behaviour of materials, and remains, owing to its imperial nature, a focus of many researchers attention. Thus, a more realistic simulation including effects of non-elastic materials, uplift of foundations, and liquefaction are now possible.

However, such analyses require an iterative causal approach, which dictates that this needs to be carried out in the time domain. Much of the literature and available software [34] is predominantly on the treatment of wave propagation phenomena in the frequency domain which naturally is more convenient.

A big limitation of dynamic soil-structure interaction analyses is the modelling of the external forces, this is especially true in the seismic case [25][26]. In addition to this difficulty the correct reaction forces from the far field soil to the applied loading need to ascertained.

The possibilities of modelling the far field in the time domain have over the past 30

years been improved by transmitting boundaries, application of boundary integral methods and coupling of boundary and finite elements. The use of boundary elements has the major draw back of the need for a fundamental solution, which for all but simple geometries can be very difficult to formulate.

After a review of existing methods of varying complexity and accuracy a novel finite element based technique to model unbounded media in the time domain was chosen for further study and evaluation. The technique is presented in a manner identical to the flow of the computer code, highlighting the analytical and numerical portions of the formulation. The new technique of configuring *essentially* boundary elements from a finite element perspective, by enforcing geometrical similarity was investigated along with it's implementation within an existing finite element code.

Re-coding of Method in FORTRAN 90 for 3-D, isotropic, compressible elastic material for the vector wave equation has been carried out. This code has been incorporated within a 3-D non-linear Finite-Element code for directly applied loading. The method of calculating the boundary reaction forces is configured to fit within the framework of an element-by-element iterative solver, with Hilber-Hughes-Taylor implicit time integration.

The technique has been applied to a realistic engineering problem, with the use of a non-linear constitutive relationship. Such an analysis would at present be impossible to perform with such confidence without the use of either boundary elements coupled with finite elements or with the new technique implemented and demonstrated.

The present study was carried out by coupling the Boundary Element style method using the convolution integral, an investigation into available methods to reduce the burden of this technique both in terms of storage and computation are highlighted. This will be a key development required in order that such techniques will become accepted not only in specialist algorithms but also enter into the domain of commercial codes.

The consistent infinitesimal finite element cell method is a significant advance in the modelling of both finite and infinite domains, with the generation of dynamic boundary element like response functions without the need of a fundamental solution. This novel formulation now enforces a new geometrical restriction, but represents an improvement for the modelling of infinite domains subject to truly transient loading conditions.

7.2 Further Work

The major short comings common to all substructure methods will need addressing by future research, before such methods become more widely accepted and used in actual practice. The intuition required on the part of the analyst and the costly modelling of greater extent of near field (to allow the wave pattern to become more predictable), make direct methods a conceptually less attractive alternative. However, to date in most commercially available analysis systems, this is the only option available to practitioners.

More knowledge of the significance of reducing the rigorous requirement of full spatial and temporal coupling is necessary before exploitation of the computational and storage advantages that become possible can take place. The errors introduced into the model by relaxing the coupling with substructure techniques needs to be understood by the analyst. In the direct method this is currently performed in practice based on intuition and experience, for example, by the calibration of springs and dashpots truncating the finite element mesh for use in a time domain analyses.

A two phase (soil and pore water) continuum model is necessary to model the near field region of soil as undrained, and also account for the possibility of liquefaction. The appropriate boundary conditions to account for the semi-infinite extent of the pore water in addition, or coupled, with the soil skeleton will need to be addressed.

In order to model non-linearities the time domain must be used. The biggest drawback at present being the burden of the convolution integral. Therefore it is the authors opinion that further research, and subsequent application of realisation techniques, whereby a direct representation of the dynamic far field is approximated from the rigorous substructure approach, offers the most promising direction of future research.

Bibliography

[1] Abouseeda, H. and Dakoulas, P. *Non-Linear Dynamic Earth Dam-Foundation Interaction Using a BE-FE Method*, (1998), Earthquake Engineering and Structural Dynamics, Vol.27, 917-936

[2] Anderson, E.; Bai, Z. et al, *LAPACK Users Guide, 2nd Edition*, (1992), Society for Industrial and Applied Mathematics, ISBN 0-89871-345-5

[3] Bannerjee and Butterfield. *Boundary Element Methods in Engineering Science*, (1981), McGraw-Hill, ISBN 0-07-084120-9

[4] Bartels, R.H. and Stewert, L.J. *Solution of the Matrix Equation* $AX+XB=C$, Communications of the ACM, vol.15, 820-826

[5] Bathe, K.J. *Finite Element Procedures*, (1996), Prentice Hall, ISBN 0-13-301458-4

[6] Bažant, Z.P. and Oh, B.H. *Microplane Model for Progressive Fracture of Concrete and Rock*, (1985), ASCE Journal of Engineering Mechanics, 118, 3, 540-556

[7] Bažant, Z.P. and Prat, P.C. *Microplane model for brittle-plastic material: I Theory, II Verification*, (1988), ASCE Journal of Engineering Mechanics, 110(10), 1672-1702

[8] Bažant, Z.P.; Caner, F.C.; Carol, I.; Adley, M.D. and Akers, S.A. *Microplane model M4 for concrete. I: Formulation with work-conjugate deviatoric stress*, (2000), ASCE Journal of Engineering Mechanics, 126(9), 944-953

[9] Bettess, P. *Infinite Elements*, (1992), Penshaw Press, ISBN 0-9518806-0-8

[10] Carol, I.; Prat, P.C. and Bažant, Z.P. *New explicit microplane model for concrete: Theoretical aspects and numerical implementation*, (1992), International Journal of Solids and Structures, 29(9), 1173-1191

[11] Carol, I.; Jirasec, M.; Bažant, Z.P. and Steinmann, P. *New Thermodynamic Approach to Microplane Model with Application to Finite Deformations*, (1998), International Center for Numerical Methods in Engineering(CIMNE), Technical Report PI-145

[12] Cervera, M.; Hinton, E.; Bonet J. and Bićanić, N. *Nonlinear Transient Dynamic Analysis of Three Dimensional Stuctures - A Finite Element Program for Steel and Reinforced Concrete Materials*, (1988), Numerical Methods and Software for Dynamic Analysis of Plates and Shells, Hinton, E. (Ed.), Pineridge Press, ISBN 0-906674-66-2, 320-504

[13] Chuhan, Z. and Chongbin, Z. *Coupling of Finite and Infinite Elements for Strip Foundation Problems*, (1987), Earthquake Engineering and Structural Dynamics, Vol.15, 839-851

[14] Chuhan, Z.; Xinfeng, C. and Guanglun, W. *A Coupling Model of FE-BE-IE-IBE for Non-Linear Layered Soil-Structure Interactions*, (1999), Earthquake Engineering and Structural Dynamics, Vol. 28, 421-441

[15] Crouch, R.S. *yaFEc-lite: A user manual for a 3-D implicit non-linear dynamic code for RC structures incorporating DSSI and FSI*, 1998, Department of Civil and Structural Engineering, University of Sheffield, UK

[16] Dasgupta, G. *A Finite-Element Formulation for Unbounded Homogeneous Media*, (1982), Journal of Applied Mechanics, ASME, vol.49, 136-140

[17] Ekevid, T. Martin, X.D. and Wiberg, N-E Adaptive Finite Element Analysis of Wave Propagation Under Moving Loads Induced by High-Speed Trains, (2000), European Congress on Computational Methods in Applied Sciences and Engineering

[18] Enquist, B. and Majda, A. *Absorbing Boundary Conditions for the Numerical Simulation of Waves*, (1977), Mathematics and Computers, 31(139), 629-651

[19] Von Erstorff, O. and Kausel, E. *Coupling of Boundary and Finite Elements for Soil-Structure Interaction Problems*, (1999), Earthquake Engineering and Structural Dynamics, Vol. 18, 1065-1075

[20] Hilber, H.M.; Hughes, T.J.R. and Taylor, R.L. *Improved Numerical Dissipation for Time Integration Algorithms in Structural Dynamics*, (1977), Earthquake Engineering and Structural Dynamics, 5, 283-292

[21] Hine, N.W.; Zienkiewicz, O.C.; Wood, W.L. and Taylor, R.L. *A Unified Set of Single Step Algorithms Part 1*, (1984), International Journal of Numerical Methods in Engineering, 20, 1529-1552

[22] Hinton, E.; Rock, T. and Zienziewicz, O.C. *A Note on Mass Lumping and Related Process in the Finite Element Method*, (1976), Earthquake Engineering and Structural Dynamics, 4, 245-249

[23] Hughes, T.J.R. *The Finite Element Method*, (1987), Prentice Hall

[24] Kausel, E. *Local Transmitting Boundaries*, (1987), Journal of Engineering Mechanics, ASME, vol.114 no.6, 1011-1027

[25] Kramer, S.L. *Geotechnical Earthquake Engineering*, (1996), Prentice Hall, ISBN 0-13-374943

[26] Krauthammer, T. *Free Field Analysis Considerations for Dynamic Soil-Structure Interaction*, (1987), Computers and Structures, Vol. 26, no.12, 243-251

[27] Lamb, H. *On the Propagation of Tremors Over the Surface of an Elastic Solid*, (1904), Philosophical Transactions of the Royal Society, Ser.A, vol.203, 1-42

[28] Laub, A.J. *A Schur Method for Solving Algebraic Riccati Equations*, (1979), IEEE Transactions on Automatic Control, vol. AC-24, 913-921

[29] Lindman, E.L. *Free-Space Boundary Conditions for the Time Dependant Wave Equation*, (1975), Journal of Computational Physics, 18, 66-78

[30] Lysmer, J. and Kuhlemeyer, R.L. *Finite Dynamic Model for Infinite Media*, (1969), Journal of the Engineering Mechanics Division, ASCE, EM4, 859-877

[31] Manolis, G.D. and Beskos, D.E. *Boundary Element Methods in Elastodynamics*, (1988), Unwin Hyman, ISBN 0-04-620019-3

[32] MATLAB *MATLAB Computer Language*, (1999), Math Works Inc.

[33] Mesmar, S. *Duvaut-Lions Viscoplastic Regularisation for Dynamic Finite Element Localisation Analysis*, (2000), PhD Thesis, Department of Civil and Structural Engineering, University of Sheffield, UK

[34] National Information Service for Earthquake Engineering *Computer Software for Earthquake Engineering*, (1995), Earthquake Engineering Research Center, University of California, Berkeley

[35] Newman, J.B. *Deformational Behaviour, Failure Mechanisms and Design Criteria for Concrete Under Combinations of Stress*, (1973), PhD Thesis, University of London

[36] Newmark, N.M. *A Method for Computation of Structural Dynamics*, (1959), ASCE Journal of Engineering Mechanics, 85(EM3), 67-94

[37] Paraneso, A. *Rational Approximation and Realization of Generalized Force-Displacement Relationship of an Unbounded Media*, 1997, PhD Thesis, Ecole Polytechnique Federale De Lausanne, Switzerland

[38] Press, W.H.; Teukolsky, S.A.; Vetterling, W.T. and Flannery, B.P. *Numerical Recipes in FORTRAN 90*, Vol 2, Cambridge University Press, 2nd Edition

[39] Qiu, Y. and Crouch, R.S. *Spurious compaction in the microplane model and a new adaptive framework*, (1997), Computational Plasticity: Fundamentals and Applications, Owen, Oñate and Hinton (Eds.), CIMNE, Barcelona

[40] Qiu. Y, *An Investigation into the Microplane Constitutive Model for Concrete*, (1999), PhD Thesis, Department of Civil and Structural Engineering, University of Sheffield, UK

[41] Quinlan, P.M. *The Elastic Theory of Soil Dynamics*, (1953), Symposium on Dynamic Testing of Soils, Am. Soc. Testing and Materials, Special Technical Publication, no.156, 35-64

[42] Reissner, E. *Stationare, axialsymmetrische durch eine Schuttelnde Masse erregte Schwingungen eines Homogen Elastischen Halbraumes*, (1936), Ingenieur-Archiv, vol.7, part 6, 381-396

[43] Richart, F.E.; Hall, J.R. and Woods, R.D. *Vibrations of Soils and Foundations*, (1970), Prentice-Hall

[44] Said, R.; Weatherill, N.P. and Morgan, K. *Unstructured Mesh Generation on Parallel and Distributed Computers*, (1999), EURO-PAR99 Third Euroconference on Parallel and Distributed Computing in Computational Mechanics, Edited Topping, B.H.V.

[45] Sainni, S.S.; Bettess, P. and Zienkiewicz, O.C. *Coupled Hydrodynamic Response of Concrete Gravity Dams Using Finite and Infinite Elements*, (1978), Earthquake Engineering and Structural Dynamics, Vol.6, 363-374

[46] Smith, I.M. and Griffiths, D.V. *Programming the Finite Element Method*, (1997), Wiley and Sons, ISBN 0-471-96542-1

[47] Smith, I. M. *General Purpose Parallel Finite Element Programming*, (1999), 7^{th} Annual Conference of the Association for Computational Mechanics in Engineering, Durham, 21-24

[48] Smith, W.D. *A Non-Reflecting Plane Boundary for Wave Propagation Problems*, (1974), Journal of Computational Physics, 15, 492-503

[49] Song, C. 'SIMILAR A Computer Programme for the Consistent Infinitesimal Finite-Element Cell Method', Software accompanying the textbook *Finite-Element Modelling of Unbounded Media*,(1996), John Wiley and Sons, ISBN 0-471-96134-5

[50] Song, C. and Wolf, J.P. *The Scaled Boundary Finite-Element Method -Alias Consistent Infinitesimal Finite-Element Cell Method - for Elastodynamics*, (1997), Computer Methods in Applied Mechanics and Engineering, vol.147, 329-355

[51] Stroud, A.H. *Approximate Calculation of Multiple Integrals*, (1971), Prentice-Hall

[52] Sung, T.Y. *Vibrations in Semi-Infinite Solids due to Periodic Surface Loadings*, (1953), Symposium on Dynamic Testing of Soils, Am. Soc. Testing and Materials, Special Technical Publication, no.156, 35-64

[53] Tahar, B. *C_2 Continous Hardening/Softening Elasto-Plasticity Model for Concrete*, (2000), PhD Thesis, Department of Civil and Structural Engineering, University of Sheffield, UK

[54] Weber B. *Rational Transmitting Boundaries for Time-Domain Analysis of Dam-Reservoir Interaction*, (1994), PhD Thesis, University of Zurich

[55] Wilson, E.L.; Farhoomand, I. and Bathe, K.J. *Nonlinear Dynamic Analysis of Complex Structures*, Earthquake Engineering and Structural Dynamics, 1, 241-252

[56] Wolf, J.P. *Dynamic Soil-Structure Interaction*, (1985), Prentice-Hall, ISBN 0-13-221565-9

[57] Wolf, J.P. *Soil-Structure Interaction Analysis in the Time Domain*, (1988), Prentice-Hall, ISBN 0-13-822974-0

[58] Wolf, J.P. *Foundation Vibration Analysis Using Simple Physical Models*, (1994), Prentice-Hall, ISBN

[59] Wolf, J.P. and Song, C. *Finite-Element Modeling of Unbounded Media*, (1996), John Wiley and Sons, ISBN 0-471-96134-5

[60] Wu, H-S. *3-D Non-Linear Dynamic Fluid Structure Interaction Analysis of Reinforced Concrete Structures*, (2000), PhD Thesis, Department of Civil and Structural Engineering, University of Sheffield, UK

[61] Zienkiewicz, O.C. and Taylor, R L, *Finite Element Method*, 1991, 4^{th} edition, McGraw-Hill

Appendix A

Flow Chart of CIFECM Code

Input from FE Code

Integers

np	number of nodes on soil-structure interface
nd	number of degrees of freedom
ne	number of elements
nstep	number of time steps
ndim	number of dimensions
nboun(ndim,np)	restrained degrees of freedom
npe(nln,ne)	element nodal connectivity
nmats	number of materials

Reals

dtim	time step size
coord(ndim,np)	nodal coordinates
minfinity(nd,nd,nstep)	unit impulse response matrices
rho(nmats)	Poissons ratio
ym(nmats)	Young's Modulus
nu(nmats)	mass density

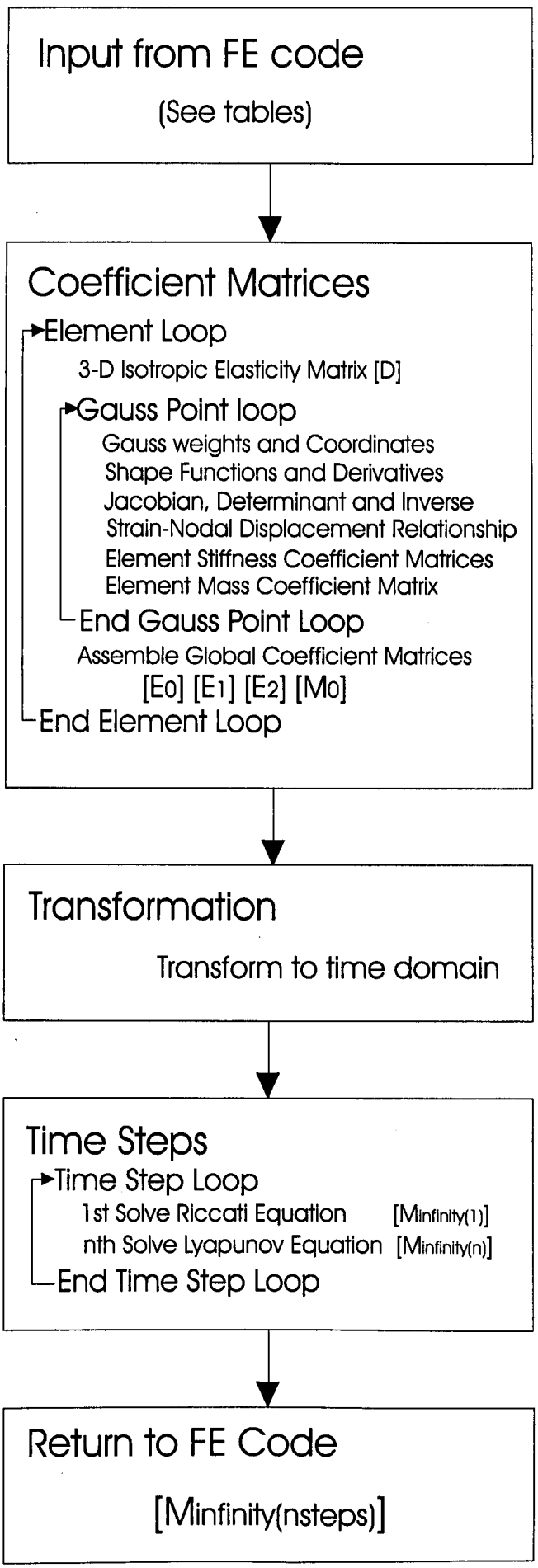
Input from FE code
(See tables)
Coefficient Matrices
Element Loop
3-D Isotropic Elasticity Matrix [D]
Gauss Point loop
Gauss weights and Coordinates
Shape Functions and Derivatives
Jacobian, Determinant and Inverse
Strain-Nodal Displacement Relationship
Element Stiffness Coefficient Matrices
Element Mass Coefficient Matrix
End Gauss Point Loop
Assemble Global Coefficient Matrices
[E0] [E1] [E2] [M0]
End Element Loop
Transformation
Transform to time domain
Time Steps
Time Step Loop
1st Solve Riccati Equation [Minfinity(1)]
nth Solve Lyapunov Equation [Minfinity(n)]
End Time Step Loop
Return to FE Code
[Minfinity(nsteps)]

Appendix A

Glossary of Terminology

Although naturally not exhaustive this short glossary is provided to help explain terms and expressions used in this thesis for which descriptions have not been provided in the main body of the work. This list has been compiled from the **NAFEMS** *Introduction to Nonlinear Finite Element Analysis* and *How to - Understand Finite Element Jargon*, for a first text in Finite Elements the reader is also directed to the excellent companion publication *A Finite Element Primer*. Details of how to obtain these publications are available on the NAFEMS website (http://www.nafems.org/).

Accuracy this has two meanings. i) the accuracy with which the finite element model represents the real structure and ii) the accuracy of the solution of the equilibrium equations

Assembly formation of the stiffness and mass matrices for the structure and the global load vector

Boundary Conditions are the loading and displacement conditions imposed on the structural model and represent the interaction of the structure with its surroundings

Compatibility implies that the displacements (or other parameters) within elements and across element boundaries are continuous

Connectivity is the relationship between individual elements and nodes and corresponding degrees of freedom in the assembled stiffness matrix

Consistent Mass Matrix is one in which the mass of an element is distributed to the nodes in an accurate manner based upon the shape functions of the elements

Constitutive equations describe the stress-strain relationship of a material

Convergence is the tendency towards an 'exact' analysis as the descretisation error is reduced

Coupled usually used to imply that two causes or effects interact

Damping is the dissipation of energy in a vibrating structure

Deformation is a general term used for deflections, displacements, rotations, distortions due to mechanical loading or thermal effects

Degrees of Freedom are the fundamental variables being solved for in a FE analysis. In structural analysis these are the displacements, and for certain element types rotations

Descretisation the process of breaking down a body into a finite number of elements of finite size

Deviatoric Strain components of the deviatoric strain tensor which is formed by subtracting the volumetric strain tensor, so that $\epsilon = E + \epsilon_v$

Deviatoric Stress components of the deviatoric stress tensor which is formed by subtracting the hydrostatic stress tensor from the stress tensor so that $S = \sigma - \sigma_m$

Element Type there are many different types of element, ranging from rods and bars, membranes, plates, shellss through to high-order three dimensional elements. The choice of appropriate element has a profound effect on the accuracy and cost

Errors errors arise from two main sources. i) poor modelling and descretisation and ii) roundoff and truncation

Explicit Time Stepping Scheme a numerical procedure where the solution at the current time is obtained entirely from the solution and conditions imposed at the previous time step

Frequency Domain solutions of dynamic problems are those in which the forcing function is expressed in terms of its frequency components and the solution is found by summing the effects of these components

Gauss Points are integration points in the Gauss Quadrature integration scheme

Hardening due to plastic flow, translation or expansion of the yield surface can occur

Implicit Time Stepping Schemes a numerical procedure where the solution at the current time is obtained from the solution at the previous time step and the conditions imposed at the current time

Incompressibility straining with zero volumetric strain (no volume change)

Incremental Formulation reduction of the partial differential equations of a structure to finite difference equations by use of finite differences in time

Incremental-Iterative method a means of solving the governing equilibrium equations in which the load is applied as a sequence of load increments and equilibrium is established using an iterative solution process during the application of each load increment

Integration Points, Integration Weights A numerical integration scheme relies on the calculation of the magnitude of a function at discrete points on an interval, and the subsequent assessment of the integral in terms of multiples of these numbers. The points at which the function is evaluated are the integration points, and the multipliers which are used to compute the integral are the integration weights

Interpolation Functions are used to calculate the value of a variable over an interval in terms of discrete values at the nodes

Isoparametric Formulation formulation of elements in which the interpolation of the geometry and the displacements are represented by functions of the same order

Iteration a process in which the equations are not solved directly. Instead an initial estimate is made and an algorithm formulated so that successive estimates improve on the previous until the estimate satisfies the equations within some specified tolerance

Jacobian Matrix relates the derivatives of the geometry of an element in the idealised space in which it is formulated to derivatives of its geometry in real space

Linear Analysis assumes that the stiffness matrix and the load vector are independant of the nodal displacements

localisation for softening materials, a tendency for nonlinear behaviour to be concentrated into local bands

Lumped Mass describes an element with a mass matrix in which the mass is distributed equally to the nodes on the element

Material Non-linearity is a change of material properties with strain, temperature etc. which causes non-linear behaviour.

Mesh is a term used to describe the discretisation of the real structure into elements connected at nodes or to describe the resulting assembly

Mode Shapes are the deformed shape of a structure vibrating at its natural frequencies, also called Eigenvector.

Natural Frequencies are the frequencies at which an undamped body will vibrate indefinitely if it is disturbed from its equilibrium condition

Newmark's Time Stepping Schemes a family of time integration methods for the solution of transient dynamic problems

Newton-Raphson Method an incremental-iterative procedure . When used for solving the equilibrium equations the tangential stiffness matrix is updated during every iteration of every increment

Path Dependancy a situation arising when the structural behaviour depends on the history of the structural response as the load is applied and the solution proceeds

Principal Stress normal stresses across planes where the direct stress has no shear stress components.

Quasi-Static means that loads vary slowly with time, thus inertial terms become unimportant

Reduced Integration the process of intentionally under-integrating the stiffness matrix of an element to prevent problems such as shear locking or to improve the performance of the element

Shape Functions describe the distribution of a variable in an element when it is assigned a value of unity at one node and zero at all other nodes in the element

Singularity has three meanings i) undefined or infinitely large values, often resulting from a division by zero, ii) insolubility of the system equations because the global stiffness matrix has a zero determinant, iii) occurence of an infinite stress / strain at a sharp internal corner or under a load point

Softening due to plastic flow, a contraction of the yield surface - leads to localisation phenomena

Stability used to describe the performance of algorithms - for example explicit time integration schemes become unstable if the time step size is too large

Substructuring a method of modelling in which the full structure is broken down into smaller parts. The substructures may be analysed separately and then assembled to form the full structure

Tangent Stiffness is the effective stiffness at a particular instant in the incremental loading of a FE model. The tangent stiffness reduces when a material passes its yield point

Time Domain refers to the method of solution of a dynamics problem in which the forcing function is expressed in terms of its time history, and applied to the system as a series of discrete pulses at each time in the solution process

Time Stepping Schemes methods for integrating in time

Topology means the model geometry is described by nodal coordinates and element connectivities

Viscoelasticty a theory of material response in which the current deformation is a function of the entire history of straining

Viscoplasticity viscoplastic theory allows the time rate effects in the plastic deformation process - thus, after yielding of the material, the plastic flow and the resulting stresses and strains are time dependant

Volumetric Strain the sum of the principal strains divided by the number of spatial dimensions

Yield Criterion in the theory of plasticity, a law defining the limit of elastic behaviour under any combination of stresses